The relationship between intracellular forces and cellular stiffness investigated by atomic force microscopy

Nicola Mandriota

Submitted in partial fulfillment of the
requirements for the degree of
Doctor of Philosophy
in the Graduate School of Arts and Sciences

COLUMBIA UNIVERSITY

2016

ABSTRACT

The relationship between intracellular forces and cellular stiffness investigated by atomic force microscopy

Nicola Mandriota

The characterization of the mechanical behavior of cells has always captured the interest of scientists and, in the last decades, it has been facilitated by the development of techniques capable of measuring a cell's deformability. However, if on one hand cells are active, living materials that regulate their physiology by generating and transmitting forces throughout their volume, common mechanical characterizations of cells involve material science approaches which mostly address them as inert materials. As a consequence, the use of mechanical characterizations of cells has so far been mostly limited to providing correlations with physiological and pathological states.

In this thesis, a cell nanomechanical platform is presented whose resolution allows the isolation of the mechanical contribution of load-bearing cellular components. We first demonstrated that tensional forces - rather than the passive viscoelastic properties of the cytoplasm - govern the stiffness of cells at the nanoscale. We then quantitatively characterized the relationship between intracellular forces and the μm-scale patterns of stiffness across the cell surface. This analysis allowed us to calculate multiple physiologically-relevant quantities such as membrane tension, cortex tension, actin bundle tension, tension-free elastic modulus, and mechanical coupling distances, all from single high-resolution cell stiffness images, allowing an unprecedented connection between distinct mechanobiology fields.

Table of Contents

List of figures

List of tables

Abbreviations

AFM	Atomic force microscopy
ECM	Extracellular matrix
FA	Focal adhesion
MTC	Magnetic twisting cytometry
PALM	Photoactivated localization microscopy
SEM	Scanning electron microscopy
SF	Stress fiber
SLA	Subcellular laser ablation
SIM	Structured illumination microscopy
STED	Stimulated emission depletion
STORM	Stochastic optical reconstruction microscopy
TFM	Traction force microscopy
THC	Torsional harmonic cantilever

Acknowledgments

First, I would like to acknowledge my advisor, Ozgur Sahin. I am very grateful for his extensive support in the design and interpretation of experiments, and for his constant help in expressing scientific ideas and navigating scientific literature. I also want to acknowledge his tremendous effort in providing the best possible work conditions inside and outside the laboratory, thanks to his fairness, trust, kindness, availability, and help with orientation. For these reasons, I could not be happier to have performed most of my Ph.D. work under his guidance.

I would also like to thank my thesis committee members Prof. Rafael Yuste, Prof. Michael P. Sheetz, Prof. Helen H. Lu and Prof. Laura J. Kaufman for their invaluable feedback on this work and throughout my committee meetings. Likewise, I'd like to thank Prof. Jean Gautier, Prof. Rodney J. Rothstein, and Prof. Martin Chalfie for the great time I spent in their lab before joining the Sahin lab. Each experience taught me a lot and helped me become a better scientist.

I'd like to thank the Sahin lab members for help and discussions, in particular John A. Jones Molina and Xi Chen for help, respectively, with the model presented and with instrumentation. Likewise, I'd like to thank former labmates Dr. Francesco Balestri, Prof. Merav Ben-Yehoyada, Prof. Peter Thorpe, Dr. Ivana Sunjevaric, and Dr. Xiaoyin Chen for help and supervision in various labs prior to my dissertation work. I'd also like to acknowledge my previous mentors Prof. Piero Luigi Ipata, Prof. Marcella Camici, Prof. Arturo Falaschi, and Dr. Gulnara Abdurashidova for their guidance and support during my college years.

I’d also like to thank the biology department at Columbia University, and the NIH institute for partially supporting my studies and experiments.

I’d also like to acknowledge my friends, who made my life better throughout these years and encouraged my work in the United States, especially Prof. Paolo A. Zacchia.

Finally, a special thanks goes to my great-uncle Erminio for inspiring scientific interest during my childhood and, most importantly, to my parents and grandparents to whom I owe pretty much everything.

Dedication

To my mother, my father, and my grandmother Agnese.

Foreword

Cells perform an enormous number of processes simultaneously to create the astounding complexity of living beings. This capability is largely enabled by an abundance of tightly-regulated biochemical reactions. Yet, cells are characterized by small Reynolds numbers, so that minute timescales are required by Brownian motion to move ions and small proteins across the animal cell volume. Cells can rely on molecular motors to transport components faster and for longer distances, however speed is still generally limited to a few μm/sec. Additionally, it generally takes hours for changes in gene expression to take place and days to observe resulting changes in cell behavior and functions [1].

Hence, biochemical processes alone might not be sufficient to properly tackle simple, yet crucial needs of the cell such as the coordination of cell movement, rigidity sensing of the extracellular environment, and the response to physical damage. For these and many other processes it would be reasonable that faster and simpler routes of communication would be used, thus improving efficiency and increasing chances of survival. One notable example is represented by action potentials, which allow exchange of information at speeds in the order of m/s, but most cells are not equipped to propagate electrical signals across their length.

In our everyday life we can observe many examples of simple inanimate materials propagating information at a very high speed. For example, a force applied to an end of a tensed rope can be felt almost instantaneously at the other end, and an earthquake can be felt at thousands of miles

from the epicenter within minutes. These mechanisms rely on physical, rather than chemical properties of materials, for example the tension within the rope and the rigidity of the Earth.

Likewise, cells are extensively equipped with intracellular components capable of transmitting stress, thus propagating information at a very high speed. These include mechanosensitive channels – able to respond to forces within milliseconds – tensed cytoskeletal elements - allowing transmission of information to the nucleus within μs [2] – focal adhesions, and a tensed membrane. Additionally, differently from inanimate objects, cells are active materials, because they can consume ATP to exert forces throughout the cell volume and move away from chemical equilibrium. Cells are indeed *mechanical objects* that use forces to unwind DNA, unfold proteins, move chromosomes, and pull on their substrate. At higher levels, cellular forces allow breathing, walking, and heart beating. The importance of these forces is even higher considering that cells cannot use gravity for the stabilization of shape and structure - as it commonly happens for macroscopic structures.

In the last decades forces and mechanical properties have been indeed recognized as increasingly important in the delineation of cell physiology. This trend is definitely going to continue as better methods are developed, allowing us to further move away from the view of the cell as a "bag full of enzymes" and start taking into account the ubiquitous importance of forces and mechanics [3].

Yet, while the knowledge of forces has given numerous insights on the regulation of cell behavior, the same cannot be said about the knowledge of mechanical properties of cells. Indeed, changes in cell deformability have been correlated with different diseases and physiological states, but so far this knowledge has spurred little understanding of cell physiology. This is surprising, because tension can increase the rigidity of objects such as cables and spider webs in the macroscopic world

– a tensed rope feels more rigid than a relaxed one - and the same behavior has been shown for reconstituted cytoskeletal networks and cells. Hence, the knowledge of cell mechanics is expected to be a powerful tools to understand the distribution of forces and thus provide insight about cell physiology. Yet, this is not currently the case, mainly due to the limited resolution of cell probing instruments, which, besides probing elastic components under force load, simultaneously probe the viscous cytoplasm, which dissipates forces. As a consequence, and with few exceptions, the study of cellular forces has remained surprisingly separated from the study of cell mechanics, and a theoretical framework connecting the two fields is still missing.

In this thesis, a tool capable of isolating the cell mechanical properties at molecular scale will be introduced, demonstrating that a connection between intracellular forces and cell deformability exists, and can be found at the nanoscale. A theoretical framework quantitatively linking the mechanical response of cells with the intracellular forces will then be discussed. This framework not only allows the quantification of physiologically-relevant intracellular forces, but also to finally unleash the power of mechanics through an unprecedented connection with forces.

Summary

Chapter 1: will first introduce basic mechanical concepts and discuss the cellular structures that are known to largely contribute to the mechanical properties of cells. It will then describe the techniques that are currently used to probe the cell mechanical behavior - including atomic force microscopy - highlighting their applicability and limitations. It will end by mentioning known correlations between disease and disruption of a cell's mechanical phenotype.

Chapter 2: will first introduce the importance of forces in cell physiology and describe the techniques that are mostly used to dissect them. It will then discuss the most popular cell mechanical models and describe the known relationships between forces and mechanics.

Chapter 3: will present a high-resolution cell mechanical properties with unprecedented sensitivity and resolution.

Chapter 4: will demonstrate that this platform is capable of isolating the mechanics of specific molecular components. We show that, at the nanoscale, mechanics depends on the intracellular force loads applied to the molecules under analysis.

Chapter 5: will thoroughly investigate this connection and describe a theoretical framework able to quantitatively connect intracellular forces with mechanical properties and their μm-scale variation patterns.

Chapter 6: will discuss capabilities and limitations of our platform and assumptions of our framework. It will also compare the forces we calculated with those estimated from current literature.

Chapter 1: Mechanical properties of animal cells

Cells are constantly exposed to a wide variety of physical stimuli in the animal body. For example, muscle cells experience stretching, bone cells experience compression, and blood cells experience shear flow. Knowing the mechanical properties of cells helps understanding how cell shape changes upon the application of a given physical force. In this chapter we will first introduce elementary mechanical concepts and definitions. We will then describe the most mechanically-active cellular structures of the cell and the methods used to characterize cell mechanical parameters. Finally, we will discuss about mechanics in disease. This connection will help delineating current limitations in the field of cell mechanics, and possible solution to increase its power in the delineation of cell physiological states.

1.1 Introductory concepts

1.1.1 Elastic behavior of materials

Before discussing the role of forces and mechanics in cell behavior, it is necessary to introduce concepts and definitions that will be mentioned throughout this essay. The most common way of determining a physical body's mechanical properties is to apply a force on it and measure its effect. An elastic materials will undergo deformation upon force application and return to its initial

position when the applied force is removed. Elastic bodies obey to the Hooke's law, which states that the force, F, needed to extend or compress an object by some distance, x, is proportional to that distance:

$$F = k\,x \qquad \text{Eq. (1)}$$

The proportionality constant is called spring constant (*k*) and is also known as stiffness - although the latter term is commonly employed to describe the rigidity of an object in a broader sense. This constant can be used to either describe the compression or extension of a solid object along its main axis – for example to quantify the elastic behavior of cells - or the lateral displacement of a suspended object – for example to quantify the bending of the free end of a cantilever (Figure 1).

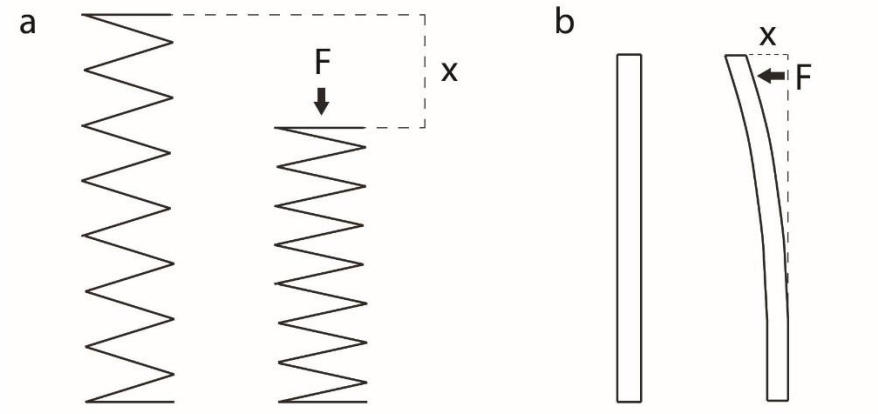

Figure 1: Definition of spring constant

The spring constant, *k*, of a physical body is the ratio between the force applied to it and its displacement, *x*. It characterizes the change in size of a fixed object (**a**), or the displacement of a cantilever object (**b**).

The spring constant is an effective property of an object, because it depends on the object shape, elastic modulus, and tension. While springs commonly used in industrial processes have spring constants typically ranging between 0.1 and 1 N/mm, spring constants of biological materials at

cellular and subcellular scales are generally few to several orders of magnitude lower. For example, proteins typically unfold with a spring constant in the order of 10 pN/nm [4], red blood cells' spring constant has been estimated to be 20pN/nm [5], and microvilli extension can be described by a 43 pN/μm spring constant [6]. Hence, to avoid damage to biological material and yield a displacement, *x*, large enough to be detectable, probing the mechanical properties of cellular materials requires the use of very compliant and sensitive sensors.

Hooke's law can be generalized to characterize the properties of the material composing a physical body through a parameter called elastic modulus (*E*):

$$E = \frac{\sigma}{\varepsilon} \qquad \text{Eq. (2)}$$

, where σ is the stress applied on the material – i.e. force per area – and ε is the strain, measured as the change in length over the original length of the material. Therefore elastic modulus relates a certain stress to the deformation it produces. Differently from spring constant, elastic modulus is an intrinsic property of the material, and does not depend on the object's shape, bending, or force load.

For many mechanical measurements, stress is applied tangentially to the object (shear stress) and the elastic characterization involves calculating the ratio between shear stress and shear strain, which is called shear modulus. For isotropic materials, shear modulus, *G*, is directly related to *E* through the following relationship:

$$E = 2\,(1 + \nu)\,G \qquad \text{Eq. (3)}$$

, where ν is the Poisson ratio of the material, which is typically estimated to be 0.5 for cells – assuming incompressibility.

Conventional materials follow a linear relationship between stress and strain until their elastic limit is reached. This point is often close to the yield limit, which is the point where the material fails and starts to deform plastically (i.e. permanently). Differently from conventional materials, biological polymers often exhibit an opposite behavior, whereas the stress required to obtain increasing strain increases with deformation. This behavior is termed strain stiffening and is believed to protect the cell's structure from sudden increase in applied pressure. The opposite behavior is also possible, whereas the stress required for increasing strain levels decreases, and is termed strain softening.

1.1.2 Viscoelasticity

The above measurements fully describe only elastic objects – i.e. the energy is totally stored in the deformation - which is typical of solid materials. Yet, in fluids, the energy transferred through the applied force can be partially dissipated through flow and heat. The speed of flow under a defined load is defined as the viscosity of a fluid. Materials that display both elastic and dissipative behavior upon deformation are called viscoelastic, and their properties can be described by the combination of a "storage" and a "loss" modulus. The energy dissipated during a deformation cycle can be determined by quantifying the area between the approach (loading) and the retract (unloading) curves of a stress–strain graph, and is referred to as hysteresis.

Cells are perfect examples of viscoelastic materials, and their storage and loss moduli depend on the frequency of stimulation, following a power law relationship. The viscoelastic nature of cells

can be explained by their heterogeneous structure and by protein turnover. First, cells are composed by a wide assortment of biological components. These include a solution containing small solutes - such as ions, sugars and proteins - biological membranes, proteins and macromolecular complexes including a combination of nucleic acids, proteins and polysaccharide chains. These materials exhibit a wide range of mechanical signatures that can depend on the interaction of their components, their geometry, and the force load applied. Additionally, cellular components are extremely dynamic and undergo remodeling and turnover, hence dissipating stress over long timescales. As a consequence, many biological networks are usually elastic on short timescales and viscous on long timescales.

A cell's ability to display elastic and viscous behaviors is also required to perform the variety of physiological functions it is capable of. For example elastic behavior is needed to be able to sense, transmit, and exert forces along membrane and cytoskeletal elements, to round up during cell division, and to squeeze cytoplasm during blebbing. On the other hand, cytoplasm viscous behavior is necessary for cells to flow during cell movement and dissipate stress.

1.2 Structures determining cell mechanical response

Animal cells, unlike plant cells or fungi, lack a cell wall, and thus require different structures to maintain their cellular integrity. This section will describe the structures that are known to largely contribute to cell mechanical measurements. Those include cytoskeletal components and other organelles such as the cell membrane and the nucleus (Figure 2).

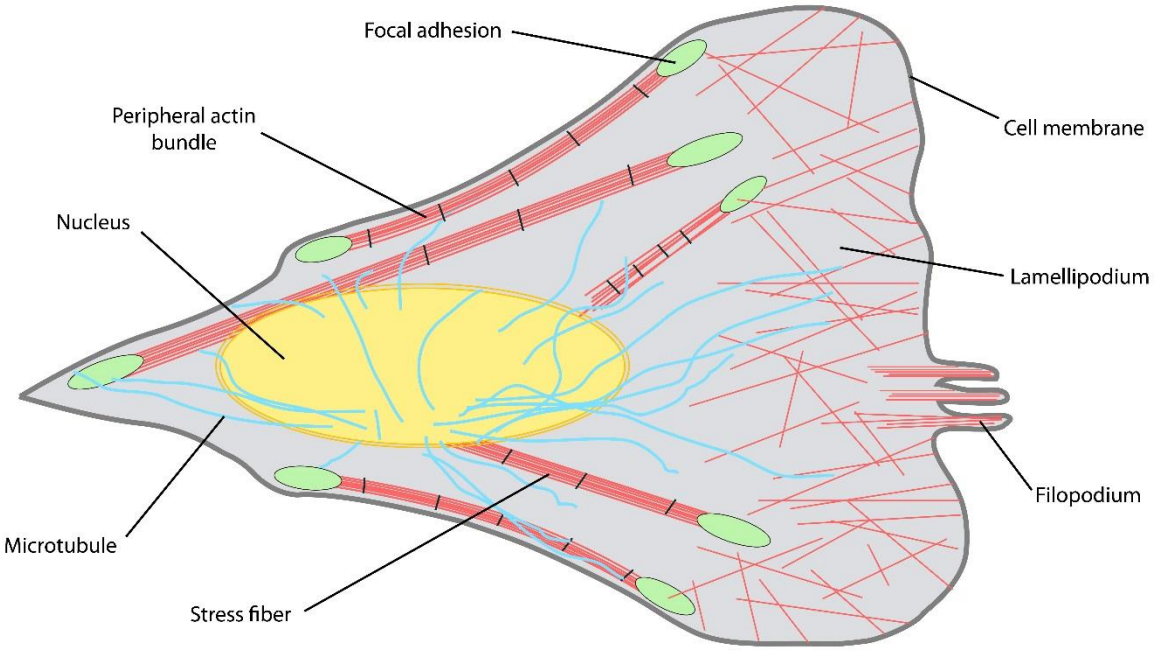

Figure 2: Main cell mechanical contributor

Drawing of the main mechanical components of the cell. Here are represented the cell membrane, the cytoskeleton – including different elements arranged in various configurations – and the nucleus. The mechanical contributors also include the actin cortex, a thin layer of crosslinked actin lying immediately beneath the membrane.

1.2.1 Cell membrane

The cell membrane is a thin semipermeable barrier separating the intracellular material from its extracellular environment. Far from just acting as a cell container, the cell membrane has been been regarded for long time as a "fluid mosaic" [7] composed of a ~ 5–10 nm lipid bilayer, and a large amount of peripheral and integral proteins, which enable the cell to interface with the outside environment, regulate solute concentration, and conduct voltage potentials. This view of the cell

membrane has been successfully harnessed to interpret its physiology for more than 4 decades [8]. Yet, this model leaves out a multitude of crucial aspects of cell physiology, such as the importance of lipid identity, domain compartmentalization, and mechanical behavior. The latter turned out to be increasingly relevant, due to the recent recognition of the importance of forces in the cell functions.

Importantly, cell membrane is under tension - defined as the force per unit length acting on its cross section. Tension regulates a wide variety of additional functions, such as cell shape, cell division, and membrane trafficking [9, 10]. On a general level, tension acts as a homeostatic regulator of protrusion. In an analogous situation to motor proteins, which are stopped by an opposing force load, actin polymerization within filopodia and lamellipodia needs to counteract the mechanical load provided by membrane tension, in order to drive cell protrusion over the substrate. This opposing relationship has been experimentally and quantitatively studied in fibroblasts using compounds that aspecifically alter membrane tension [11], and has been shown to be sufficient to explain the phenotypic variability and the migration speed in a population of fish keratocytes [12]. Tension increase due to actin polymerization against the cell edge also acts as a coordinator of exocytosis and contraction in spreading fibroblasts, providing a fast mechanism to coordinate multiple biochemical events [13]. Tension not only can block protrusion locally, but prevents actin assembly throughout the cell, and acts as a long-range inhibitor of cell protrusion to prevent the formation of secondary leading edges in neutrophils [14]. Additionally, membrane tension regulation is necessary for the successful repair of torn membranes, commonly occurring in normal tissue [15].

Plasma membrane tension can be modulated by a variety of factors, including membrane composition, shape, and the activity of associated proteins, but is ultimately controlled by the ratio between a cell's surface area and volume [16]. Thus, the most direct way to change its value is by addition or subtraction of membrane surface. A quick decrease in membrane tension can be achieved through the unfolding of tension-free "reservoirs". Many of them are created by discrete attachment of the cell membrane to the cortex at discrete spots via linker proteins. These attachment sites behave as membrane pinned ends, enabling the presence of excess membrane folding inwardly or outwardly. A prominent type of membrane reservoir is represented by caveolae, which are stable bulb-shaped membrane invagination ~70 nm in diameter residing underneath the cell membrane of many cell types [17]. Caveolae sense membrane stress and can flatten in response to sudden membrane stretching, providing a mechanism of cell defense against lysis [18]. Other reservoirs include microvilli, blebs, caveolae, and vesicles, which are expected to perform similar functions [16]. On the other hand, endocytosis can increase membrane tension step-wise due to subtraction of membrane.

Membrane tension measurements are relatively easy in membrane vesicles, because they can be performed through pipette aspiration by simply applying the Laplace law (See section 1.2.7). The presence of underlying cortex tension does not allow the same type of measurement in living cells, unless the membrane tension contribution is comparatively large enough – such as in specialized systems like red blood cells [19]. Hence, in the last few decades membrane tension has been measured optically by measuring nanoscale thermally-driven fluctuations [20] or, more commonly, by pulling tethers and measuring the cell's restoring force (See section 2.2.6).

1.2.1.1 Glycocalyx

The glycocalyx represents the outer coating of the cell membrane. It is composed of glycosylated portions of membrane proteins and the carbohydrate moiety of glycolipids. Although the glycocalix is present over most eukaryotic cells - where it gives protection and acts as a fingerprint to distinguish self from non-self [21] - it is particularly prominent over specialized systems. In endothelial cells - where it can reach up to 4.5 μm thickness in large arteries - it prevents direct contact between flowing blood cells and endothelium, determines vascular permeability, acts as a mechanotransducer of shear stress, and serves as a docking site for cells and molecules [22]. It is also abundant over epithelial cells of the digestive system, where it provides scaffold for digestive enzymes and protection from the acidic environment of digestion. Being the outermost cell layer of cells, some studies have deemed glycocalix as an essential component of the cell mechanical response of the endothelium [23]. However, the present work mainly discusses mechanics in fibroblasts, were glycocalix should extend only over a very thin layer. Furthermore, glycocalyx thickness appear to be reduced in static culture conditions [24].

1.2.2 Nucleus

The nucleus is the largest cell organelle and can be structurally subdivided into the nuclear envelope - consisting of a double membrane and the nuclear lamina - and the nuclear interior. Mechanical forces transmitted from the cell exterior and from the cell volume can be transmitted to the nucleus, where they can be potentially transduced into changes in gene expression [25]. Therefore the nucleus contains two very mechanically active structures, such as the lamina and the chromatin – lamina components lamins will be discussed in section 1.2.3.2.

The overall compressibility of isolated nuclei can be readily studied through micropipette aspiration [26]. These studies have shown that the nucleus is generally more rigid than the rest of the cell and its high elastic modulus has been ascribed to the structural role of lamin proteins. However, due to the deep location of the nucleus within the cell, surface measurements, such as those performed with AFM, might not be able to unequivocally probe mechanical contributions from the nucleus [27]. This is especially true for our work, due to the confining of our measurement to the outermost layer of the cell. Therefore, nuclear mechanics will be not experimentally considered in this thesis.

1.2.3 Cytoskeleton

The cytoskeleton is an interconnected ensemble of filamentous proteins lying in the cytoplasm and performing countless functions during a cell's lifetime. The cytoskeleton consist of three distinct classes of proteins that differ in size and function, but are in intimate communication with one another: microtubules, intermediate filaments and actin filaments. These three elements are associated to a variety of classes of regulatory proteins, including crosslinkers, filament nucleators, capping proteins, severing factors, and catalyzers of (dis)assembly. These regulatory factors help assemble the cytoskeleton into different structures, whose mechanical properties vary according to their emergent structure and the changing needs of the cell.

Among its main functions, the cytoskeleton organizes the cell's content, provides a scaffold for the association of structural and signaling molecules, segregates chromosome, coordinates cytokinesis, and directs intracellular transport. One peculiar feature of the cytoskeleton is its ability to generate forces, namely through polymerization of monomers and association with motor

proteins able to generate contractions. This force-generating ability allows the cytoskeleton to give cell mechanical support, determine shape and movement, and transmit mechanical signals and force loads throughout the cell volume.

The functionality and the mechanical characteristics of the cytoskeleton depend on the emergent properties and the high-order interactions stemming from its overall structure, rather than the sum of the molecular interactions of its building blocks. The overall cytoskeletal organization, in turn, depends on signaling systems interpreting and transducing a variety of physical and chemical cues. Reorganization of the cytoskeleton occurs constantly to match ever-changing needs of the cells, but, surprisingly, it does without affecting its ability to function. This is because, although turnover occurs on molecular lengthscales and second timescales, the overall structural integrity of the structure is maintained [3].

It has recently hypothesized that the cytoskeleton response to mechanical and biochemical stimuli might also depends on the previous history of the cytoskeleton, which is a record of a cell's previous mechanical interactions. This could potentially create variability of cell fate and behavior in an otherwise identical environment [28].

Due to the importance of cytoskeleton in the mechanical response of the cell, its different classes of components will be described separately. An overview of reconstituted cytoskeletal networks will then follow.

1.2.3.1 Microtubules

Microtubules are hollow tubes ~30 nm in outer diameter characterized by very high rigidity. Thanks to this feature, they serve as long tracks for intracellular motors, contribute to define cell's

shape, and are the core components of motility organelles, namely cilia and flagella. Their rigidity also determines their persistence length (5.2 mm) [29], which is extremely high compared to cell size (~50 μm). Despite this, microtubules often look highly curved in living cells. This bending likely reflects buckling, due to the high compressive load they bear [30]. According to the tensegrity hypothesis (See section 2.3.5), this force load, together with substrate elements, counteracts actin contractile stress to help a cell maintain its shape. Consistent with this hypothesis, disruption of microtubules with colchicine results in a 13% increase in traction forces on the substrate [31].

Microtubule mechanics is also very important during cell division. In this phase, the microtubule cytoskeleton reorganizes into a mitotic spindle, which is responsible for the segregation of chromosomes. When chromosomes align on the metaphase plate, tension develops along the spindle as a result of the combined action of microtubule depolymerization occurring at the plus ends and the action of motor proteins [32, 33]. Chromosome segregation is an accurate and robust process and fine-tuning of forces, together with biochemical signals, is required to avoid disease, birth defects, and cancer. For example, when a spindle fiber is artificially severed, dynein force restores spindle integrity by anchoring the severed fiber to neighboring fibers [34].

1.2.3.2 Intermediate filaments

Intermediate filaments consist of a group of filamentous polymers with approximate 10 nm diameter classified into 6 groups, based on sequence similarity. Most of intermediate filaments are very compliant at small deformation but dramatically stiffen upon larger stretch, providing cells with mechanical strength and resistance. Some intermediate filaments are only present in

specialized systems, including keratins – forming hair, nails, horns and skins in epithelial cells – desmin – connecting Z-discs in muscle cells – and neurofilament proteins – abundant in mature neuronal processes, where they sustain the structure of long, thin processes. Others are ubiquitous, such as vimentin – present in fibroblasts, smooth muscle cell, and leucocyte – and nuclear lamins – component of the nuclear envelope in most of the cells [21].

Lamin proteins lie underneath the nuclear envelope, providing structural stability to the nucleus. Due to their role, changes in their expression can affect nuclear shape, possibly explaining the symptoms of laminopathic diseases – rare genetic and pleiotropic disorders [35]. Additionally, cells with reduced lamins have more deformable nuclei and can therefore migrate faster through micrometer-sized pores [36], possibly favoring intertissutal migration in living organisms and a higher rate of DNA mutations [37]. Lamin is also extensively connected with the rest of the cytoskeleton through the LINC complex. As a consequence, defects in lamin expression can lead to loss of mechanosensitivity. This relationship has been recently further proved by a study showing that lamin A works as a "mechanostat", whose levels of expression correlate with the elasticity of the human adult tissue under examination [38]. Due to the depth of the nuclear envelope within the cell, lamins contribution to the nanomechanical response of the cell were not analyzed in the present study.

Vimentin's main function is to confer structural stability to the cells, but its role in cell adhesion, signaling, and migration has only recently started to be delineated [35]. Vimentin forms a network extending from the perinuclear region to the cell membrane. Yet, particle tracking experiments have shown that while vimentin does affects the stiffness of regions corresponding to the internal cytoplasm, it doesn't affect the regions closer to the cell surface, corresponding to the cell cortex

[39]. Additionally, knockout of vimentin in mice is viable and does not affect intracellular force distribution, reinforcing the idea that the primary role of vimentin is mainly structural [40]. Contribution of vimentin, as well as of other intermediate filaments, to the mechanical properties of cells has so far been relatively neglected by the research community [41], but progress in the next decade might uncover new information useful for the characterization of animal cell mechanics.

1.2.3.3 Actin filaments

Actin filaments (f-actin) result from the polymerization of monomeric actin (g-actin) into 8.4 nm-diameter helical filaments. These filaments have a polarity, designated by a (+) and a (-) end. Actin is ubiquitous and its huge role in structural integrity and physiological regulation of the cell is exemplified by the number of proteins having actin-binding domains - exceeding 150.

Actin cytoskeleton generates two main types of forces: protrusive and contractile. Protrusive forces are generated by f-actin elongation, pushing the leading edge forward against membrane tension and extracellular matrix impediments, while contractile forces depend on the actin-binding molecular motor myosin and exert forces that cause parallel f-actin filaments to slide past each other. Because the ends of some actin filaments are ultimately secured to the cell's substrate through focal adhesions (See section 1.2.5), this sliding force can causes the onset of pre-stress or tension within the actin network and the presence of traction forces on cellular substrates. Tension forces are distributed throughout the actin cytoskeleton, forming a mechanical continuum with the surrounding extracellular matrix.

Contractile forces have varied functions. First, they allow the cell to anchor to the substrate to resist fluid shear forces, and mechanical forces from neighboring cells and matrix. Forces also help cells to sense and measure the rigidity of the substrate and mechanical signals from neighboring cells, which can be mechanotransduced into biochemical signal to influence processes such as cell movement, proliferation, and gene expression. Contractile forces also allow cell movement and proliferation, for example by allowing the retraction of the cell's leading edge and squeezing cell material to allow blebbing-mediated migration and cytokinesis.

In non-muscle cells, f-actin can be assembled in different fashions, according to the cell location and the function to be performed, but the main architectures types can be roughly subdivided into networks and bundles. Branched networks are the main constituents of lamellipodia, which are thin (140 to 200 nm) and flat regions supporting cell protrusion typically found at the leading edge of the cell. The branching of the filament network is induced by the Arp 2/3 complex, which nucleates the formation of new actin filaments at a ~70° angle from pre-existing filaments [42]. This branching structure is thought to be particularly suited for the generation of a protrusive force at the lamellipodium, which has been estimated to be ~ 1.18 nN, and to be generated through ~100 filaments/µm pushing with an average force of ~4 pN [43]. Isotropic networks are the main constituent of the actin cortex, which is a major contributor to the cell mechanics and will be treated separately in its dedicated paragraph (See section 1.2.3.4). Actin bundles are the constituent form of actin in stress fibers (See section 1.2.6), filopodia, and other actin structures similar to stress fibers, including peripheral actin bundles (See section 1.2.7). Filopodia are finger-like protrusions of the plasma membrane 100 to 300 nm in diameter supported by tightly-bundled actin filaments. Just as for lamellipodia, the polymerization from the (+) ends of actin filaments powers

their extension. Filopodia are often found protruding from lamellipodia and the concerted action of these two elements defines the initial steps in cell migration. Filopodia mediate cell adhesions, support wound healing [44], and work as “antennae” that probe the extracellular environment for physical stimuli and the presence of chemoattractants, Finally, most of the aforementioned structures disassemble during cell division to reorganize into a contractile ring, which pinches and divides the mother cell into two daughter cells.

Actin networks properties and functions are especially sensitive to their surrounding conditions and environmental cues. In particular, the structure of the network strongly depends on the type of stress they are subjected to. While branched networks in lamellipodia and filopodial bundles are usually subjected to compression caused by polymerization against an obstacle such as the membrane or ECM elements, cortical isotropic networks and contractile bundles are under actomyosin-generated tension.

1.2.3.4 Reconstituted networks

Because of the widely-recognized importance of the mechanical properties of cytoskeleton and a lack of conventional materials able to reproduce them, a number of studies has been trying to recreate their behavior *in vitro*, through the assembly of reconstituted networks. When measuring the elasticity of networks, persistence length and contour length become two important factors. Persistence length, L_P, is the approximate length over which the filament orientation changes due to thermal motion, while contour length, L_C, is the length of the extended filament or its length between hinge points, such as those created by crosslinker binding. For flexible polymers ($L_C >> L_P$), such as neurofilaments, the measured elasticity mostly depends on entropy, i.e. the energetic

cost associated with the reduction in the number of configurations during indentation. For stiff polymers ($L_C << L_P$), such as microtubules, the elastic response is dominated by enthalpy, i.e. by the energetic cost to strain monomers away from their equilibrium positions, which is described by the bending modulus, K_B, of the material. Yet, most of biological polymer - including actin – are "semiflexible", because they display an intermediate behavior ($L_C \sim L_P$) and their measured elasticity can be attributed to both enthalpic and entropic contributions [45]. The relative importance of enthalpic and entropic components and, hence, the mechanical properties of in vitro networks strongly depend on the sample preparation and its architecture, including presence and stoichiometry of actin filaments, crosslinkers and other regulatory proteins [46]. A variety of mechanical phenotypes is also present in living cells, empowering them with a rich variety mechanical responses to best suit their physiological demands.

Perhaps one of the most surprising properties of living materials is their ability to exhibit strain stiffening at increasing force loads, which is believed to prevent cellular damage. While strain stiffening is not present in conventional materials such as polyacrylamide, it is typically found in the majority of biological polymers – such as actin, collagen, fibrin and vimentin. It has been argued that this property is mainly due to entropic effects and emerges spontaneously for any semi-flexible and isotropic polymer network in the presence of low-to-intermediate strain, independently from its geometrical configuration [47]. On the other hand, actin reconstituted networks can switch from strain stiffening to strain softening behavior when subjected to high force loads. This phenomenon might be due to the elastic buckling of networks filaments, just like for microtubules [30], and might therefore reflect an increase in the importance of enthalpy upon

increasing force loads. This behavior is thought to prevent catastrophic failure of the network and is therefore considered an additional protection mechanism for the cells upon physical stimuli [45].

The study of reconstituted networks can also provide hints about previously-unidentified capabilities of the cytoskeleton. One example is the discovery that the growth velocity of branched actin networks not only depends on the current, but also on the previous force load applied, potentially allowing a sophisticated feedback between cell protrusion and physical environment [48].

One of the main goals of reconstituted networks goal is to reproduce mechanical behavior of the in vivo cytoskeleton, which has been consistently shown to be a major contribution to the mechanical response of the cell surface. Yet, the stiffness of reconstituted networks has been shown to be strikingly different from that typical of the cell surface. Whereas the stiffness of the *in vivo* cell surface has been shown to be in the order of kPa, most of the reconstituted networks display elastic moduli in the order of 1-10 Pa. This three orders of magnitude-difference has been shown to largely depend on the lack of prestress within the reconstituted network. Indeed, preparations introducing prestress within the networks displayed elasticity increasing linearly [49] or as 1.5 power dependence [46] with prestress, eventually reaching stiffness values comparable to those of living cells - 100 times higher than networks without tension. These critical experiments demonstrates that presence or rearrangement of molecular components *per se* is not sufficient to reproduce the mechanical phenotype of the cell, while application of prestress might create more physiologically-relevant mechanical conditions.

Overall, reconstituted network studies have been able to reproduce a broad diversity of mechanical behaviors displayed by *in vivo* networks, such as strain stiffening. Additionally, these studies allow

to isolate the physical component necessary for a given mechanical response and identify the order of network assembly. Yet, the cytoskeleton is a living structure whose architecture varies dramatically along its length, and is constantly re-shaped by active processes dependent on constant intracellular and intercellular communication. Additionally, the whole cytoskeleton is completely interconnected - allowing the propagation of stress and information along the entire cell's length – and its mechanical properties are therefore a result of the coupling between distinct elements such as microfilaments and microtubules. Finally, the *in vivo* actin cytoskeleton is under tension, while tension is mostly absent in most of the studies involving reconstituted networks, or cannot reach critical values, due to network failure [49]. For these reasons *in vitro* studies can currently mimic only a small fraction of the cytoskeleton mechanical behavior and further exploration and connections with other cell components (e.g. cell membrane) are needed to make them more relevant to cell physiology.

1.2.4 Actin cortex

The actin cortex (also known as the cell cortex) is a thin layer of crosslinked actin filaments located immediately adjacent to the plasma membrane of animal cells. The network runs parallel to the membrane and is mainly isotropic, with mesh size ranging between 50 and 250 nm [50] and a thickness of 30-40 nm [51]. As a consequence, the cortex occupies a significant part of cellular volume within the numerous flat, peripheral regions of a spreading cell, leaving only a ~100 nm separation between its dorsal and ventral layers. The cortex is also rich in myosin and crosslinking proteins such as α-actinin, filamin and fimbrin, as well as actin nucleators such as Arp2/3.

The actomyosin contractility causes the levels of prestress within the cortex to rise, resulting in tension build-up. Additionally, tension levels can be potentially modulated by cell shape changes due to actin (de)polymerization, changes in crosslinkers and changes in cortex architecture in a myosin-independent fashion. Measurements mainly based on micropipette aspiration [52] and force application through AFM (see next chapter for details) estimate such tension to range between tens and thousands of pN/µm, depending on the technique and the organism under analysis. Assuming a typical tension of 500 pN/µm and a typical mesh size of 50 nm, an isometric tension of a few tens of pN can be expected for single actin filaments, consistent with the contraction of several myosin heads per filament. This tension is possibly counteracted by intracellular pressure [16], microtubule buckling [53], or by a combination of the two.

The cortex is connected to the membrane via molecular linkers. These become under tension when the cortex separates from the membrane, tightly coupling the mechanical behaviors of the two structures [54]. For example, membrane and cortical tensions might add up (hence creating "cell tension") to counteract large-scale cellular deformation.

In addition to tension, the cortex also exhibits some degree of viscous behavior, which is dependent on the timescale of the analysis. The interplay between elastic and viscous behaviors determine the cortex functions and allows the cell to display a variety of physiological behaviors. The apparent elasticity provided by tension, and the intrinsic elasticity provided by the elastic modulus, allow the cell to exert forces during mesenchymal-type movements [55], cytokinesis and cell polarization, oppose the hydrostatic pressure caused by its own contraction, and resist mechanical deformation [56]. Cortical forces are also essential in meiosis, when a local decrease in cortex tension mediated by myosin depletion is responsible for the off-center positioning of the spindle,

thus allowing correct chromosome segregation [57]. Finally, cortex tension is responsible for detachment of the trailing edge from the substrate during cell protrusion and triggers blebbing during migration [58]. On the other hand, the molecular components of the cortex undergo turnover within a second timescale, allowing network reorganization, stress dissipation and certain types of shape changes. While the viscoelastic behavior of the cortex offers cells ways to adapt mechanical behavior to a wide variety of physiological needs, it results in the need of characterizing the mechanical response of the cortex at different timescale.

1.2.5 Focal adhesions

Focal adhesions (FAs) are µm-sized multi-protein structures commonly found at the ventral surface of the cell, close to the cell edge. Their main function is to mechanically and biochemically link the actin cytoskeleton and the extracellular environment, allowing bidirectional communication. They transduce a variety of signals from the extracellular matrix (ECM) – including chemical composition, shape and stiffness - that influence many cell processes such as proliferation, differentiation, movement, and determination of cell fate. Moreover FAs share some biological functions with stress fibers - due to their physical continuity - such as firm attachment to the substrate, reorganization of the substrate and detachment of the trailing edge to allow cell movement.

FAs were initially identified as discrete sites of close (10 to 15 nm) contact between the cell and substrate by interference reflected microscopy, an optical microscopy technique used to probe vicinity of cell to the substrate [59]. While newer techniques such as TIRF, FLIC and those based on surface plasmon resonance might have improved the contrast and quantification of these

distances [60, 61], it was since then accepted that the great majority of the cell ventral surface is indeed “suspended”, being separated from the substrate by a distance between 100 and 150 nm, and that focal adhesion represent the only sites of direct contact between cell and substrate.

Structurally, focal adhesions are massive multiprotein complexes composed of nearly 100 proteins - as of 2006 - and associated with other many other interacting proteins [62]. FA components are organized in a multilayered structure, best revealed by high-resolution fluorescence techniques such as iPALM [63]. At the base of this structure are found integrins, which physically link ECM components with the FA. Integrins are heterodimeric transmembrane receptors whose clustering and subunit combination largely determines the response of FAs to physical stimuli. For example, it has been shown that, while integrin α5β1 preferentially mediates adhesion strength, integrin αvβ3 enables mechanotransduction [64]. Associated with integrin are FAK and paxillin, two proteins often associated with integrin signaling upon ECM binding. Above these molecules there is an intermediate layer which contains talin and vinculin, proteins typically associated with force transduction and, for this reason, later discussed in this paragraph. The superior layer of FAs is mainly composed of actin filaments and associated proteins, such as VASP, zyxin and the crosslinker α-actinin. Actin filament organization can be readily visualized by electron microscope techniques - which have been very popular in the last decades of the twentieth century – and their 3-D organization in FAs has been recently dissected through cryo-EM. This analysis revealed the presence of stress fibers occupying ~25% of the FA volume and consisting of hundreds of actin filaments that are parallel to the main axis at the core of the FA and unaligned at its periphery [65]. Overall FA shape can also very accurately revealed through atomic force microscopy, which

reveals FA thickness to be approximately 100 nm, with height and width respectively increasing and decreasing towards the stress fiber-associated end [66].

FAs are found at the end of stress fibers (discussed in the next paragraph), which are tension-generating structures exerting traction forces in the order of nN on the substrate [67, 68]. This places FAs in a perfect position to transmit mechanical forces and transduce physical signals into biochemical signals. Although some believe that focal adhesions should not be considered necessarily mechanosensors and other factors such as strain, curvature, and actin retrograde flow [69] can explain aspects of cell physiology attributed to mechanosensitivity [70], basic biochemical features and physiological considerations seem to attest the importance of focal adhesion mechanosensitivity in cell's physiology.

First, integrins support the formation of catch bonds with their ligand fibronectin. Forces in the physiological range (10 to 30 pN) induce conformational changes in α5β1, bringing integrins to a high affinity state [71] and, hence, contributing to activation of intracellular signaling. Catch bonds are also present in the intercellular counterparts of focal adhesions. Here the minimal complex cadherin-catenin-actin is stabilized under a ~10 pN tension force [72], further supporting the idea that adhesions support regulatory mechanisms dependent on force.

Second, it has been shown that FA proteins undergo force-induced conformational rearrangements that might be responsible for biochemical changes. The most popular example is represented by the large protein talin. *In vitro* experiments based on single molecule photobleaching have shown that the talin rod domain unfolds at ~35 pN force, thus exposing multiple cryptic binding sites for vinculin binding [73]. This property has been confirmed *in vivo*, where the labeling of both ends of the talin protein showed that an exceptionally large 100 to 350 nm stretching (several times the

native protein length) occurs along the direction of actin flow and is largely dependent on myosin activity [74]. Overall these experiments strongly indicate that talin is a molecular mechanotransducer, because vinculin is activated by talin and is a known key player in cell signaling and cytoskeletal organization. Talin stretching is perhaps unsurprising, due to its diagonal positioning between actin and integrin [65], but is not the only molecule displaying stretching due to physiological forces. Careful analysis of cryo-EM data also revealed 25 nm-diameter particles that decrease in their size upon incubation with Rho kinase inhibitors (size decrease is by 60%) and blebbistatin [65]. Likewise, *in vitro* extension of FA protein p130Cas leads to its Src family kinase-dependent phosphorylation, thus potentially triggering the subsequent downstream cellular signaling [75].

Finally, the maturation of focal adhesions is a force dependent process. Seminal experiments showed that high substrate rigidity is necessary to reinforce the connection between integrins and the actin cytoskeleton [76] at the very early stages of adhesion formation, consistent with a sensing mechanism relying on tension. As initial contacts between cell and the substrate – named focal complexes – form at the lamellipodium, they are generally smaller than FA, containing only a fraction of their proteins. Focal complexes then come in contact with actin filaments, which flow centripetally at a rate of few μm/s, due to the monomer binding and unbinding kinetics – this process is known as treadmilling. The engagement between actin and extracellular matrix creates a variable friction between the retrograde actin flow and the substrate [77] – known as molecular clutch – which simultaneously slows down actin flow, leads to a local increase of f-actin protrusion at the cell edge, and allows the onset of isometric tension within the underlying fibers and the creation of traction forces [78]. This tension is then required for maturation of the FA, which

increase in size and in the number of components. Intermolecular FRET-based studies indeed specifically showed there is a direct relationship between the presence of 2.5 pN tension across vinculin and adhesion assembly, while the loss of tension coincides with FAs disassembly [79].

1.2.6 Stress fibers

Stress fibers (SF) are conspicuous bundles of 10 to 30 actin filaments containing large amounts of myosin and held together by the crosslinking protein α-actinin. These two proteins localize as alternating and periodic bands along the length of the fiber, forming peculiar, highly-organized tandem repeats. This organization closely reminds a sarcomere, and indeed stress fibers are contractile units. Yet, the organization – including the polarity of actin filament blocks - and function of stress fibers differ significantly from their muscle cells counterparts. Based on their location and architecture, SF can be classified into three types. Ventral SFs are located at the base of the cell and terminate into two focal adhesions, dorsal SFs have one side anchored to a focal adhesion and one side terminating into a loose matrix of actin, while transverse arcs lie under the dorsal side with a shape recapitulating the convex edge of protruding cells [80]. A fourth type of thick stress fibers can be found covering the nucleus, constituting the so-called actin cap. Here, parallel fibers have one end attached to the nuclear envelope and the other end secured either to the leading or to the trailing edge of the cell [81].

Functional SFs have been initially isolated from fibroblasts and endothelial cells, allowing the study of their mechanical properties as isolated systems. These studies initially showed that isolated SFs are not only capable of contracting, but also of generating simultaneous rotational force [82]. They also showed that, in living smooth muscle cells, SFs are shortened by ~20 %,

compared to their *in vitro* relaxed state. An application of forces could reproduce that shortening, indicating an approximate value of isometric forces of 10 nN for *in vivo* SFs [83] - in agreement with studies performed with pillars and traction force microscopy. Additionally, in the latest few years, contractile SF-like bundles have been reconstituted *in vitro* [84]. This approach will help clarifying long-standing problems of SF physiology, such as the distinct roles of different actomyosin isoforms, the relationship between contraction and polarity of contractile units, and the molecular basis of the attachment to the substrate [85].

SFs have also been extensively studied *in vivo*, mainly through subcellular laser ablation (See section 2.2.3), micropatterned substrates and AFM indentation (See section 1.3.4.2). Taken together, these studies have unequivocally confirmed that FAs exert forces and are under isometric tension, and the latter has been found to be responsible for their mechanical response. They have also shown that SFs behave as mesoscale mechanosensors – although the evidence is not as extensive as for FAs - and identified the protein zyxin as one of the major mechanosensors. In fact, processes like SF maturation and reorganization upon physical stimuli are highly dependent on forces levels, suggesting the presence of intrinsic tensional homeostasis mechanisms [85].

The biological functions of SFs are varied and can be almost exclusively ascribed to their contractility. Upon actomyosin contraction, SFs generate forces that can deform and reorganize the substrate, and/or harbor isometric tension. FAs are also believed to transform isometric forces into chemical signals, due to their mechanotransduction machinery. Contrary to intuitive belief, SFs do not participate in the advancement of the cell on the substrate and their role in motility could be limited to powering cell tail retraction upon dissociation of FAs at the cell rear [86]. Indeed, increased presence of stress fibers is correlated with reinforced cell adhesions to the

substrate. For example, stress fibers reorganize in the presence of shear forces and cyclic stretching of the substrate and tend to align in the direction of the applied force [87] and are typically more numerous in stationary cells. SF have multiple functions in tissues, including regulating vascular tone, inducing the dorsal closure of embryos and the closure of wounds - whereas myofibroblast SFs pull and reorganize the ECM, and epithelial cells SFs contract to induce coalescence and cover the wound. SF-containing cells also line glands, releasing their content upon increase in actomyosin contractility.

1.2.7 Peripheral actin fibers

Structures similar to SFs can be found lining the concave, non-protrusive edges of the cell periphery. These peripheral bundles completely follow the outline of cell edge arcs, lying between two FAs that have their main axis tangential to the cell edge. For these features, these structures have been named “peripheral actin bundles” and “actin edge bundles”, while they are known as “dense peripheral bands” in endothelial cells.

Based on their dynamics and on the localization of SF markers, these structures would be almost indistinguishable from SFs residing in other cell areas [88]. Yet, compared to standard SFs, peripheral bundles show small differences in size, different sensitivity to distinct inhibitory molecules and different timing of contraction, hinting that cells could regulate actin bundles differently based on their location [89]. Also, studies based on femtosecond laser ablation (See section 2.2.3) showed that, compared to standard SFs, peripheral bundles display very different viscoelastic retraction profiles and trigger wider and larger rearrangement of cell shape and

cytoskeleton upon ablation [90], pointing towards an important role in the balancing of forces at the cell edge.

Peripheral actin fibers are indeed crucial regulators of the cell shape at the cell periphery. Specifically, they belong to a mechanical system, whose equilibrium can be simply described by a modified Laplace law. The Laplace law relates the pressure difference across two fluids to the shape and the tension of the interface between them. Under equilibrium conditions, assuming uniform curvature and a very thin interface, the Laplace equation can be expressed as:

$$\Delta p = \frac{\gamma}{R} \qquad \text{Eq. (4)}$$

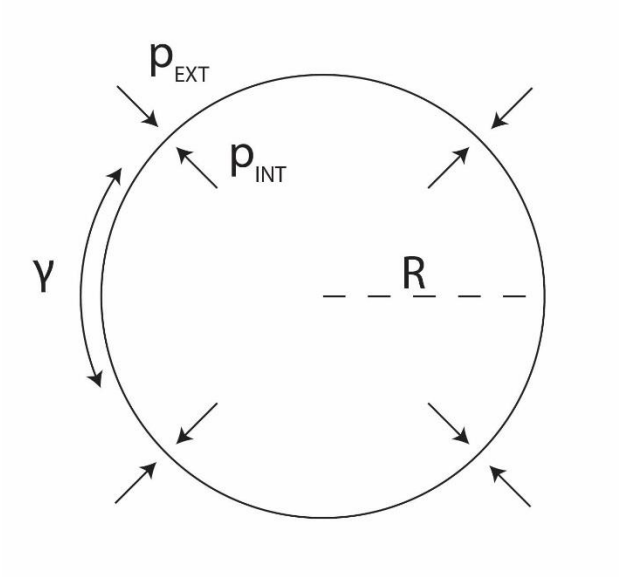

Figure 3: Laplace law for a fluid droplet

The Laplace law relates the pressure difference across two fluids, Δp, to the surface tension across their interface, γ, and the shape of the latter. Depicted is the simplest case of a fluid droplet, representing, for example, the behavior of an inflated balloon. The droplet will develop a radius, R, proportional to the surface tension of the droplet, γ, and inversely proportional to the difference of pressure across the two fluids, $\Delta p = p_{INT} - p_{EXT}$.

, where Δp is the pressure gradient between the two fluids, γ is the surface tension of the interface and R is the radius of the interface (Figure 3).

This law describes, for example, the mechanical behavior of soap bubbles. While the difference of air pressure across the bubble acts to expand the bubble, the surface tension of soapy water tends to make the bubble smaller, and an equilibrium between the two opposing forces is instated at a certain bubble radius, R. In a very similar formulation, this relationship is widely used by biophysicists to estimate cortex tension in living cells (See section 2.2.4) and membrane tension of lipid vesicles.

In 1999, it was hypothesized that the Laplace relationship could as well describe cell shape, provided that the previous variables would be adapted to existing cell parameters. Based on the analysis of the two-stage pattern of latrunculin A-induced cell retraction, Bar-Ziv et al. envisioned a mechanical equilibrium between the membrane tension which pulls the cell edge inwards, and an elastic resistance provided by the actin cytoskeleton between two fixed adhesion points – i.e. focal adhesions. This model could effectively explain the shape of untreated cells, as well as the physical changes following drug treatment, including the pearling instability caused by the collapse of thin cellular tubes [91]. Although the authors hypothesized that passive cortex rigidity

would be responsible for opposing membrane tension, it was previously reported that inwardly-curved cell edges typically harbor peripheral actin bundles and that these are necessary to prevent the collapse of concave edges [92]. These cables might represent better candidates to contribute to the term γ and oppose surface tension, as later supported by independent studies [93].

Hence, based on the aforementioned studies, the Laplace relation can be applied to cell edges with the following formulation:

$$\sigma_m = \frac{T}{R} \qquad \text{Eq. (5)}$$

, where a cell's membrane tension, σ_m, acts in the same direction as the pressure differential described by the Laplace law, and can thus substitute Δp. The surface tension, γ, seen in Eq. (5) becomes the tension along the actin bundles, T, because this opposes the pressure gradients and is located at the interface. Finally, R becomes the radius of curvature of the edge arc under analysis [94]. Therefore, the radius of peripheral actin fibers is at an equilibrium position due to the line tension component, γ, which acts to straighten the bundle, and to the membrane tension which acts uniformly and centripetally along the bundle and would tend to curve the bundle further.

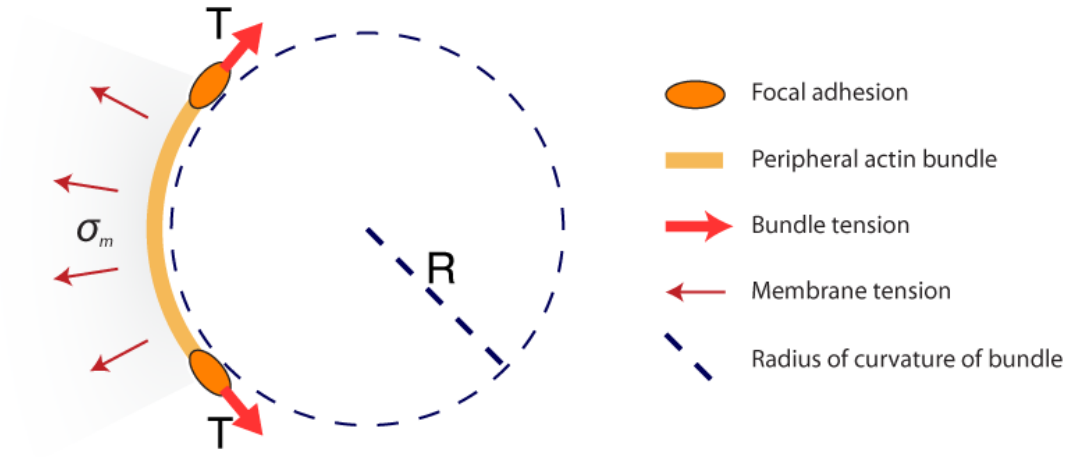

Figure 4: Mechanical equilibrium at the cell edge

A peripheral actin bundle lining a cell edge is anchored via focal adhesions to the substrate, allowing the onset of an isometric tension, T. The cell body exerts a uniform centripetal force resulting in the curving of the bundle towards the cell center. The ensuing equilibrium condition results in the circular shape of the arc, which has radius of curvature governed by Eq. (5).

The presence of this force balance can be easily verified by severing the connection between the bundle and the cytoplasm, which leads to complete straightening of the bundle, or by disruption of the actin cytoskeleton, which leaves membrane tension alone to decrease the radius of curvature of the cell edge [91].

Although a considerable part of the mechanobiology community broadly agrees on the basic principles of this model, there is debate about specific assumptions. One of the most controversial questions is whether both membrane and cortex should contribute to the inwardly-generated force on the peripheral actin bundle. Based on the decrease of radius of curvature in the presence of actomyosin inhibitors and the powerful predictions made by Bar-Ziv et al., we believe the membrane tension largely contributes to this term, and we will discuss this in more detail in

paragraph 6.8. The γ component is also under debate, since some believe it can be due to elastic deformation of the contractile network by the cell edge [94], in agreement with the original formulation of the model [91], rather than resulting from peripheral actin bundle prestress. Others claimed that traction force distribution can be predicted by considering the cell a gel exerting a uniform contractile tension which is balanced by a uniform line tension – with unspecified molecular composition. In this scenario cell shape would be a variable that a cell would use to distribute traction forces, rather than the result of force equilibrium [95].

In summary, the presence of tension along macromolecular structures not only determines a variety of physiological processes, but also strongly contributes to cell shape. This notion was previously envisioned by the tensegrity theory, predicting that cells would derive the shape of their flat regions based on the sole combination of cell tension and compression between adhesive substrate elements [96]. The modified Laplace theory can thus be seen as a quantification tool in broad agreement with the tensegrity principles.

1.3 Methods to probe mechanical properties of cells

Animal cells are compliant, viscoelastic materials characterized by an elastic modulus ranging within five orders of magnitude, but generally lying between 100 Pa and 10 kPa [97]. These values are few to several order of magnitude smaller than those typical of common materials, such as plastics and metals. This makes quantification of mechanical properties an arduous task, due to the instrumentation sensitivity required to characterize the corresponding stresses and strains. However, in the latest decades the advent of technologies such as improved piezoelectric materials,

high-resolution optics, and nanofabrication have made the mechanical characterization of cells easier. In the next paragraphs, I will discuss the most popular methods currently used to quantify the response of cells to deformations.

1.3.1 Whole-cell methods

Whole cell techniques are useful to characterize the collective response of large portions of cellular materials to applied forces. While some of these techniques were more commonly used during the previous decades, they still provide choice methods to help understanding the collective cell behavior during mesenchymal migration, or in response to fluid drag, intratissutal compression and changes in osmotic pressure. We can classify these technique based on the type of mechanical stimulation applied, i.e. stretch, compression, or shear.

Cell stretching can be obtained via microfluidic channels [98], dielectrophoresis [99], optical methods - directly [100] or through beads [101] - or by a flexible substrates on which they are grown [102]. In this case, mechanical parameters can be calculated by either monitoring the force necessary to apply a certain uniaxial or biaxial strain or from the recoil resulting from the termination of the stress. Compression can be achieved between two flat plates [103] or between a plate and a gel [104]. Shear can also be obtained through a variety of tools, including microfluidic devices and the application of fluid drag allows the measuring of the cell's shear modulus. In this case, it is important to distinguish the effects of different Reynold's numbers of the flow. While low Reynold's number relate to the laminar flow typically found in the human body, high Reynold numbers can be related to the conditions typical of altered blood circulation or bifurcations in circulatory system.

Whole-cell methods also include micropipette aspiration, but the latter will be treated separately, due to its importance and wide use in the community.

1.3.2 Passive and active bead microrheology

This family of techniques relies on the incorporation of microbeads of known size, mass and drag within the cellular volume and their subsequent tracking. Alternatively, beads can be attached specifically or aspecifically to the cell surface. Tracking can be performed either based on the passive – i.e. thermally-driven - motion of the bead or upon the application of an external force.

In the first case (Particle tracking microrheology), the mean square displacement of the particle's spontaneous trajectory - which is mainly driven by Brownian motion - can be related to the elastic and viscous local components of the cell [5, 105-107]. Furthermore, the dissociation of the particle from a purely thermal-driven behavior can give information about local cellular constrains and the presence of intracellular forces. These techniques collectively show that the cytoplasm of adherent cells, such as endothelial cells and fibroblasts, has greater viscous component at timescales greater than 10 – 20s, and greater elastic component at timescales between 0.1 and $\sim$10s [108].

Yet, particle tracking microrheology techniques are limited in scope, due to the limited amount of information that can be extracted from the thermal excitation of the beads. To extract additional mechanical information, forces can be applied externally on the beads through optical tweezers, magnetic tweezers and magnetic twisting cytometry (MTC). Laser tweezers, for example, measure forces through the displacement of a transparent bead from a laser's focal point. When bead displacement is measured upon quasi-static force application, a creep-relaxation curves can be obtained [109]. This formulation can provide mechanical parameters to characterize the cell

response to quasi-static physiological forces, such as blood flow in circulation or actomyosin contractility generated during wound repair.

Yet, cells are routinely exposed to deformation at different timescales, and their mechanical response is highly dependent on those timescales. Hence, bead microrheology experiments can also rely on sinusoidal force application at different frequencies [110]. For a purely elastic materials, bead displacement is in phase with force application, while a $\pi/2$ delay between force application and bead displacement can be expected from a purely viscous materials. Cells typical display intermediate – i.e. viscoelastic – behavior, and the ratio between the viscous and elastic components, α, is a widely-used parameter to describe cell mechanics.

Bead microrheology techniques not only confirmed that cell's mechanical response depends on the speed of measurement and on the measurement tool used, but it also depends on the temporal and regional characteristics of the cell region under analysis [111]. On the other hand, the scope of these techniques is limited by the difficulty to control and infer bead positioning and the potential toxic effect of fluorescent microbead injection in living cells. Additionally, while the knowledge of local elasticity and viscosity of confined cytoplasmic regions at different frequency can be potentially associated to different cell behaviors, the direct relation between these findings and specific intracellular processes has so far being limited.

1.3.3 Micropipette aspiration

In micropipette aspiration, a cell is sucked into a glass pipette through constant negative pressure, as the aspirated volume is tracked through video microscopy. Negative pressure, radius of pipette and aspirated volume can then be related to different mechanical quantities (such as cell's elastic

modulus or viscosity), depending on the assumption underlying the cell's mechanical behavior [112].

During a typical experiment, cells are first aspirated with a negative pressure, such that the aspiration length, L_P, becomes equal to pipette radius, R_P. Then, a further increase in the suction pressure can have two different effects, according to the system under study.

Cells with prominent viscous behavior – e.g. granulocyte - gradually and completely flow into the pipette and recover their shape upon release, due to the restoring effect of surface tension. The interpretation of these early experiments gave rise to the "liquid drop" model, which is still currently widely employed [113]. According to this model, a cell is physically equivalent to a drop of water, whereas the cell interior is assumed to behave as a viscous liquid, while the cell exterior – i.e. cortex – is considered a viscous fluid under tension and with negligible bending modulus [114]. This physical description allows the interpolation of cortex tension (See section 2.2.4) and cell's interior viscosity, μ, which has been estimated to be approximately 135 Pa *s for neutrophils [115] - about 10^5 higher than water's.

Other cells are characterized by more prominent solid-like behavior, because their surface extends into the pipette to a new equilibrium position [116]. In this case, the elastic modulus, E, of cellular material can be calculated from the following equation:

$$E = \frac{3R_P\,\Delta p}{2\pi\,L_P} \qquad \text{Eq. (6)}$$

, where, Δp, is the pressure difference between cell and pipette. Early micropipette measurements estimated cells' elastic modulus to be approximately 400 Pa [116].

Micropipette aspiration is best suited for studying the physiology of rounded cells, such as blood cells, cancer cells and cells in metaphase, although it is technically applicable to spread cells as well [52]. Micropipette aspiration is cheap and simple to use and implement, and can be used with a wide range of negative pressure. Yet, its force resolution is limited by the resolution of the optical setup and it involves large cell strains [117], resulting in cell damage, measurements confined to large cell portions and measurements preformed within second timescales. Additionally, micropipette aspiration estimates cell tension, rather than cortex tension itself. Because membrane tension is usually smaller than cortex tension (Compare Table 1 with Table 2), cortex tension is usually approximated with cell tension. Yet, this might not be the case for cells displaying particularly high membrane tension, or for certain physiological situations.

1.3.4 Atomic force microscopy

Indenters produce opposite deformations to aspiration, in that cell surface is depressed into the interior of the cell rather than being extended into a pipette. Early forms of indenters included various forms of microneedles and a calibrated "cell poker" [118]. Yet, these methods suffered from poor sensitivity and low throughput of measurement and were subsequently and almost entirely replaced by Atomic Force Microscopy (AFM).

1.3.4.1 Basics of AFM imaging

The modern AFM is mainly composed of a piezoelectric scanner, an optical detection system, and a force sensor consisting of a sharp tip attached to the free end of a μm-sized cantilever. The scanner is placed under the sample and allows the latter to come into contact with the force sensor in a controlled fashion. The cantilever deflection due to tip-sample interaction can be monitored

via a laser, which is focused on the back side of the cantilever and reflected to a four-quadrant photodetector (Figure 5).

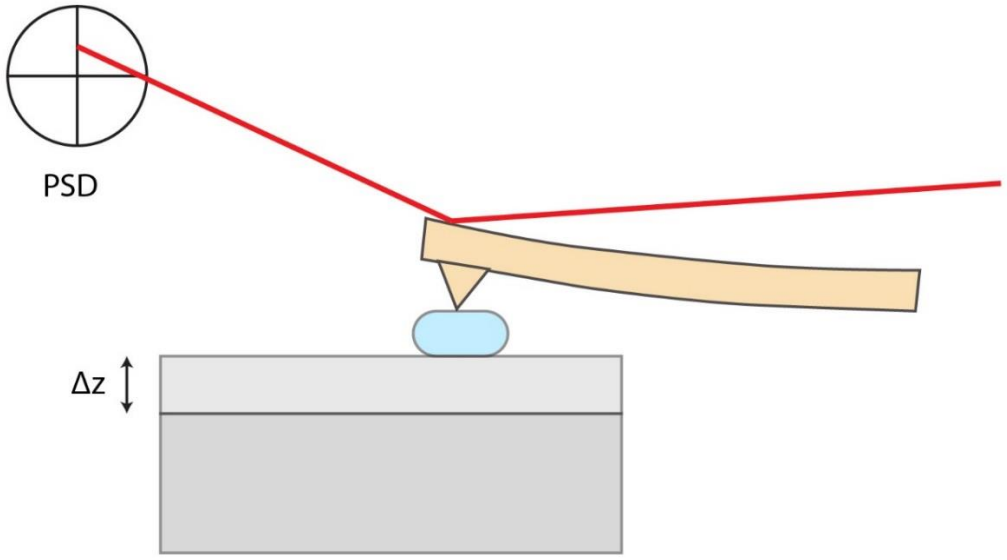

Figure 5: Basic AFM setup

A basic AFM is composed of a piezoelectric scanner (in grey), a cantilever harboring a tip (in yellow) and a Photo-Sensitive Detector (PSD). The scanner expansion, Δz, brings the sample (in light blue) in contact with the cantilever, thus bending the latter. The monitoring of cantilever bending is enabled through the reflection of a laser (in red) from the back side of the cantilever to the PSD.

Depending from the experimental needs, AFM can be operated in different modes. The most basic mode is the Contact mode, whereas the raster-scanned sample is brought in contact with the cantilever quasi-statically, so that a constant cantilever deflection can be used as a feedback signal. Another popular imaging mode is Tapping mode, whereas the cantilever is vibrated close to its resonance frequency and, as the sample is brought closer to the cantilever, the oscillation gets damped until it reaches a feedback value (tapping mode is further discussed in Section 3.1).

AFM was initially designed to image stiff and relatively-flat samples, such as semiconductor materials. It was later adapted to the imaging of organic materials, biological molecules, and, in 1992, to living cells in near-physiological conditions [119]. AFM imaging has superb imaging capabilities in terms of speed and resolution. For example, AFM has been used to "watch" myosin V walk on actin filaments and a rotorless F_1 ATP-ase rotate [120]. Some have even argued that AFM is able to recognize hydrogen bonds [121]. Although AFM has been successfully used to characterize a variety of biological structures and solve numerous biological problems, this work will solely focus on its impact on the imaging of living cells, in particular their mechanical mapping.

Different types of information about the sample can be acquired through AFM, the most basic of which is topography – henceforth called height. As the tip scans across the sample surface, height is approximately equal to the stage expansion necessary to maintain the imaging feedback. Other conventional imaging observables include the feedback error, and, in case of tapping mode, the phase delay and the oscillation amplitude. Right from its start on living cell imaging, these channels have been used to uncover cell structures at a higher resolution than conventional optical microscopy. Notable examples include the display of rapid rearrangement of cytoskeletal components [119], the appearance of large membrane pits and smaller depressions, revealing the presence of vesicle fusion pores during exocytosis [122] and the dramatic rearrangements of the nuclear pore complex in response to aldosterone [123].

However, AFM capabilities extend well beyond the mere topographical mapping of the sample, because tip-sample interaction forces (and hence mechanical properties) are stored in the cantilever motion and can therefore be reconstructed from it. Force reconstruction can be either done from

the cantilever quasi-static deflection or from changes in cantilever oscillations. Specifically, when quasi-statically approaching the sample, the cantilever behaves as a Hooke's spring. Hence, tip-sample interaction forces are simply directly proportional to the cantilever deflection. This characteristic can be used to estimate cell-originated forces, such as those involved in lamellipodial protrusion [43] and those acting isometrically on actin edge fibers [124] and is also exploited by force volume imaging mode - described in the next paragraph – and by its higher speed variations - See section 1.3.5.

1.3.4.2 Basics of force volume mode

Force volume (also known as force mapping) is an imaging mode providing a pixel-by-pixel map of the sample stiffness. Each pixel results from a single indentation cycle, whereas the tip progressively indents the sample until a setpoint is reached, and is then progressively retracted (Figure 6), enabling the monitoring of cantilever deflection over piezoelectric expansion. After some corrections, the previous plot can be transformed into a force vs. distance recording, which can be used for mechanical parameter interpolation [125].

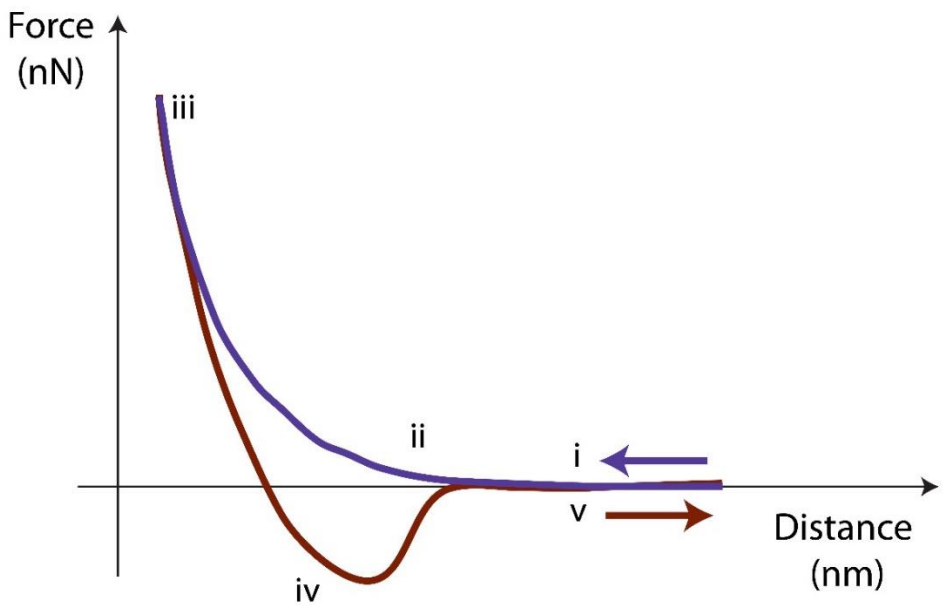

Figure 6: Representation of a force volume indentation cycle

An AFM indentation cycle can be divided into an approach (in purple) and a retract curve (in brown). Initially (i), the cantilever and the sample are separated and no interaction force is detected. As the scanner brings the sample closer to the cantilever, the latter starts bending (ii) until a setpoint is reached and the maximum tip-sample interaction force is detected (iii). As the cantilever is retracted, significant adhesion forces can persist between the tip and cantilever, bending the cantilever downwards (iv). As those adhesion forces are overcome, the cantilever returns to its initial state (v).

Force-volume experiments require calibration of the instrument, including the knowledge of the cantilever deflection sensitivity (in nm/V) and spring constant (in pN/µm). Cantilever deflection sensitivity can be routinely acquired by measuring its deflection on a surface extremely stiff compared to the cantilever, such as a glass slide. Spring constant can be estimated by the amplitude of thermal vibrations at the cantilever's resonance frequency [126]. Cantilevers typically used for cell mechanical imaging have spring constant ranging between 0.01 and 0.1 N/m, with the softest

cantilever compromising on noise and imaging stability for higher sensitivity. Overall, these features allow AFM cantilever to detect deformation in the nm and μm range and forces in the pN and nN range.

As shown by Eq. (2), the elastic modulus (*E*) of a material simply corresponds to the ratio between stress (σ) and strain (ε) and is therefore a measure of its deformability. Elastic modulus of cells, however, cannot be directly calculated through this simple relationship in AFM experiments, because σ and ε cannot be immediately known, partly due to the contact area which constantly changes during an indentation cycle. To solve this problem, different contact mechanics models can be applied to estimate elastic modulus from force vs. indentation cycles, each having different dependencies of measured force from sample indentation and geometrical parameters of the indenter. For example, if the indenter can be approximated as a spherical bead – μm-sized beads are usually employed for estimation of whole cell deformability - the so-called Hertz model is applied. According to the Hertz model, forces grow with indentation according the following relationship:

$$F(\delta) = \frac{4\ E\ R^{0.5}}{3\ (1 -\ \nu^2)}\ \delta^{1.5} \qquad \text{Eq. (7)}$$

, where R is the radius of the spherical indenter, v is the Poisson ratio of the cell, and δ is the indentation of the cell material.

A variation of the Hertz model, the Sneddon model, can be used to model the interaction between the sample and a conical tip – conical tip assumption was used in this work. According to Sneddon's model the force vs. indentation relationship can be expressed as:

$$F(\delta) = \frac{2\,E\,\tan(\alpha)}{\pi\,(1-\,v^2)}\,\delta^2 \qquad \text{Eq. (8)}$$

, where α is the opening angle of the cone.

These models can be modified to account for adhesive forces between the tip and the sample, which often appear and become important as the cantilever is retracted from the cell. Between these, the JRK model is well suited for strong adhesion forces and when the tips radius is bigger than the indentation depth, whereas the DMT model [127] – used in this work – is better suited in case of weaker adhesion forces and tips radius smaller than indentation depth.

In addition to characterizing the elastic response of the cell, force volume can also quantify the viscoelastic hysteresis of the sample, which is represented by the area between the approach and the retract curves [128]. This allows AFM to analyze the viscoelastic behavior of cells at different frequencies, providing an alternative to experiments involving injected microbeads [129].

1.3.4.3 Force volume applications

Mechanical measurements carried in force volume have been very popular during the last two decades, mostly due to their versatility, availability of commercial instruments, and relative ease of measurements [130]. In its most basic implementation, force volume has been used to estimate the elastic modulus of a wide variety of living animal cells, with values generally ranging between 0.1 and 10 kPa [117, 131]. Variation in elastic modulus derive from cell-to-cell variability, probing location, systematic error, and specific differences between different cell types. For example, leucocytes are consistently softer than erythrocytes, while fat and bone cells are respectively among the most compliant and rigid cell types.

Force volume popularity generated many publications investigating the relationship between stiffness and cellular structures. For example, Rotsch et al. analyzed the distinct height and elastic modulus patterns displayed by motile and stable cell edges along their lengths, hypothesizing a link between cell protrusion and a decreased cortical tension [132]. Others combined force volume mapping with topographical and fluorescence imaging of the cytoskeleton to show that stress fibers colocalize with regions of higher stiffness [27]. Relationships between stiffness and specific elements could as well be established by harnessing AFM compatibility with a wide variety of treatments, such as drug administrations. This allowed to relate cytoskeletal changes with the resulting mechanical phenotype. These studies started in 2000, when Radmacher et al. systematically analyzed the effects of several cytoskeletal drugs on cell mechanics [133]. Besides revealing that actin - but not tubulin – depolymerization always causes a global decrease in cell stiffness, this study also revealed distinct, drug-specific patterns of disruption of actin cytoskeleton, providing a tool complementary to optical microscopy for the characterization of effects of the drug on the cytoskeleton assembly. Of particular interest for this dissertation is the measurements of mechanical changes due to incubation with myosin-inhibiting drugs. These studies were initially performed by Radmacher et al., who showed that blebbistatin and Ml-7 treatments induced a net reduction in elastic modulus across the whole surface of fibroblasts [134, 135] and by Grütter et al, who showed an increase in stiffness due to incubation with contractile agonist 5-HT [128].

As mentioned in section 1.2.3.4, force volume-based assays have also been used to characterize mechanical behavior of reconstituted networks, including strain softening [45], and the dependency of actin network growth speed from previous loading history [48].

Likewise, force volume studies have also provided numerous insights into an abundance of cellular processes, for example they have characterized the forces of lamellipodial protrusion [43], cell rounding forces during mitosis [56] and cortical stiffening over the equatorial regions immediately before the appearance of the cell division furrow [136]. One of the most successful examples of relating stiffness changes to physiological processes is represented by the work of Oberleithner et al., who found an antithetic action of sodium and potassium on the endothelial cell: while sodium increase endothelium stiffness and reduces nitric oxide release, potassium does the opposite [137]. This is a particularly fruitful example of how a link between cell mechanics and physiology can benefit the medical community, because of the well-known relationships between nitric oxide and sodium/potassium intake on the development of hypertension and cardiovascular disease.

Finally force-volume has been used to identify features of diseased cells and has been suggested as a diagnostic tool, for example in aging cartilage [138] and in type 2 diabetes, whereas red blood cells not only displayed stiffening compared to healthy counterparts, but also increased adhesion forces towards silicon nitride tips [139]. As a consequence, force volume has been hypothesized as a label-free diagnostic tool in cancer detection. Some have even suggested the use elastic modulus as a single parameter for the detection of metastasis [140] and the identification of varying stages of breast cancer [141]. Others, through the interpretation of force vs. distance curves, hope to identify cancer cells based on their unique brush layer, composed of elements with two different lengths and densities [142].

Force volume limitations

Force volume is a very popular technique due to its versatility, ease of implementation and relative success in different communities. Yet, it has some limitations that have only been started to be addressed in the latest years.

First, force volume is relatively slow (~1 s per force measurement). This is mainly due to excessive viscous drag encountered by the cantilever and the need of avoiding z scanner overshoot – which can cause exceeding of force feedback and sample damage. These factors, combined with the necessity of getting topographic images of the sample at different times, makes this technique inadequate to reasonably follow many biological processes.

Second, force volume mapping of living cells has limited lateral resolution compared to other cell mechanical techniques, other AFM modes, and its own capabilities over stiffer samples [143]. This is because cells are particularly compliant, and large indentations are required to produce the nN-range forces required to perform elastic modulus fitting. The limited resolution is not simply due to the radius of the indenter and the ensuing convolution of cell structures with the AFM tip, but most importantly, by the total surface of contact between the indenter and the cell. For example, when indenting 1µm of cell material with a 1-µm radius sphere, the mechanical information represented by a 10 nm-edge square pixel actually convolves the collective response of a few μm^3 of cellular material, which mostly includes viscous cytoplasm. This issue could in theory be limited by the use microneedle-like tips. Yet, this tip shape would make imaging more challenging and the ensuing increased pressure applied by the indenter would pierce the cell membrane, resulting in massive cell damage. This limitation effectively prevents force volume from reaching the resolution necessary to probe cell mechanics at the molecular level (1-10 nm).

Another limitation of force volume is represented by the possibility of mechanical bleed-through of the cell's substrate. Indeed, to avoid mechanical contribution from the underlying substrate, the contact mechanics models used for elastic modulus fitting are valid only for indentations of no more than ~ 10% of total cell height. Hence, most of the current force-volume measurements are carried on sufficiently tall regions of the cells (few to several μm) such as the nucleus or its close proximities, so that the initial 200/300 nm of the indentation cycle can be fitted for elastic modulus. This not only results in an intrinsic spatial bias of mechanical measurements, and in large errors arising from the uncertainty of the contact point, but also in the inability to measure the mechanics of the cell periphery without using an appropriate correction algorithm [144]. This limitation is particularly detrimental to the development of the cell mechanics field, because most of physiological processes associated with cell movement, mechanotransduction and cytoskeletal reorganization occur close to the cell edge (See sections 1.2.5 and 1.4.1.1), which are usually the thinnest parts of the cell.

Finally, the commonly-used and previously-described indentation models assumes the cell as purely elastic, isotropic and homogeneous. This is clearly not the case, given the breadth of structures they possess and the viscoelastic responses they can display. This assumption limits the possibility of elastic modulus of being a universal and reliable parameter describing cell mechanics.

1.3.5 Emerging AFM cell mechanical techniques

During the last several years, a few groups and companies developed techniques to address the issues presented in the previous paragraph. These efforts can be roughly divided into two types of

approaches: those aiming to increase the imaging throughput and those aiming to acquire higher force harmonics.

To increase throughput, in turn, different strategies were devised. The company Bruker, for example, developed and commercialized a "peak force" system, which uses a fast z-scanner to drive the non-resonant movement of cantilever through a sinusoidal voltage. This, together with a feedback system based on peak force interaction, helped limiting the z-scanner overshoot, thus allowing the acquisition of force vs. distance curves at a 1 to 10 kHz rate [145]. Another approach to increase throughput was the adaptation of high-speed technology to cell mechanical imaging [120]. For this purpose, Shäffer et al. designed 10 μm-long cantilevers and adapted high-speed scanner to create a high-speed force volume capable of mapping the dynamic changes in mechanics of fibroblast within a minute timescale [146]. Cantilever size reduction (to 40 μm) and the use of the peak force technology were combined allowing the rapid mechanical imaging of actin cortex in fibroblasts, revealing two organizational motifs: large parallel bundles and a tight meshwork of filaments [147].

In the aforementioned techniques, forces are simply extracted from the quasi-static deflection of the cantilever and the application of Hooke's law. On the other hand, dynamic modes - such as tapping mode – rely on cantilever vibrations near resonance frequency and the interaction between the sample and the cantilever causes a modulation of this vibration, resulting in an increase of its harmonic content. In principle, tip–surface forces could be reconstructed from the frequency spectrum of the tip motion. Yet, conventional dynamic modes are unable to excite or detect more than a single frequency, hence they lose great part of the mechanical information contained in the

modulated vibration, and their ability to obtain high-resolution mechanical images of soft samples is thus compromised.

During recent years, the advancement in instrument sensitivities, the design of new sensors capable of responding to higher-order flexural vibrations [148], and progress in the formulation of theoretical frameworks capable of harnessing harmonic content [149] allowed the development of so-called multifrequency methods, capable of exciting or detecting multiple frequencies [150]. These methods are amenable to living cells, because harmonics are enhanced in liquid, as opposed to in air. Hence, living cells readily display discernable patterns of harmonic distributions that relate to their stiffness [151]. To exploit this, Raman et al. combined zeroth, first, and second harmonic amplitudes to map mechanical properties like stiffness and dissipation over the surface of fibroblasts and red blood cells. Because this information was extracted in tapping mode, this method allowed significant improvements in speed and the visualization of dynamic changes of mechanical properties [152]. Acquisition time were further reduced by an order of magnitude through subsequent developments [153]. An alternative approach to enhance the harmonic content of the tip-sample interaction was developed by Butte et al. through the development of cantilevers incorporating diffraction-grating-based force sensors [154]. Through the collection of entire force vs. indentation waveforms in liquid, this method allowed the fine mechanical characterization of the spectrin network under the red blood cells membrane and the stiffness tomography of HeLa cells [155].

To conclude, these recently developed methods greatly improved the speed and resolution of living cells mechanical imaging. Yet, while some of them rely on small indentation, but have limited signal/noise ratio, others have good signal-to noise ratio but rely on large indentations. The current

work is also based on development of multifrequency methods. In our case, force reconstruction relies on the detection of torsional harmonic signal, rather than modulated flexural vibrations. As described in section 3.1, this leads to an increase force sensitivity, higher signal-to-noise ratio and a decrease in viscous drag detection.

1.4 Mechanical properties in disease

The past decades have witnessed an increasing interest in how changes in the biomechanical properties of cells influence, and are influenced by, the onset and progression of human pathologies. As a result, it has been claimed that diseases such as asthma, osteoporosis, deafness, atherosclerosis, cancer, osteoarthritis, glaucoma and muscular dystrophy are either caused or catalyzed by changes in cellular mechanics [117, 156].

While cell deformability could be simply an indirect consequence of a pathological process rather than its cause - just like changes in ATP concentration or in expression of housekeeping genes can be expected due to a disease - a single measurement representing the elastic modulus of a whole cell has been hypothesized to be used as a marker of a disease or its progression. This turned out to be the case for the stiffening of red blood cells due to *P. falciparum* infection – the agent causing malaria. In this case, changes in deformability gradually follow the different stages of disease progression [157]. Stiffness measurements were also presented as a promising tool for the early detection of osteoarthritis, due to the structural and mechanical changes associated with age-dependent ECM fiber rearrangement and degradation [138].

Taken together, these experiments show that mechanical phenotypes can be associated with diseases and that cell elastic modulus measurements could be potentially employed as a diagnostic tool. While this might be true and extremely useful in some situations, changes in deformability can result from a wide variety of possible scenarios, both physiological and pathological, resulting in a potential abundance of false positive and false negative diagnosis. For example, stiffening of red blood cells also occurs in type 2 diabetes patients, compared to control subjects [139].

To better understand disease, one has to look at the mechanisms regulating cell physiology and its regulation. While a big part of that lies in the genetic makeup and biochemical reactions, scientists are increasingly appreciating how forces are also part of that regulation (See Chapter 2:). Because forces can determine mechanical properties (See section 2.4), mechanics has a far bigger potential than the simple detection of cell-level elastic modulus. In the following paragraph we will provide an example of the interconnections between mechanics and forces by briefly discussing the mechanobiology of cancer progression.

1.4.1 Mechanical properties of cancer

Cancer is the pathology that has been related to mechanical dysregulation through the higher number of studies. This is partly motivated by the multifaceted complexity of cancer. In fact, not only each cancer type can be considered a distinct and separate disease, but cancer progression involves a multitude of stages, each of which might be regulated differently by a multitude of mechanical factors. Cancer is indeed considered a journey, characterized by constant changes in genome, structure, extracellular environment and stimuli [158]. Although the causal relationship

between mechanical changes and cancer is currently mostly anecdotal, all cancer steps require change in mechanics.

1.4.1.1 Initial stages

Cells partly regulate their physiology by constantly sensing, processing, and adapting to the mechanical information provided by their extracellular environment, including its rigidity and topography [159]. For example, it has been shown that rigidity higher than ~100 kPa determines an elongated and polarized shape in fibroblast cells in a protein kinase-dependent fashion [160] and a change in substrate stiffness can be sufficient to start the differentiation of mesenchymal stem cells into a neurogenic, myogenic and osteogenic lineage [161]. Additionally, cells might preferentially migrate along directions dependent on substrate rigidity [162]. These physical cues, together with the tensional homeostasis within the cell, are particularly important during embryonic development [163], but also retain a huge importance during homeostasis of fully-developed tissues, where together with soluble factors, they contribute to the creation of a so called cell niche.

When equilibrium in the mechanical communication changes, disruption of cell structure and morphology can occur. For example, plating cells on ECMs with different stiffness can be sufficient to induce epithelial transformation in the mammary epithelium, which is characterized by a transition from a keratin- to a vimentin-based cytoskeleton, a hallmark of epithelial-to-mesenchymal transition in the initial stages of breast cancer. These types of events, in turn, can start a positive feedback loop, characterized by further and progressive molecular changes – for

example in integrin expression and contractility - as well as disruption of the mechanical environment [158].

1.4.1.2 Invasion and metastasis

ECM changes can be so significant that they can trigger cell detachment from its origin tissue and invasion. This process often coincides with the appearance of invadopodia, structures characterized by localized actin polymerization, digestion of the ECM, and replacement of the latter with new ECM fibers working as tracks for the following steps of invasion. These steps are generally associated with ECM stiffening, which generally triggers an increase in cell contractility. Yet, even if matrix digestion is suppressed, cells can dramatically deform to squeeze through pre-existing ECM, potentially resulting in nuclear deformation-induced damage [37].

Additionally, the increased proliferation of cells within a confined space causes compression forces within tissues, which, together with the outward proliferation forces exerted by the cell, might cause tissue basal membranes to thin out or collapse, thus favoring the following stages of cancerogenesis. Increased compression also leads to formation of a niche, where tumour-specific growth factors can be concentrated and drug delivery hindered.

Cells that escape the primary tissues are then subjected to shear forces, collisions, and immunological stress within the vasculature, which are known to influence cell mechanics and physiology. Finally, cells might reach the secondary tissue either through capillary occlusion or via adhesive forces towards the endothelium. In either case, cancer cells must then cross the endothelial layer, which involves extending processes to penetrate the adherens junction-filled

intercellular space and large deformations to squeeze their content through narrow spaces [158, 164].

1.4.1.3 Mechanics vs. cancer

Cancer stiffness determination is nowadays already a powerful tool to diagnose tumour progression and cancer, being routinely used during palpation, ultrasound imaging, and intracranial pressure measurements. “Microscale palpation” could further enhance the capability of mechanics of predicting and diagnosing cancer stages. In fact, different techniques such as optical stretchers [165] and AFM indentation [140, 141] have already consistently found that breast cancer cells and metastatic cells are softer than their healthy counterparts and that different stages of cancer can be related to distinct mechanical signatures. Therefore single-cell mechanical measurements have been suggested as simple and powerful diagnostic tools.

Mechanical characterization can indeed undeniably provide an additional tool for tissue classification and can be particularly useful in determinate cancer types, such as breast cancer. Yet, one has to be careful to solely rely on cell-level stiffness for diagnostic purposes, given the great variety of stages of cancer development and the plethora of different invasion strategies [166]. This notion is especially relevant in light of the extreme variability and ability to change cancer cells are capable of. Indeed, some cancer cells types have been found to be stiffer than their healthy counterparts [167].

Yet, while elastic modulus can be occasionally used as a diagnostic marker, and explain some aspect of intravasation and extravasation, it is possible that, alone, might not be sufficient to tackle the complexity of cancer development. On the other hand, mechanics is intrinsically related to

forces to the point that virtually no change in mechanical properties can occur without a change of forces and vice versa [158, 166]. Therefore while cell deformability alone might not recapitulate the complex mechanics of cancer, mechanical characterization can further help cancer diagnosis and understanding, when related to the forces that cause the mechanical phenotype.

1.5 Conclusions

Advancements in instrumentation sensitivity have recently allowed the application of refined mechanical method to living cells, which are orders of magnitude compliant than common polymers and common materials. Both instruments and models used to interpret these experiments generally derive from the material sciences toolbox, thus providing useful information that thoroughly characterize the bulk properties of inanimate materials such as elastic modulus, viscosity, and bending modulus.

On the other hand, a cell is a mosaic of different mechanical structures. Mechanical variations across its volume can derive from a wide variety of factors such as shape, architecture, material properties, density and crosslinking of building blocks, and the affinity between them. This picture is further complicated by a striking temporal heterogeneity, because cells are dynamic, living structures and therefore their mechanical properties change according to their physiological needs and in response to stimuli. Differently from conventional materials, cells can spend energy, undergo rapid molecular turnover without changing architecture, or abruptly change the latter. They can reinforce their cytoskeleton through polymerization, crosslinking and adhesion

maturation to generate and transmit forces, or they can increase their viscous behavior and remodel to crawl and move through tissues.

Hence, a multitude of techniques measuring mechanical response at different spatial resolution and at different timescales were developed to tackle this complexity. For example, some techniques such as micropipette aspiration can address the collective cell mechanical response within seconds and others, such as particle tracking, can measure the local rheological behavior of parts of the cytoplasm at shorter timescales.

These approaches are useful to understand the physiological responses of cells to stresses, such as shear flow of blood and compression from neighboring tissues and characterize their deformability. Knowing the cell response to shear is important to better understand impact of blood flow in physiological and pathological conditions, or the impact of extracellular fluid movement in ECM. Knowing the cell's response to compression is also extremely valuable. It helps us better understand late stages of cancer progression, where cell squeeze through different layers of cells to metastasize - or the three-dimensional migration of cells powered by intracellular pressure. It is also essential to characterize the physiological extravasation of cells, which can occur as a result of inflammatory process, immune response and wound healing.

However the difference between cells and inanimate object is not limited to spatial and temporal heterogeneity. Cells also actively push, yank, change shape, sense forces, move, and slide. These forces can in turn affect the mechanical signature of the cell, as will be clear in the following chapters. Because these forces are largely responsible for a cell's behavior, a mechanical understanding that goes beyond the concept of bulk properties and incorporates contributions from forces is necessary to make progress in the cell mechanics field.

The next chapter will discuss the role of forces in cell physiology, the techniques used to measure them and evidence showing how forces can determine a cell's mechanical response under certain circumstances.

Chapter 2: Intracellular forces

2.1 Introduction

A great deal of biological regulation occurs through chemical interactions, which have been characterized for over a century, allowing us to understand most of the cell physiological regulation we currently know. Yet, cells are also capable of spending ATP to exert forces, which are generated throughout the cell volume. These forces are generally in the pN and nN range, therefore their detection has been inaccessible for a long time, due to a lack in techniques able to measure them. With the development of new technology, the detection of this forces has become possible and, since then, the importance of physical forces in cell's behavior has been increasingly recognized.

There are different ways forces can be generated within the cell. A significant percentage of cellular forces is generated by molecular motors allowing direct transport of materials along cytoskeletal structures or isometric contraction. Another common mechanism of force generation is the polymerization of cytoskeletal filaments, allowing, for example, the expansion of the leading edge [43]. Osmotic pressure can also be harnessed by cells to generate forces, which is believed to be mainly caused either from actomyosin contractility [56] or by local water influx [168]. Cellular forces can also have molecular origin, and be used to melt dsDNA, degrade proteins, and rearrange chromosomes.

When forces are applied to molecules and structures pinned at their ends, they cause isometric tension within those structures. The physiological roles of tension in cell membrane, and cytoskeletal filaments, including the cell cortex have been previously described.

In addition, forces can be sensed and transmitted from the extracellular environment and neighboring cells – such as those cause by blood flow and pressure, muscle contraction, lung inflation – and share mechanotransduction responses with those typical of ECM rigidity sensing [169]. External forces can be either directly transmitted to the cytoplasm cell without biochemical conversion and travel as far as the nucleus [2] or first transduced into biochemical signals controlling cell fate and physiology. The latter mechanism has been studied in more detail [1] and is highly dependent on mechanosensors – such as stretch-activated channels and the previously-described mechanosensitive elements of FAs and SFs - and on the ability of cells to generate their own forces.

The importance of forces is so high that most of the major diseases affecting human beings have defects in components of the mechanotransduction machinery [170]. For example, heart failure can be due to pressure overload, atherosclerosis to reduced ability to signal disturbed flow patterns [163] and cancer to force deregulation (See section 1.4.1).

Yet, due to the wide heterogeneity of force origins and values, no technique is able to currently measure all types of cellular forces simultaneously, but many techniques are able to dissect subsets of these forces with great accuracy and precision at a given scale and with a given sensitivity. For example, traction force microscopy can quantify the nN-level cell traction forces transmitted at the substrate, FRET sensors can measure the pN isometric tension within a single molecule, optical tweezers can characterize the pN forces required to unfold proteins *in vitro*, and micropipette

aspiration can measure cell surface tension in the order of hundreds of pN/μm. Here follows a discussion about the technique currently used for intracellular force measurements, including their cellular targets, force range and limitations.

2.2 Methods to measure intracellular forces

2.2.1 FRET sensors

Förster resonance energy transfer (FRET) is a non-radiative energy transfer that can occur between donor emission and acceptor absorbance upon spectral overlap. FRET can only take place when the two fluorophores are within molecular distances (usually less than 10 nm), and its efficiency decays as a sixth-power of the distance between the two fluorophores. This feature makes FRET extremely sensitive to intermolecular distance, thus favoring its use a molecular ruler in many biological studies [171].

FRET can also be used to measure pN-range forces exerted across a single molecule by incorporating the two fluorophores separated by a small linker peptide into such molecule. As higher forces are applied on the molecule, the linker peptide will gradually stretch, thus reducing the FRET efficiency and an optical tweezers setup can then be used to precise characterize this relationship, thus calibrating the force sensor.

Thanks to this technical development, FRET has been recently harnessed to measure forces across single molecules with sub-pN sensitivity. For example, it has been initially used to show that the average tension across the FA component vinculin is 2.5 pN, and to characterize the spatiotemporal

distribution of forces in maturing and disassembling FAs [79]. FRET sensors have also been used to understand force transmission in the intercellular counterparts of integrins, i.e. cadherins. It has been shown that E-cadherins can be under constitutive pN-tensile forces transmitted by catenin molecules, regardless of localization to cell-cell contacts [172]. FRET sensors also offer the possibility of being combined with other techniques, such as subcellular laser ablation (See section 2.2.3). The combination of these tools has allowed to map the change in tension distribution across focal adhesions upon single stress fiber ablation [173].

Other sophisticated tools based on fluorescence microscopy have been used to map traction forces. For example, molecular beacons have been used to map tension transmitted at extracellular sites [174, 175] and double fluorophore labeling has allowed to prove and study the stretching of focal adhesion components *in vivo* [74]. Yet, in these cases, tension detection is mostly qualitative. In comparison, FRET offers the possibility to simultaneously map tension across the whole cell with relative ease and incredible precision. However, its fine sensitivity to intermolecular distance can be regarded as a double-edged sword, because it limits the range of measurable forces [176]. Additionally, FRET sensors are unable to determine force directionality and rely on the assumption that sensors behave as Hookean springs [177]. For this reasons, FRET sensors' accuracy has been questioned by some groups.

2.2.2 Traction force microscopy and micropillars

Less than 3 decades ago, a seminal work showed that cells form prominent wrinkles on a thin and flexible membrane they were plated on [178]. That was the first time traction forces exerted by a

single cells were directly visualized. This work paved the way for the development of a multitude of substrates harboring multiple mechanical sensors.

In traction force microscopy (TFM), cells are plated on gel substrates containing a large amount of fluorescent microbeads. Traction forces cause a change in bead position, creating a so called "displacement field". Forces can then be reconstructed through large-scale matrix computation, upon knowledge of the substrate elasticity. TFM has shown that, in motile cells, the small nascent FAs found at the leading edges exert larger forces than the large, mature adhesions away from the cell front [179]. It has also revealed a seemingly-different situation in stationary cells, where a linear relationship between FA size and traction stress exists, with a slope of $5.5 nN/\mu m^2$ [68], leading to the idea that the strongest traction forces are generated only by relatively stationary cells to tightly anchor them to the substrate [180].

Yet, TFM is computationally-intensive, sensitive to noise and does not lead to unique solution for force calculations [181], mainly due to the transmission of forces within the continuous substrate. To address these issues, cantilevers embedded in the substrate were initially devised as alternative methods. This method was used to characterize the oscillatory characteristic of traction forces and their transition between the rearward and forward directions [182]. Although this method can in principle provide very accurate measurements, drawback include its limited throughput and impractical design. To overcome these issues, arrays of PDMS micropillars were developed through conventional photolithographic tools [183]. Pillar tops can be coated with ECM proteins to increase their physiological relevance. Cell spread, attach to, and deflect these posts arranged in a hexagonal lattice and the pillar top deflection can be monitored through optical microscopy and converted to local traction forces measurements via the following relationship:

$$F = \frac{3}{4}\pi E \frac{r^4}{L^3}\,\Delta x \qquad \text{Eq. (9)}$$

, where E, r, L and Δx are, respectively, the Young's modulus, the radius, the height, and the deflection of the post. The spring constant of the pillars can be tuned by controlling the radius and the height of the pillar or through UV crosslinking, thus allowing fine control of the substrate rigidity. Compared with TFM substrates, pillars are independent force sensors, because each deflection occurs independently of the neighboring posts. Micropillars not only allowed measurements of local traction forces - for example those between large discontinuous gaps in ECM [184] - but also significantly contributed to a better understanding of cell–matrix interactions, as well as the coupling between forces and the contributing molecular components. For example, it was shown that the direction of the traction force guides fibronectin fibril remodeling and orientation [185] and that focal adhesion maturation is sensitive to tension, but largely insensitive to the tension levels, after a certain threshold [69].

The relatively ease of sensor parameters tuning allows the study the effect of substrate rigidity on cell forces, movement, and mechanotransduction. Yet, the change in diameter of micropillars also causes significant effects. It was recently shown that submicrometer pillars display unique patterns of localization in adhesion proteins and myosin, resulting in rigidity-sensing events that are completely missed using larger pillars. These events are characterized by a maximum of 60 nm local contractions between adjacent pillars during early spreading events [186]. Higher resolution tracking on the same substrates later allowed the observation of 2.5 nm steps between opposing pillars, possibly leading to the first-time *in vivo* observation of single steps in sarcomere-like contractions units. This helped understanding that the number of steps taken before reaching a 20 pN force level is an initial, crucial step in rigidity sensing [187].

To conclude, TFM and micropillars are widely used tools and have provided a wide variety of useful insights into mechanosensing, spreading and differentiation [188]. Yet, their use has a few drawbacks that limits their application. First, they can only address the ventral traction forces of the cells and force characterization is mostly limited to the nN range. Second, it is not clear what percentage of force measured at adhesion sites is actually being transmitted to the underlying cytoskeleton and how that stress is redistributed between distinct elements such as stress fibers, membrane tension and cortex tension. Also, their application seems limited to mesenchymal-type movement, as blebbing cells display little to no force on deformable substrates [189]. Finally, their shape constrains sets limits on their applicability and implementation.

2.2.3 Subcellular laser ablation

Lasers have been extensively used in biology to excite and bleach fluorophores and subsequently perform optical microscopy experiments. Less commonly, lasers have also been employed to ablate entire cellular regions to study the cell behavior in the absence of a certain structure – for example to study blebbing in the absence of cortex - and the cell's response to physical damage [190]. Yet, the extension of the damage caused to the cell has been limiting this application. The laser disruption of SFs would be important to characterize force distribution within cells, because they are under tension and other techniques cannot unambiguously characterize their mechanical properties - for example, FRET sensors can only characterize pN tensions across single molecules, and micropatterned substrates don't allow the unambiguous calculation of traction forces across single stress fibers. To address this, femtosecond laser have been tuned to confine vaporization of cellular material to a diffraction-limited spot [191], therefore confining the cellular ablation to a

single stress fibers. This tool, known as laser nanoscissor or subcellular laser ablation (SLA) has been initially used to pioneer the study the viscoelastic retraction of stress fibers upon tension dissipation and its rigidity-dependent effects on traction forces and cell shape [90, 192]. It has also lead to confirm the hypothesis that zyxin has a force-sensing role of in FAs [193, 194]. This tool shows promises to tackle cortex mechanics as well [195] and can readily be combined with other sensors such as TFM to study the change in traction force distribution upon fiber ablation [192]. Yet, the quantification of forces upon SLA is problematic and the disruptive nature of the technique prevents the uninvasive monitoring of physiological processes.

2.2.4 Micropipette aspiration

Micropipette aspiration - previously described for the characterization of cell elastic modulus and viscosity - has also been used to measure cell cortex tension. A cell can be aspirated into the pipette until the aspirated length, L_P, is equal to the pipette radius, R_P. At this point the Laplace equation - Eq. (4) - can be modified to include the negative pressure exerted by the pipette:

$$P_P = 2\,\gamma\,\left(\frac{1}{R_P} - \frac{1}{R_C}\right) \qquad \text{Eq. (10)}$$

, where P_P is the negative pressure exerted by the pipette, R_C is the cell's radius and γ is the cell's surface tension – mainly indicative of cortex tension. This equation can be solved for γ, which gave values of 35 pN/nm for the cortex tension of granulocytes in early studies [113]. Although cortex tension values acquired through aspiration vary more than two orders of magnitude, most values lie between 40 and 400 pN/µm for animal cells [50]. Tension measurements by micropipette aspiration have shown that cortex tension is tightly regulated during cell division, shape control, and migration [50]. In the latter case, it has been shown that bleb formation and size depends on

the levels of cortex tension [190], and an increase in cortex tension can be sufficient to trigger a transition from lamellipodium to bleb-driven protrusion [58].

2.2.5 Microbead tracking

Micrometer beads - previously described for the characterization of the rheological behaviors of cells - can be also used to measure intracellular forces. In most of these cases, they are coated with extracellular matrix protein. This allows them to bind to actin cytoskeleton via integrins, therefore connecting to force-transmitting intracellular structures. Both optical and magnetic tweezers can be used to move them and/or detect their displacement. For example, optical tweezers have been used to quantify the strength of the minimal bond between fibronectin and cytoskeleton [196] and to discover the strengthening of cytoskeletal linkages and pulling forces upon substrate binding [76], while magnetic tweezers have been used to clarify the role of different integrin receptors in adhesion and mechanotransduction, while quantifying bond strength [64].

2.2.6 Tether pulling

Tether pulling experiments are a particular type of particle tracking experiments aiming at measuring cell membrane tension and its impact on cell physiology. Most of these studies use laser-trapped beads which are coated with cell surface ligands and bind to the plasma membrane. The trapped bead is pulled from the cell at a constant velocity by a motorized stage, allowing the bound membrane to be pulled into a long, thin tether that remains associated to the cell, but is free from cytoskeletal attachment. The required force, f, to hold the tether at constant length can be monitored by the defection of the bead in the trap, perpendicular to the optical axis. Tether pulling can also be performed through AFM, and in that case force is simply measured via cantilever

bending. When the membrane is pulled, the cells responds with a force coming from three distinct components: the in-plane membrane tension, σ_m, the membrane bending modulus, B, and the adhesion between the membrane and the cytoskeleton, γ. However, the σ_m and γ terms are difficult to separate and therefore are combined into a single term: the apparent membrane tension, σ_{mAPP}. Apparent membrane tension can be calculated from f and B through the following equation:

$$\sigma_{mAPP} = \sigma_m + \gamma = \frac{f^2}{8\pi B} \qquad \text{Eq. (11)}$$

, where σ_m only reflects the properties of the lipid bilayer - independently of how it interacts with the cytoskeleton - and *B* is the term that resists the generation of membrane curvature, and depends on the composition of the membrane. For physiological membrane bending, this force component is generally extremely small, so that thermal energy is sufficient to lightly bend the membrane. Yet, it can become significant during vesicle formation and for the drastic curvatures typical of tether experiments [197].

Dai and Sheetz were the first to adapt laser tweezers to the measurement of forces from neuronal growth cones-pulled tethers [198] and the relationship between tether forces and σ_m, σ_{mAPP} and B was later soon determined [199].

The contribution from the cytoskeleton attachment to the measured force can vary greatly, according to the cell type and the cell region under analysis. For example *C. elegans* sperm cells and mitotic HeLa cells appear to have little cytoskeleton contribution, while renal epithelial and melanoma cells' measured forces are largely a result of the cytoskeleton attachment term [197]. To separate the two contributions, tethers can be pulled from membrane regions devoid of cytoskeleton. Blebs represent a perfect example of this condition, because of the lack of cortex

under their nucleation site, thus making the γ component equal to zero. Measurements performed on normal membrane and bleb tethers in renal epithelia cells and melanoma cells show that in-plane bilayer tension accounts for less than a quarter of the apparent membrane tension [200].

Membrane tension estimation using tether extraction is based on the assumption of a definite membrane bending stiffness, which can be calculated from the tether forces knowing the tether radius, R:

$$B = \frac{f\,R}{2\pi} \qquad \text{Eq. (12)}$$

B has been estimated to be 2.7×10^{-19} N*m in chick neural growth cones [199], and $1.4\ 10^{-19}$ N*m in rapidly moving keratocytes [201], displaying values very similar to those found in *in vitro* giant lipid vesicles [202].

Yet, the correct estimation of this parameter relies on the estimation of tether diameter through differential contrast or quantitative fluorescent densitometry, which might be inadequate due to limits in optical resolution. Furthermore, the absence of cytoskeletal attachment from neighboring regions is still debatable even in blebs, due to the lengths of tethers and the presence of attachment in the neighboring regions. For these reasons, despite tether pulling has been an excellent tool pioneering and clarifying the role of membrane tension in cell's physiology, additional techniques able to unequivocally separate membrane tension from other distinct cell's force components might benefit the scientific community.

2.3 Mechanical models

The mechanical behavior of cells is extremely rich, and the cell mechanical response can readily change due to a great variety of factors, including cell type differences, spatial and temporal heterogeneity and internal reorganization. In addition to that, the techniques used to probe it differ by the frequency of stimulation, the amount of strain applied, probe geometry, and the spatial scales of probing (e.g. bulk vs μ-scale). Due to these challenges, it is hard to come up with a universal model of cell mechanical behavior, and the mechanical model so far postulated can only explain a small portion of the whole spectrum of the possible mechanical behaviors. In particular, most of existing mechanical models were initially designed to fit and interpret a particular set of data, often acquired through a specific set of techniques. Hence, while many models can provide very good fitting for the data and behaviors interpreted, a universal framework describing the full range of possible cell mechanical behaviors is far from being devised.

Mechanical models can be categorized based on different ideas. One way is to distinguish between top-down approaches - which are based on the initial analysis of the collective behaviors – and bottom-up approaches – whereas the molecular composition and microstructure are first considered. Another approach is to distinguish between “continuous” models - whereas the cell is approximated as a single-phase homogeneous material – and “structural” models – whereas some sort of component heterogeneity is considered. In the next paragraphs, the most popular cell mechanical models will be presented, along with the type of experiments intended to interpret, and their limitations.

2.3.1 Viscoelastic models

Viscoelastic models are continuous models whereas the response of cell to deformation can be represented by a finite number of springs (representing the elastic components) and dashpots (representing the viscous components) in series or in parallel. This model was initially devised to interpret the nonlinear creep displacement of leucocytes within microaspiration pipettes [203], but has been further developed in the following decades.

A significant approximation is provided by the solid elastic model, which assumes that an equilibrium is achieved after force loading, thus ignoring the time-dependent component of the viscoelastic model [114]. The solid model can be applied to describe the response of cells to a variety of techniques. In micropipette aspiration, for example, it can be used to estimate the elastic modulus of a cell [116]. The elastic approximation is also widely used by the AFM community, since all the most commonly-used contact mechanics model are based on the assumption of a homogeneous, elastic half-space (See section 1.3.4.2).

On the other end of the spectrum, it is possible to approximate the cell as a liquid (cortical shell-liquid core model). Like the solid model, the simplest formulation of liquid model – the liquid drop model – was developed to explain cell behavior during micropipette aspiration. This framework allows estimating the cell cortical tension and viscosity by measuring the pressure required to reach an equilibrium position within the pipette, and the velocity of cell's flow into the pipette, respectively [113] (See section 2.2.4). Due to partial disagreements between theory and experimental measurements, liquid models became more sophisticated. An example is represented by the compound liquid drop model, predicting the presence of three separate cellular layers.

Interestingly, tension would be present within two layers: the outer layer, which includes cell cortex, and the core, which includes a tensioned nuclear envelope surrounding a dense nuclear material [204].

Viscoelastic models are continuous model, therefore representing a gross approximation of the highly-varied content of the cell. Although they can predict cell deformation under many circumstances, their lack of structural information confines their validity to the collective behavior of multiple cell structures.

2.3.2 Power law and soft glass material models

Power law models are geared towards the phenomenological interpretation of experiments involving cell stimulation over a range of frequencies, such as those involving active bead microrheology and AFM. Under vibratory conditions, the ratio of stress to strain is termed complex modulus, G*. By knowing the phase delay of the strain upon force application, it is possible to separate the complex modulus into its elastic, G'(ω) and viscous, G''(ω), components:

$$G^*(\omega) = G'(\omega) + iG''(\omega) \qquad \text{Eq. (13)}$$

Experiments consistently showed that dynamic modulus follows a weak power law dependency for a wide range of frequencies:

$$G' \propto \omega^{\alpha} \qquad \text{Eq. (14)}$$

and that the ratio between G'' and G' is surprisingly constant (around 0.3) over a wide range of frequencies [110] – i.e. the behavior is mostly elastic. Different models have been devised to interpret and fit this type of data. The most popular of these postulates that cells behave like a "soft

glassy material" – a type of material that like foams, pastes, and colloid suspensions is close to a glass transition. In soft glass materials, the structural elements are disordered and metastable, due to structural relaxation occurring prior to reaching a minimum energy level. In other words, the transition to a stable configuration – i.e. glass - would require energies higher than thermal contributions [205]. Soft glass materials are mostly elastic, but when enough energy is provided in the form of oscillatory stimulation, they undergo transition into glass, thus partly dissipating the energy and recapitulating the phenomenological behavior [110].

An interesting observation from the analysis of cell power-law behavior is that the ratio between G'' and G' is only constant for some orders of magnitude of frequencies. For frequencies over ~10 Hz the ratio ceases to be constant and G'' starts to grow faster with frequency. As a result, the curve representing G'' and G' are expected to display a crossover at frequencies around 100 Hz, suggesting that the cell mechanical behavior at high frequencies should be dominated by viscosity. This notion has been tested by multiple works of Fredberg et al. using magnetic twisting cytometry [110, 206, 207] or AFM [208] and has been confirmed by other groups via AFM [209]

Although the soft glass model offers a description that recapitulates the frequency-dependent behavior of cells, it might not be the only description of the cell able to do that [210]. Additionally, models interpreting power law behavior are limited to the description of collective and phenomenological behaviors - similarly to common viscoelastic models.

2.3.3 Sol-gel model

The ability of reconstituted cytoskeletal networks to reproduce cell mechanical behaviors (See section 1.2.3.4) has sparked the postulation of different cell mechanics models. The most popular

is probably the sol-gel model, which is inspired by the transitions between fluid-like (solution) and solid-like (gel) behavior of cytoskeletal actin networks upon the addition of crosslinkers, increase in f-actin concentration and f-actin length [211]. This model postulates that cells undergo solution-to-gel (hence sol-gel) transitions like their reconstituted counterparts by increasing their mechanical linking. This transitions would allow cells to switch from a state able to crawl, protrude, spread and invade [212] to a regime able to resist elastic deformation and generate forces.

The sol-gel model is substantially different from the soft-glass material model, because while the first predicts cytoskeleton components to dwell at energy minima, the latter envisions metastable components trapped in energy wells [110]. Despite the sol-gel model elegantly predicts rapid and physiological transition, it postulates the cell to be structurally similar to a reconstituted network, hence it is subjected to the limitations described for reconstituted networks.

2.3.4 Poroelastic model

The poroelastic model is based on the idea that a cell can be approximated as a biphasic material consisting of a solid elastic porous meshwork – including cytoskeleton, organelles and large molecular complexes – and an interstitial fluid – mainly composed of water and soluble molecules. Hence, the cell can be considered as a fluid-filled sponge, whereas the fluid readily moves within the porous network. According to this view, if the pores are small enough, a pressure gradient caused by a sudden increase of pressure might not equilibrate instantaneously, resulting in cytoplasmic flows occurring in the timescale of seconds. In this scenario, the movement of water across cell regions in response to pressure gradients becomes a limiting factor in cell deformation and might thus dictate the rate at which cell shape changes [168]. A notable example of how cells

could harness this gradient is represented by blebs, whereas pressure gradients could be used to locally expand the cytoplasm [213] - although other studies predict instead a uniform intracellular pressure coupled to contractile forces [190].

By subministering a local hyperosmotic solution and simultaneously tracking organelles and injected quantum dots, a hydration gradient has been experimentally observed [214]. The poroelastic theory was recently further supported by the implementation of quantitative predictions. According to the poroelastic theory, the timescale of water movement within the porous network – i.e. poroelastic relaxation time - has an upper bound represented by:

$$t_P = \frac{\sqrt{R\delta}}{D_P} \qquad \text{Eq. (15)}$$

, where R is the radius of the indenter, δ is the cell indentation, and D_P is the diffusion coefficient of the cytosol - which is proportional to the square of the average pore radius. If an indentation is applied with a timescale $t_r << t_P$, the creation of intracellular pressure gradients becomes possible. The analysis of AFM indentation experiments performed in the poroelastic regime confirmed the validity of this argument [215].

This theory allows the presentation of daring and intriguing hypothesis whereas cells could locally activate ion antiporters to create a local osmotic change – K^+ and Cl^- export would allow volume decrease, while Na^+ import would allow volume increase. These osmotic gradients would then be able to generate forces to power changes in cell shape, for example powering protrusion at the lamellipodium and cell contraction during cytokinesis [168].

Differently from viscoelastic and power-law models, the poroelastic framework provides an interpretation for the dilatational changes of cytoplasm and non-equilibration of pressure gradients

across the cell body. It also interprets cell viscoelasticity based on the biphasic nature of the cell. Yet, it neglects the role of prestress and other active force components of the cell, which are known to regulate physiology.

2.3.5 Tensegrity model

To address the limitations of current mechanical models, other aspects of cell physiology need to be taken into account. As previously discussed in this chapter, cells are not just biochemical entities, but exert contractile forces, which are generated and transmitted throughout their volume. These forces are not only important regulators of physiological processes, but also important determinators of cell shape.

In engineering, structure determination and stabilization through tension is possible using a building principle called tensegrity. Tensegrity structures consist of a continuous network of tensed structural members which are stabilized by incorporation of support elements resisting compression. Notable examples of these structures are camp tents, spider webs, a boat's rigging, and Snelson's sculptures. The latter show a network of tensed, suspended steel cables holding isolated steel bars in position. This type of architecture derives its stability from its tensional integrity (hence the name tensegrity) [96, 216]. This is in contrast with conventional structures, such as houses, which are stabilized by the compression of its components under gravity – and are dependent upon the elastic properties of the object such as elastic modulus, spring constant and bending modulus.

In 1981, Ingber et al. speculated that loss of equilibrium between mechanical elements can lead to loss of shape control and malignant phenotype, hypothesizing that cells behave as tensegrity

structures. It was later clarified that cells are indeed multimodular tensegrity structure, whereas for each module tensional forces are mainly borne by actin filaments and intermediate filaments, whereas compressional struts are carried by microtubules and ECM adhesions. This is consistent with the linear shape of actin and the curved shape of microtubules and the localization of actin and tubulin in living cells – respectively deep within the cell, and spanning the cell volume. Experiments based on TFM in the presence of microtubule-depolymerizing drugs have shown that microtubule carry 5-30% of the compression, while the remainder is ascribed to the compression of the extracellular matrix between adhesions. Adhesions would thus act like external support element withstanding the cytoskeletal tension forces generated during attachment and cell movement. Just like other cell mechanical models, tensegrity can explain a variety of cellular behaviors, including strain stiffening and the shape of adherent cells upon dissociation from the substrate.

While initially just an intuitive formulation, tensegrity has been subsequently developed into a mathematical model. Although relatively simple [217] - based on 24 tensed cable and 6 compressed struts – the first tensegrity mathematical model enabled *a priori* predictions of cell mechanical behaviors, which have been proven over the course of over three decades. This is a valuable differentiation aspect compared with other cell mechanical models, which are merely limited to the description of the particular behaviors object of the experiments. One of the predictions stemming from the tensegrity model is that applied stresses would not distribute uniformly within the cell or throughout the cortex, but would be preferentially channeled through discrete cytoskeletal elements, due to the non-uniform prestress – and hence rigidity - of cytoskeletal elements. Initial experiments agreed with this notion, showing that magnetic beads

bound to integrin molecules – which transmit physiologically-relevant forces between ECM and internal cytoskeleton – display strain stiffening, whereas beads bound to other receptors do not. Furthermore, strain stiffening was dependent on other cytoskeletal filaments systems [218]. These observation were later confirmed by the observation that stresses applied through integrin-bound beads – but not other receptor-bound beads - caused rearrangement of mitochondria tens of μm away from the bead [219]. Because mitochondria are intimately associated with microtubules, this experiments further proves the interconnectivity of the cytoskeleton and the discrete nature of its load-bearing elements, spanning from the cell surface to the center of the nucleus. According to the tensegrity theory, these load-bearing cytoskeletal structures would work as communication "highways" of the cell, capable of transmitting stress at a speed of ~30 m/s, so that signals would travel from the membrane to the nucleus within a few μs. This capability could be in principle harnessed by cells to trigger mechanotransduction at a very higher speed compared with mechanisms based on chemical diffusion and motor-driven transport. Communication would also have a much higher efficiency compared to a uniform viscoelastic model - which would predict stress to decay with the square of the distance within - and travel at a larger distance, potentially reaching the nucleus and regulating gene expression [2].

A second important prediction formulated by the tensegrity model is a linear correlation between the levels of prestress within the cytoplasm and the stiffness of the cell [217]. This relationship has been confirmed through a variety of techniques and its verification will be discussed separately in section 2.4, due to its importance.

Another notable aspect of differentiation of tensegrity compared to other cell mechanical theories is that it can be extended to a strikingly wide range of lengths scales to explain structural stability

of biological materials. For example, single proteins can be viewed as tensegrity structures. Indeed, while intermolecular bonds tend to crumple amino acids together, secondary structures such as α–helices and β-sheets counteract that by forcing different shapes, thus creating an equilibrium between tension and compression within the amino acid chain. On the other side of the spectrum, body parts as well can be described by tensegrity, because the compression of the bones counteracts the tension developed by entire groups of muscles [96].

Tensegrity is the most popular model integrating the role of forces in the mechanical behavior of cells. Yet, despite its predictive values, it has been criticized in favor of other mechanical views of the cell whereas a more uniform cortex tension plays a major role in the cell's mechanical response and can explain behaviors such as the prestress vs. stiffness relationship [220]. It has also been argued that the interconnectivity displayed by the actin cytoskeleton upon force stimulation of integrin molecules can be simply ascribed to the high-frequency response of a viscoelastic material. Also, it has been argued that extreme strain stiffening strain can be simply due to the activity of crosslinkers such as α-actinin [5] – although these observations derive from *in vitro* measurements of reconstituted networks. Finally, others believe that tension-induced compression loads are mainly carried by the cell's hydrostatic pressure and possibly by the compression of other cell's elastic components [112], rather than ECM compression and microtubules.

2.4 Intracellular forces control the mechanical properties of cells

As discussed in the previous paragraph, the tensegrity model predicts that the deformability of cells would depend linearly on its levels of prestress. Specifically, it has been hypothesized that, the higher the prestress, the smaller the geometrical rearrangements of its components – including rotation and extension – under an applied strain. This prediction has indeed been indeed verified in living cells using a variety of different techniques to measure mechanical properties of cell, and to control or measure strain, traction forces or local prestress.

Most commonly, cell stiffness has been mapped throughout the cell surface via AFM in the presence of drugs modulating non-muscle myosin II activity. Independent AFM experiments have shown that fibroblast cell stiffness decreases ~3 fold upon treatment with blebbistatin [134] and with ML-7 [135]. While M7 inhibits myosin indirectly by blocking the active site of myosin light chain kinase – which might be responsible for activating other enzymatic cascades, blebbistatin is a very specific myosin inhibitor, ruling out other potential factors that might cause a decrease in stiffness. Conversely, blebbistatin inactivation via photoinactivation results in a ~1.6 fold increase in cortex tension [221], while increase in contractility due to 5-HT drug treatment results in a dramatic increase of elastic modulus in airway smooth muscle cells [128].

Living cell stiffness has also been mapped through oscillatory MTC (allowing quantification of shear modulus, which is closely related to elastic modulus for isotropic materials) and has been shown to linearly depend on the traction forces developed on TFM substrates [219]. However, it has been argued that local prestress cannot be exactly determined through the knowledge of local

traction forces. To tackle this problem a slightly different computational approach has been recently developed to measure shear modulus and local cell strain. This work confirmed the trend that, on average, cell shear modulus (and therefore stiffness) increases with prestress [222].

The prediction has also been verified at a single SF level via AFM. AFM-based indentation has shown that SF stiffness depends on the SF's contractile levels, since blebbistatin and calyculin treatments respectively decreased and increased their stiffness. Furthermore, the stiffness at the SF center was found to be lower than at their periphery [223], in agreement with mechanical properties of a rod object determined by tension - Eq. (29) - or by a combination of tension plus elastic response of the underlying cytoplasm (See section 5.1.1).

The prediction has also been extended to the tissue level, as shown by studies performed on fibroblast-populated matrices. Here, actin-depolymerizing drugs have been shown to cause a decrease in contractility, which in turn tightly correlates with a decrease the stiffness averaged over the cell population [224].

The linear relations between tension and stiffness has also been reproduced *in vitro*, once the right conditions were established – involving actin filament shortening to physiological lengths and their crosslinking via filamins. The onset of tension caused a very significant increase in stiffness, compared with values of previously-assembled actin networks - which are generally in the Pa range - and became very close to those measured in living cells [49, 225]. This observation also indicates that tension is indeed an essential contributor for cell mechanics.

2.5 Conclusions

Taken together, the previous chapters showed how mechanical properties and intracellular forces are intimately related. This concept has been consistently shown when discussing mechanotransduction, mechanical models, and various techniques, which can probe bulk mechanical properties or forces, according to the system under study, and the underlying assumptions.

Given these extensive interconnections, it is surprising how the precise relationship between intracellular forces and stiffness has never been rigorously tackled – with the exception of specialized systems [19] - and a theoretical framework relating the two is missing. The tensegrity theory, indeed, does predict a linear relationship between prestress and stiffness, but cannot relate the tension borne by specific elements to the local mechanical response of the cell. Additionally, it ascribes the predicted increase in stiffness to entropic contributions and neglects the role of cortical tension and membrane tension.

Yet, for any physical body under isometric stress, tension contributes to its mechanical response proportionally to indentation with a reaction force, T_V, equal to

$$T_V = 2\,T\,\sin(\alpha) \qquad \text{Eq. (16)}$$

, where T is the tension applied to the physical body and α is the indentation angle. As previously described in Chapter 1, the outermost layer of cells almost exclusively contains structures which are under tension in physiological conditions, i.e. cell membrane and the actin cytoskeleton.

As technical developments will allow to increase force sensitivity of mechanical measurements, we would expect to be able to confine mechanical probing to the surface layer of the cell, and therefore isolate its mechanical response from the viscoelastic cytoplasm.

The following chapter will present a high-resolution AFM platform with pN sensitivity capable of confining mechanical measurement to the outermost layer of living cells. We will show that this platform is indeed sensitive to tension borne by intracellular elements.

Chapter 3: A novel, high-resolution platform to probe cell mechanics

3.1 Torsional harmonic cantilevers (THCs)

Tapping mode is a widely-used AFM imaging mode able to provide high-resolution images of a variety of biological materials. In tapping mode, a cantilever is vibrated close to its resonance frequency, causing the oscillating tip to intermittently contact the sample. This interaction modulates the vibrations and reduces its amplitude, which is kept under constant feedback during imaging [226].

Compared with imaging schemes based on static cantilever deflection, tapping mode offers several advantage, including the minimization of sample wear due to smaller forces applied, the reduction of lateral forces, and the presence of new observables - such as phase and amplitude. Most importantly, the use of tapping mode would theoretically allow the reconstructions of tip-sample interaction from the harmonic content of modulated vibrations.

These advantages would be particularly beneficial for cell imaging, because they would limit damage to the cell's delicate structures, allow the isolation of the mechanics of molecular components from the cytoplasm, and greatly improve the mechanical imaging of thin regions of cells, currently limited by the mechanical contributions of the underlying substrate.

As discussed in section 1.3.5, a few multifrequency approaches have been recently successfully used to reconstruct mechanical parameters or tip-sample interaction forces from the modulated cantilever vibrations, allowing tapping mode to be employed for mechanical characterizations of living cells. However, the mechanical images provided by these methods still suffer from limited resolution, and the inability to resolve the mechanical response of defined intracellular components. This is mostly caused by the small amplitude of flexural force harmonics.

An alternative approach to force reconstruction in tapping mode is offered by the design of sensors that allow excitation of torsional modes upon tip-sample interaction. To achieve this, a torsional harmonic cantilever (THC) harbors its tip at an offset from its long axis. Similarly to symmetrical cantilevers, THC are excited close to their flexural resonance frequency. Yet, tip-sample interaction not only results in modulated flexural vibrations, but also in a torque acting on the cantilever, thus causing the excitation of the torsional modes [227]. Forces can then be reconstructed from the analysis of the flexural harmonics of the torsional vibrations.

The use of torsional vibrations presents some significant advantages in terms of mechanical characterization of the sample. First, torsional vibrations generate force harmonics with much larger signal/noise ratio compared to flexural vibrations, allowing striking improvements in force sensitivity. Also, torsional resonance frequency is typically > 10 higher than flexural resonance frequency. This allows mechanical measurements at a higher bandwidth, which in turn allows to resolve tip-sample forces with a substantially higher temporal resolution (sub-microsecond) [228].

THCs have been previously used on samples with stiffness ranging from ~1 MPa to ~10 GPa, where they were able to collect nanometer-scale elastic modulus maps [229] and have been

employed to mechanically detect the hybridization of complementary DNA and miRNA on immobilized target DNA with unprecedented sensitivity [230].

THC were later adapted to mechanical imaging in liquid environment through reduction of their spring constant. This allowed them to characterize protein flexibility under physiologically-relevant deformations at a microsecond timescale [231] and to precisely and three-dimensionally locate binding sites inside a protein complex [232].

3.1.1 Optimization of THCs for cell mechanical imaging

THC could be potentially used to image animal cells. Yet, cells are compliant materials and while previous THC measurements addressed elastic modulus measurements within the MPa and GPa range, the vast majority of cells exhibit elastic modulus between 0.1 and 10 kPa [131]. Therefore, changes in cantilever design were required to adapt high-resolution mechanical imaging to cells.

On one hand, force sensitivity is very important for cell mechanical imaging, because it allows to confine the measurement to molecular components without extending the indentation to the underlying cytoplasm. This concept is particularly relevant to cells, because AFM-measured forces scale with the elastic modulus of sample. On the other hand, high bandwidth is not a strict requirement for mechanical imaging of very soft samples, because tip-sample contact occupies a large percentage of the period of oscillation [228]. Hence, high force harmonics have a lower impact in the reconstruction of force vs. distance curves, compared with stiff samples [233]. Therefore, cell imaging THCs were designed shorter and thinner (Figure 7a) to trade bandwidth for increased force sensitivity.

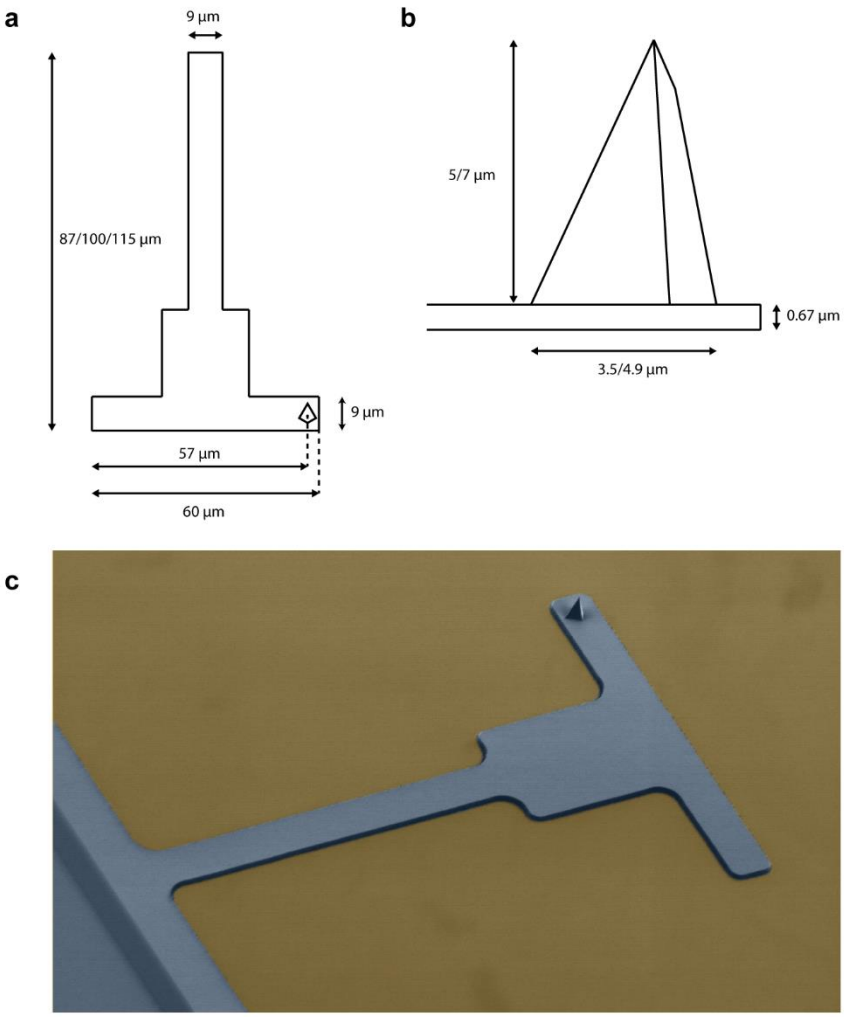

Figure 7: Cell imaging THC

(**a**) In-scale representation of the cantilever used for cell mechanical imaging, seen from above. The tip is located on the right side of the cantilever, with a 27 µm offset from the long axis. (**b**) In-scale representation of the tip of the cantilever, seen from the side. (**c**) False-colored SEM image of the cell imaging THC.

The use of THC presents another important advantage compared with symmetrical cantilevers, namely the reduction of detected viscous drag. Indeed, when a resonator is placed close to a surface, the displacement of the fluid between the resonator and the surface introduces additional mass and

viscous damping. This effect is called ”squeeze film damping” [234] and can have a particularly-negative impact in liquid, as it can be misinterpreted as cell-originated force. The use of THC minimizes this problem, because the tip is placed at an offset, so the viscous drag acts on both the arms of the cantilevers and can thus be decoupled from measurements.

Cell imaging cantilevers were manufactured by conventional manufacturing protocols (Bruker-Nano) with a pyramidal tip, approximately 10 nm in diameter at its end – as measured by SEM and using an imaging calibration standard. Although a sharp tip is necessary to reach the highest resolution, it makes imaging less practical. We indeed observed that cantilevers harboring sharp tips are occasionally vertically pulled by the feedback system 2 to 5 µm upwards during imaging. This tends to occur especially at the topographically-highest regions of the cell (endoplasm). We suspect this might be caused by membrane rupturing under the tip pressure, which in turn results in the formation of membrane tethers – as reproducibly documented by others [235]. Hence, we devised strategies to increase the tip radius. As a first attempt, we scanned tips at high-speed under high static force feedback (~ 50 nN) over a stiff surface (glass). This procedure produced duller tips – as demonstrated by surface profiling over an imaging standard – but turned out to be time consuming and not reproducible. We then resorted to deposition of a thin (few nm) layer of Cr and Au, respectively via thermal and e-beam evaporation. This procedure, while causing material to be added to the whole length of the cantilever – not only to the tip - turned out to excessively change the resonating behavior and the spring constant of the cantilever. We therefore reasoned that the deposited material should mechanically behave as similarly as possible to the material constituting the cantilever (silicon). We therefore resorted to plasma-enhanced chemical vapor deposition of silicon nitride. Although silicon nitride was deposited on both sides of the cantilever

in addition to the tip, this procedure made the tip duller without altering the functionality of the cantilever. Indeed, the silicon nitride layer did increase cantilever thickness and spring constant, but these changes were taken into account by cantilever calibration and did not disrupt the mechanical functionality of the cantilever.

3.1.2 Cantilever calibration

Flexural and torsional deflection sensitivities of the cantilevers were found through an unpublished calibration method considering flexural and torsional motions to be described by springs in series. The accuracy of this method was tested by comparing its results with two other procedures. One of them was based the Sader's method [236] and its torsional counterpart [237]. The other procedure was based on titin domains, which are known to unfold upon the application of ~ 225 pN forces [4].

Flexural (~ 200 pN/nm) and torsional (~ 1 N/m) spring constants were determined from the amplitude of thermal vibrations, as conventionally performed within the AFM community. Spring constants were in line with the values expected through estimation based on physical dimensions.

3.2 Experimental setup and methods

3.2.1 AFM hardware and software

AFM experiments were performed on two commercial AFM systems: Bioscope II (Bruker) and Bioscope Catalyst (Bruker), both of which equipped with a Nanoscope V controller (Bruker). We acquired topography images through the built-in AFM software Nanoscope. Force-sample waveforms and mechanical parameters were calculated from torsional vibrations via custom software, as previously described [227]. Briefly, raw flexural and torsional signals were sent to a computer equipped with LabVIEW (National Instruments) via a data acquisition card (NI-S6115), where a custom module performed inversion of the transfer function of the torsional signal and optimized force reconstruction by eliminating the cross talk deriving from the bleedthrough of flexural vibrations.

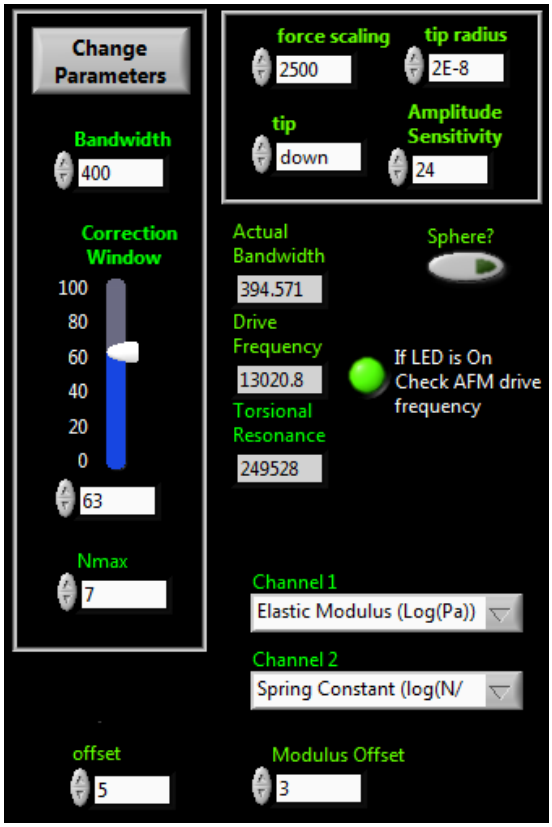

Figure 8 Fine tuning of tip-sample forces reconstruction

Screenshot showing the graphical interface of the LabVIEW module used for force vs. distance curve reconstruction. Fine tuning of force waveform could be achieved through the modification of the displayed parameters.

A Labview module allowed the real-time fine-tuning of force reconstruction through the modification of certain parameters (Figure 8). For example, it allowed averaging vibration waveforms over a variable number of consecutive oscillation cycles to reduce noise and to adapt the frequency of mechanical measurement output to the number of acquired pixels. While increasing averaging reduces noise levels, it also results in loss of mechanical information. The LabVIEW interface also allowed to define the width of the force curve, to fit flexural bleedthrough correction, based on the remainder of the cycle. We observed cellular forces for ~60% of the

oscillation period, while most of previous THC measurements performed on more rigid samples displayed forces within less than 20% of the period. This difference can be explained by the compliance of cells, leading to a widening in the force waveforms [228]. The module also allowed to define the number of harmonics used for force reconstruction, and was usually set to 7. This number is smaller than those typically used for previous THC measurements, due to the compliance of cells and the liquid imaging conditions.

The module allowed the real-time extraction of a multitude of mechanical parameters from the force waveform, including adhesion, dissipation, peak force, elastic modulus and spring constant - the present work is mainly based on the analysis of the last two. The elastic modulus was calculated by fitting force vs. distance curves with a DMT model, assuming a conical or hemispherical indenter, while the spring constant was calculated by fitting the initial 70% of the force vs. distance curve slope.

3.2.2 Cell culturing and treatments

In this work we imaged different cell lines, although most of the findings were based on the analysis of fibroblast cells. M2 cells [238] (generously provided by T. P. Stossel), CHO cells (generously provided by L. Chasin), HUVEC cells (acquired from Lonza, Ltd), mouse hippocampal cells (generously provided by R. Yuste) and RPTPα+/+ mouse fibroblast cells [239] (generously provided by M. P. Sheetz) were grown according to the provider's instructions or standard culturing procedures.

Mouse fibroblasts were grown in basal DMEM medium (Life Technologies) supplemented with 10% FBS (Atlanta Biologicals and Life Technologies) and 5% Penicillin-Streptomycin (Life

Technologies) at 37°C in a 5% CO_2 incubator and harvested with 0.05% Trypsin-EDTA (Life Technologies). These cells were plated on extracellular matrix-coated Petri dishes (Corning) or on glass-bottom dishes, custom-coated with human fibronectin.

Baculovirus (Life technologies) transduction was generally used to induce the expression of fluorescently tagged proteins (Actin-RFP, Actin-GFP, Talin-GFP, and Tubulin-GFP), and cells were imaged 1 to 2 days after transduction.

Growth medium was generally replaced with fresh L-15 medium (Life Technologies) before the experiments. For myosin inhibition experiments, blebbistatin (EMD Millipore) was pipetted and mixed to a final 100 µM concentration into the culture dish mounted on the stage. For washout, the drug-containing solution was aspirated, and replaced with fresh solution.

3.2.3 Optical microscopy

An inverted epifluorescence microscope (AxioObserver.A1, Zeiss) equipped with a 20X air or a 100X oil-immersion objective was used to acquire bright field, phase, and fluorescence images. Images were captured with a standard CCD camera device (Hamamatsu). The camera dark noise was subtracted for fluorescence quantification. Alignment between optical and AFM images was performed via the alignment of fiducial markers, such as stable cell edges and actin fibers. Data analysis of optical data was performed with built-in functions of the software ImageJ.

3.2.4 Imaging set up

For experiments, cultured cells were mounted on the stage of the AFM. The AFM head, containing the cantilever, was subsequently positioned over sample and stage (Figure 9a). Laser was first

aligned over the cantilever and then its reflection was centered on the four-quadrant photo-sensitive detector. The cantilever was driven very close to its resonance frequency (we chose the frequency that produced an amplitude at 70-80% of the resonance peak, on the left side of that peak). Depending on the length and the thickness of the cantilevers, the resonance frequency of the cantilever in liquid ranged between 5.5 and 14 kHz (generally around 12 kHz), while the flexural spring constant ranged between 0.08 and 0.3 N/m and the torsional spring constant ranged between 0.85 and 1.5 N/m. Driving the cantilever at high amplitudes helped increasing signal-to-noise ratio of mechanical measurements, therefore the oscillation amplitude was typically kept at approximately 50 nm.

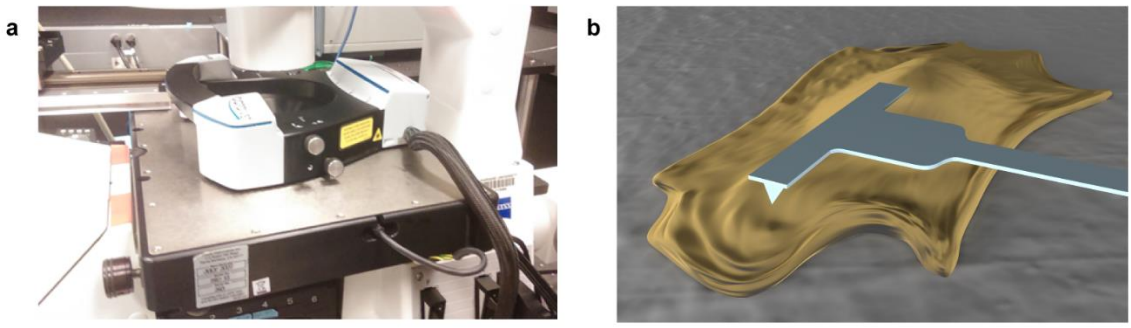

Figure 9: Mechanical imaging setup

(**a**) During experiments, the AFM head was placed on top of the AFM stage. The latter is sitting on an inverted fluorescence microscope. (**b**) Schematic representation of the experiment, showing the THC (in blue) on top of a living cells (in yellow).

3.2.5 Data processing

Stiffness values presented in this work are color-coded in logarithmic scale and displayed either as raw data or after limited processing. Processing generally consisted of median filtering and

removal of known artifacts typical of AFM imaging using the software Scanning Probe Image Processor (Image Metrology A/S). 3-D overlays were generated using the same software. To improve the clarity of the overlays, topography images were flattened, and outlier values were removed.

Radius of curvature of actin bundles was determined by fitting a circle through the coordinates of the bundle, which were identified by the ImageJ plugin JFilament [240]. Stiffness profiles along actin bundles were acquired using a 2-by-2 pixels sliding window averaging signal to reduce noise. Pixels with negative spring constants were not included. k_B values were obtained by averaging the spring constant values along such stiffness profiles. Stiffness profiles along the cortex near actin bundles were obtained by first averaging stiffness values along straight lines parallel to the actin bundle (or along concentric arcs) and then plotting them vs. their distance from the bundle. Coupling distances were obtained using the trust-region-reflective algorithm of Matlab (The Mathworks, Inc.).

3.3 Force vs. distance curves

Figure 10 shows nanomechanical force vs. distance curves acquired from a living fibroblast cell, where the maximal forces range between 30 and 55 pN - with a 10 pN RMS in noise - and the maximal cell indentations are approximately 30 nm.

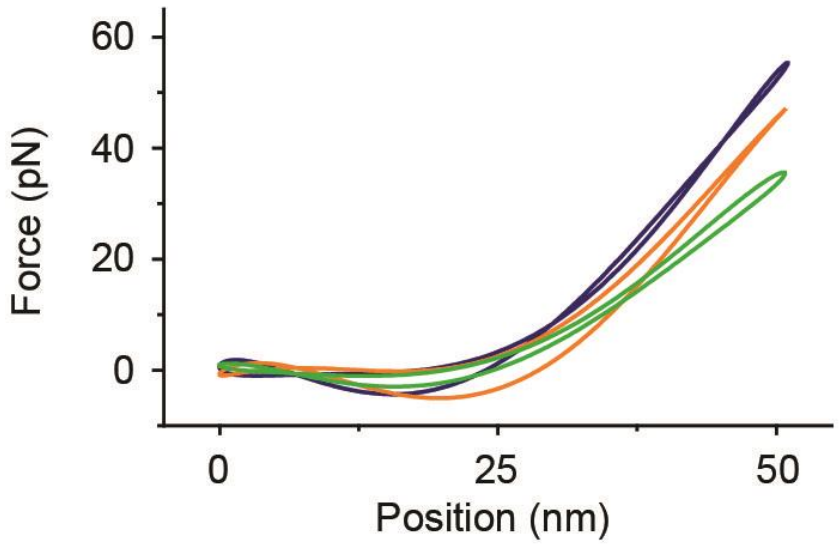

Figure 10: Nanomechanical force vs. distance curves acquired over living cells

Tip-sample forces are shown as a function of cell indentation. Different curves represent measurements acquired on different regions of the same cell. The two traces for each curve represent the approach and the retract portions of the curve.

These technical features represent a simultaneous improvement in force sensitivity and a drastic reduction in the volume of cell under mechanical probing, which has been difficult to obtain for conventional force volume and for the recent developments presented in section 1.3.5. Finally, forces display a surprising linearity as a function of indentation and a lack of hysteresis. These features will be further discussed in section 6.7.

Analogously to typical AFM mechanical measurements on living cells, we often observe a small increase in attractive forces as the tip comes into direct contact with the cell surface (known as jump-to-contact), due to Van der Waals forces.

Because of the negative resting membrane potential of fibroblasts (around -45 mV) [241] and the surface charge density on the AFM tip created by silicon nitride deposition [242], we expect some

electrostatic force to be present in force vs. sample interactions. However, we also expect this contribution to be negligible, due to the lengthscales of electrostatic screening (~ 1 nm). Furthermore, we do not observe large adhesion forces upon contact between tip and sample - this situation could change in excitable cells, i.e. neurons.

3.4 Nanomechanical images of living cells

Height and elastic modulus maps were simultaneously acquired from living cell as the AFM tip was raster-scanned at ~12 kHz over defined cellular regions. Figure 11 shows three-dimensional overlays of these two components, whereas the three-dimensional topography is colored according to the local elastic modulus. We were able to image melanoma, endothelial, fibroblast, ovary, and neural cells, representing a wide variety of cell types, include human.

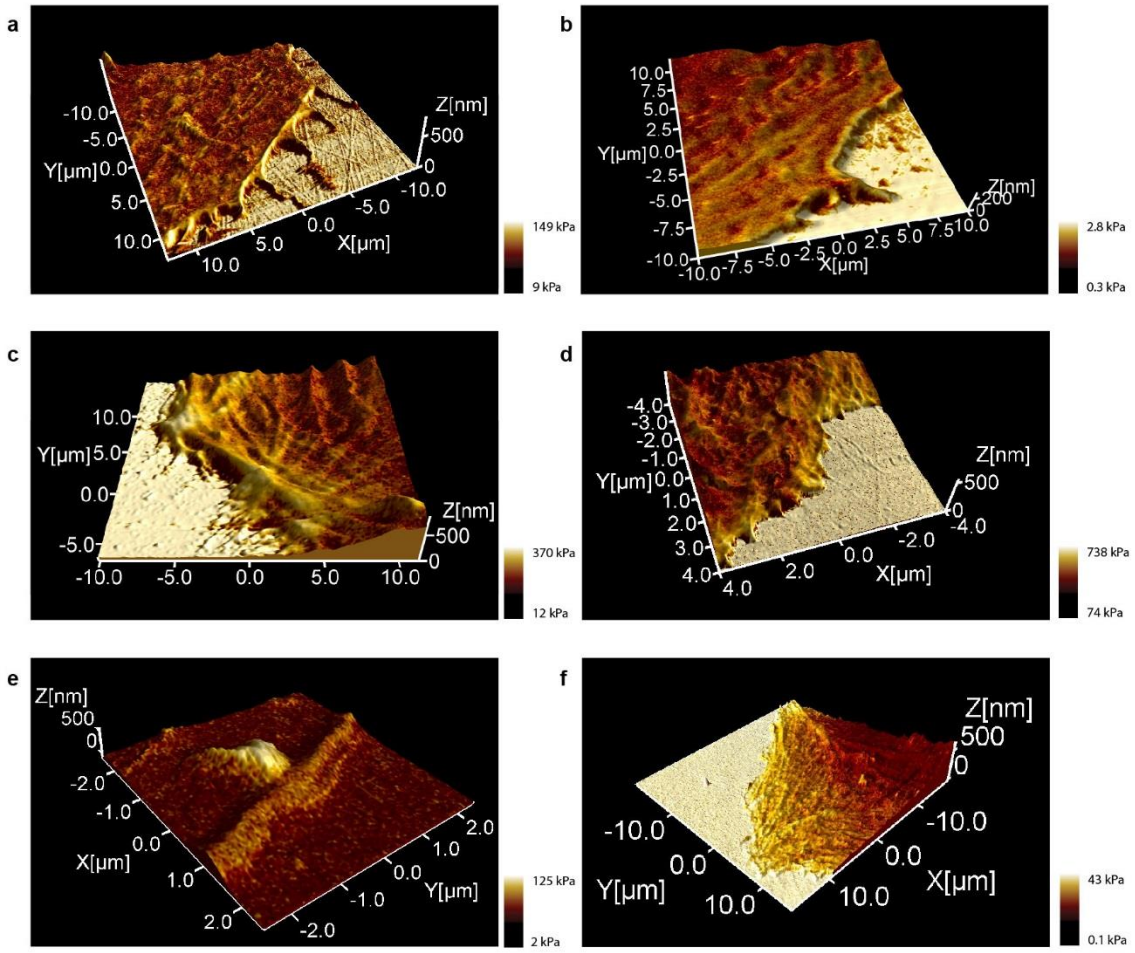

Figure 11: Mechanical imaging of a wide variety of living cells

3D overlays of topography and elastic modulus overlay were acquired from (**a**) Filamin-deficient human melanoma cells, (**b**) Human Umbilical Vein Endothelial cells, (**c**) Mouse fibroblasts, (**d**) Chinese hamster ovary cells, (**e**) Mouse neurons, and (**f**) Human transformed fibroblasts.

In this work we concentrated our mechanical analysis on the peripheral areas of the cell. Despite the substrate is various orders of magnitude stiffer than the cell, it can occasionally appear softer than the cell in our mechanical maps. This is caused by the choice our imaging parameters, carefully set to avoid application of large forces while probing cells. A differentiating aspect of our platform is indeed its ability to get mechanical maps of the cell periphery without mechanical

contributions from the substrate. This represents a much needed improvement for the field, considering that the majority of the processes known to be regulated by forces and mechanics - such as cell sensing, mechanotransduction and movement - occur close to the cell edge.

It is important to notice that the nanomechanical maps shown in Figure 11 display an abundance of nanometer-sized structures resembling known cytoskeletal components, which emerge with high contrast from the background. For example, Figure 11a, d, and f show multiple actin filaments, while Figure 11a, c, and f show some adhesion structures. This supports the idea that the increased force sensitivity and the reduced indentation of our platform is able to isolate the mechanical contribution of molecular components. It is also worth noting that Figure 11e shows the mechanics of dendritic spines, which appear as very rigid structures.

3.5 Improvement in spatial resolution

The small indentation and the high signal-to-noise ratio of our platform allow a net increase in spatial resolution of distinguishable mechanical features. Figure 12a represents an elastic modulus map over the edge of a mouse fibroblast. Plotting the values along the white dashed profile line shows that our platform is capable of distinguishing structures only 30 nm apart (distance between the brown dashed lines in Figure 12b).

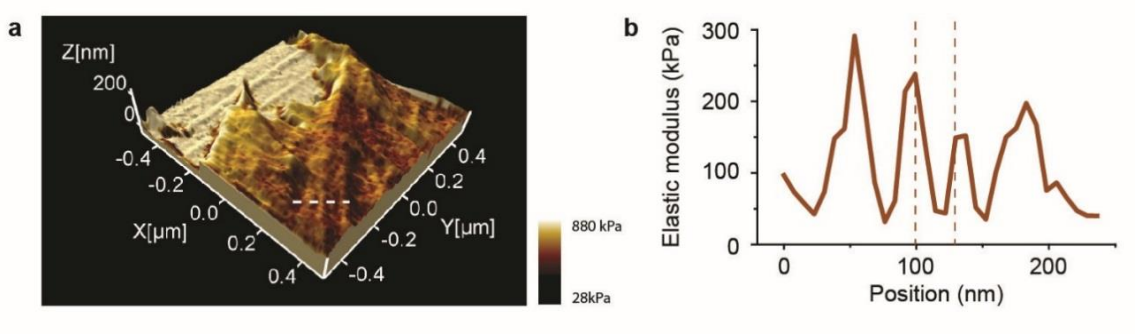

Figure 12 High-resolution capabilities of the platform

(**a**) Overlay of topography and elastic modulus acquired from a mouse fibroblast edge. (**b**) Elastic modulus values acquired along the white dashed profile line in **a** are plotted vs. their position.

We believe the represented structures are single actin filaments, due to their size, linearity, and presence of an adhesion-like structure at their end. Single actin filaments are the cytoskeletal filaments with the smallest diameter [243] and probably represents the smallest nanoscale unit contributing to the cell mechanical behavior. This is, to our knowledge, the first reported case of single actin filaments being mechanically-distinguishable through AFM.

3.6 Time-resolved mechanics of biological processes

Our nanomechanical measurements can be acquired within a minute timescale, as 5 to 10 minutes are most commonly required to acquire a high resolution mechanical map spanning hundreds of squared µm. At this temporal scale, it is possible to follow a multitude of biological processes - such as cell migration, cell adhesions, and response to damage - that were not possible to be followed in force volume mode.

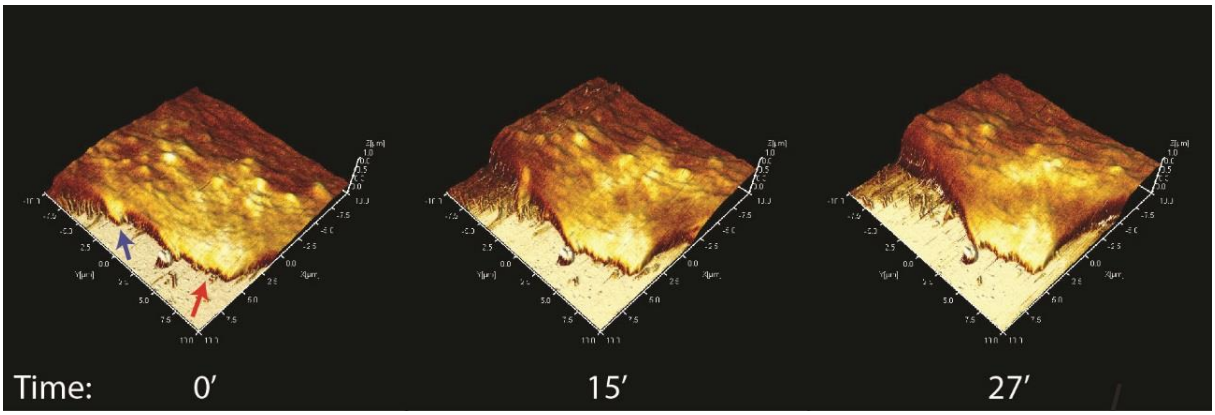

Figure 13: Temporal changes in the mechanics of retraction

The same cell was imaged over time. Topography and stiffness changes were monitored to dissect the mechanical changes associated with cell retraction. Arrows indicate focal adhesions.

As an example, a retracting cell is shown in Figure 13. The red arrow marks a focal adhesion which remains in the same position and stays stiff during the course of imaging. The blue arrow indicates a smaller adhesion which undergoes disassembly, while, at the same time, is becoming more compliant. The loss of the adhesion is locally associated with a net increase in height and with the appearance of retraction fibers. Because substrate adhesions transmit forces between the cell and the substrate, this analysis seems to confirm the hypothesis that a force balance between actin filaments and focal adhesions keeps cells flat against the substrate, while a loss of tension leads to cell round-up. This example demonstrates the ability of our platform to dissect the mechanical steps associated with dynamic physiological processes through the analysis of consecutive overlays.

Chapter 4: Nanomechanical behavior is determined by tension

4.1 Varying relation between cytoskeletal elements and nanomechanical response

Because nanomechanical images display a variety of distinguishable structures, we sought to precisely pinpoint the cellular counterparts responsible for their nanomechanical contrast. This task was facilitated by the high-contrast of the mechanical features (Figure 11), which resemble cytoskeletal components based on their size, shape and position within the cell. We therefore labelled cytoskeletal components and simultaneously performed mechanical measurements (Figure 14).

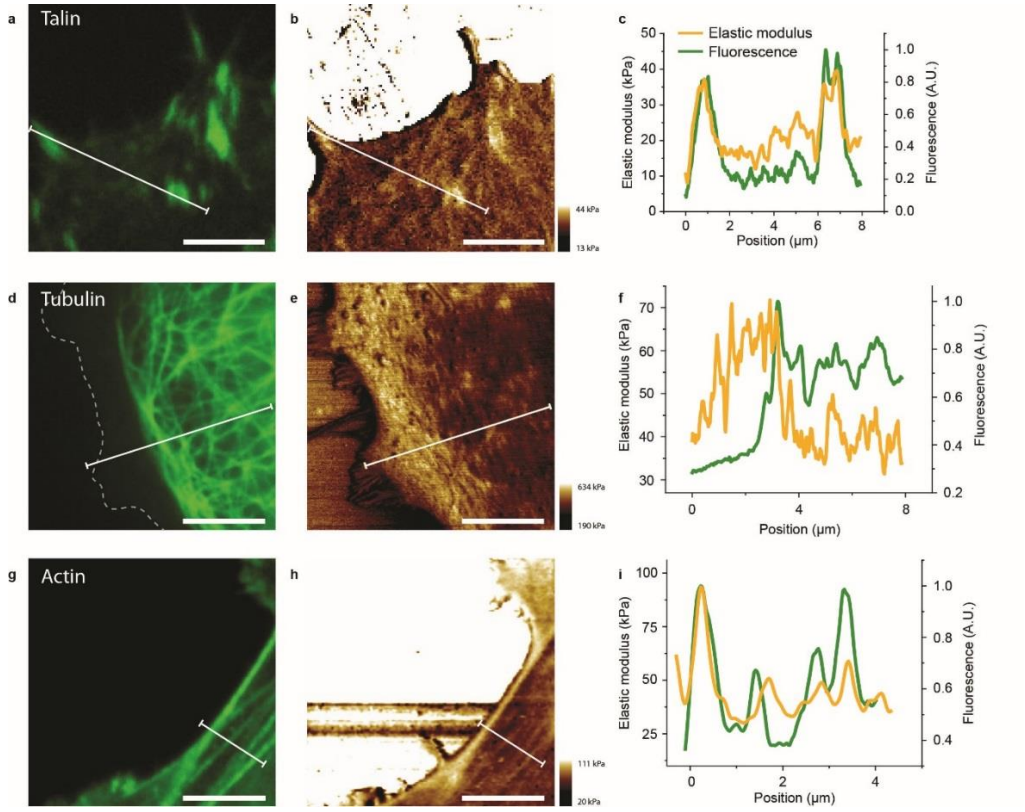

Figure 14: Nanomechanical stiffness vs. cytoskeletal components

Living cells were labelled for talin (**a**), tubulin (**d**), and actin (**g**) and probed mechanically (**b**, **e**, and **h**). Graphs in **c**, **f**, and **i** display the fluorescence and elastic modulus values along the white profile lines shown on the corresponding fluorescence and elastic modulus images. The dotted line in **d** corresponds to the cell edge. Scale bars, 5 μm.

First, we found that focal adhesions invariably correspond to stiff regions. Focal adhesions are indeed the stiffest cellular structures we detect – along with dendritic spines -, being up to thirty times stiffer than surrounding regions. We also found that microtubules – known to buckle under force loads in physiological conditions [30] - are confined to compliant regions. Surprisingly, the boundaries of these compliant regions display very sharp transitions with neighboring stiff regions – characterized by a ~ 40% difference in elastic modulus. Finally, comparisons of stiffness images

with f-actin – tensioned in physiological conditions – presents a more complicated picture, because we observe variable correspondence between f-actin and stiffness. Figure 14c shows an example where colocalization between high-stiffness regions and f-actin occurs.

This analysis seems to suggest an unprecedented scenario, whereas f-actin presence per se does not entail stiffness. We reasoned that, albeit cytoskeleton [28] - together with cell membrane [244] - is known to be the main contributor of cell mechanics and shape, force load can dramatically alter its mechanical behavior (See section 2.4). We therefore hypothesize that the force load applied to cytoskeletal components could play a major role in the cell mechanical response at the nanoscale.

4.2 Time-dependent changes in nanomechanical stiffness

To visualize the time-varying response of nanomechanics to force load, we simultaneously monitored actin localization and the corresponding nanomechanical response of fibroblasts over time.

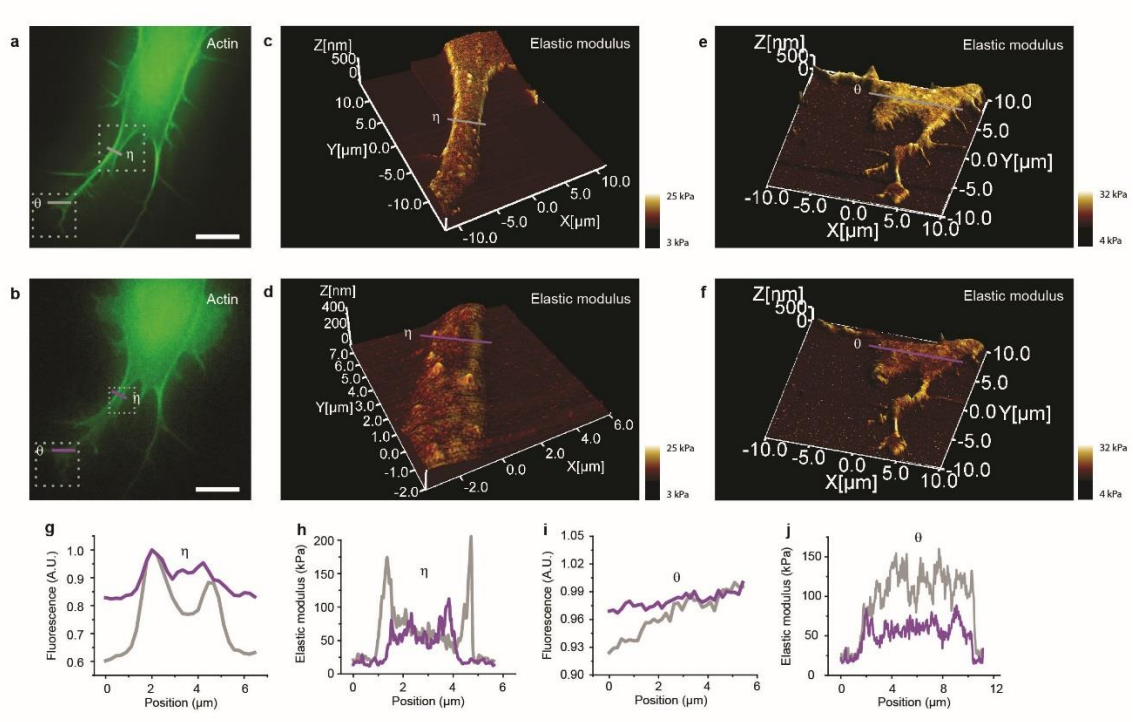

Figure 15: Time-dependent changes in nanomechanical response

a-b, Actin localization in a fibroblast cell at the beginning (**a**) and at the end (**b**) of the experiment. **c**-**d**, Mechanical maps acquired 17 minutes apart, corresponding to the dashed upper squares in **a** and **b**. **e-f,** Mechanical maps acquired 30 minutes apart, corresponding to the dashed lower squares in **a** and **b**. **g,** Fluorescence intensity profiles along the gray and purple lines (**η**) within the dashed upper squares in **a** and **b**. **h**, Elastic modulus profiles along the gray and purple lines in **c** and **d**. **i**, Fluorescence intensity profiles along the gray and purple lines (**θ**) within the dashed lower squares in **a** and **b**. **j,** Elastic modulus profiles along the gray and purple lines in **e** and **f**. We observed dynamic changes in the stiffness of actin fibers (**c, d**) and confined cortex regions (**e**, **f**), which occurred independently of actin redistribution (**a, b**). Scale bars, 25 μm.

In Figure 15, we monitored the nanomechanical response of two regions, enclosed by dashed squares in panels a and b. The first region (upper square) represents a cell process delimited by two actin bundles. The second region (lower square) represents a cortex region at the cell extremity,

likely characterized by extensive Arp2/3 complex activity, due to the abundance of ~ 70° bifurcations in its shape. We detected dynamic changes in the stiffness of actin fibers (Figure 15c, d) and of confined cortex regions (Figure 15e, f), which occurred independently of actin redistribution (Figure 15a, b). This supports the hypothesis that tension within actin bundles and the cortex is the responsible for the variation of nanomechanical response and spurred us to perform additional experiments to verify this hypothesis.

4.3 Blebbistatin-dependence of mechanical response confirms role of tension

To support our hypothesis, we sought to induce a decrease in tension at specific and defined times. Actomyosin contractility is considered the main responsible for tension build-up in cortex [50] and actin bundles [245], so we decided to block its activity through blebbistatin, a specific inhibitor of nonmuscle myosin II [246].

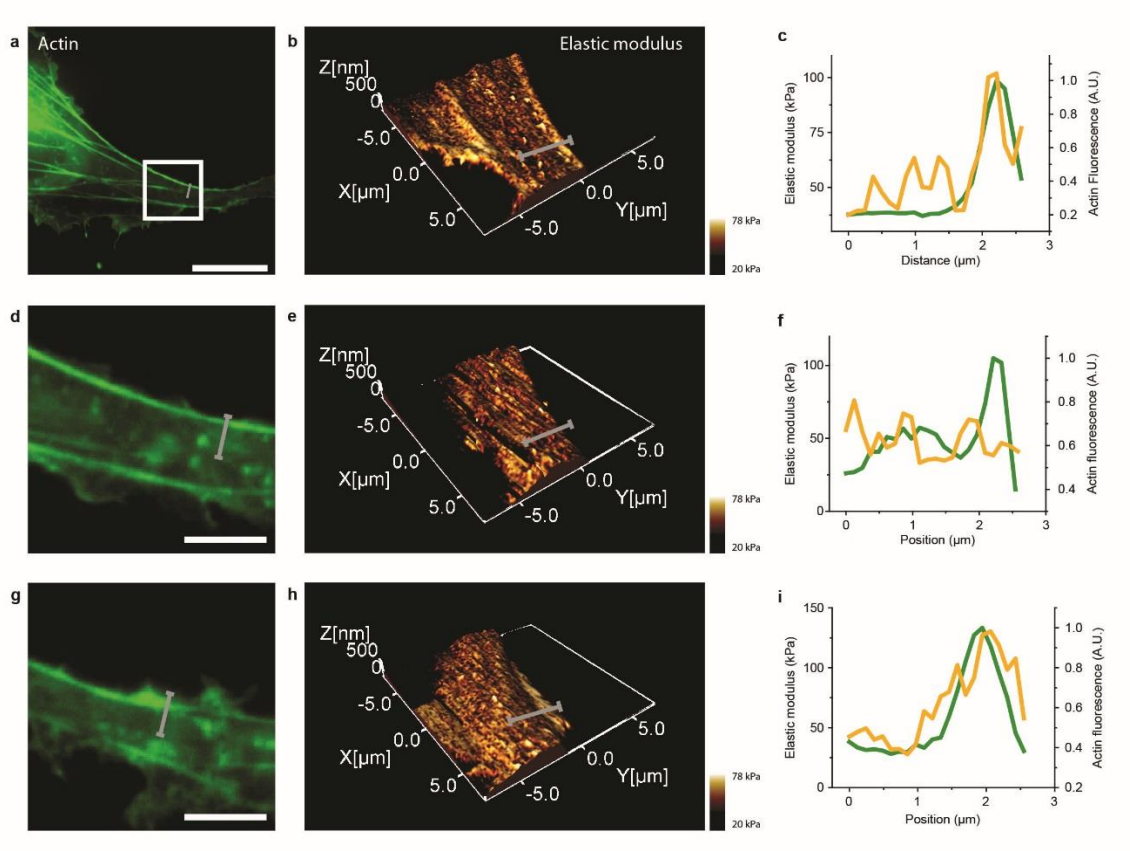

Figure 16: Blebbistatin-sensitivity of the nanomechanical response of cells

a, Fibroblast region showing actin bundles (in the white box) that are initially stiff (**b**). Myosin inhibition does not significantly alter actin distribution (**d**), but causes a decrease in their stiffness (**e**). After drug washout, actin reorganizes (**g**) and stiffness builds up again (**h)**. **c, f, i** Comparison between actin signal (green) and elastic modulus (yellow) along the profiles respectively shown in **a, d,** and **g**. Scale bars are 25µm for panel **a** and 5 µm for all other panels. The mechanical information corresponding to the substrate was removed for clarity purpose.

In Figure 16, we analyzed the mechanics of a cell harboring actin bundles on its edges. The actin bundles are initially stiff, but become more compliant upon addition of blebbistatin. This mechanical change occurred independently of major structural rearrangements of actin bundles, as their integrity appears intact after drug incubation. We also took advantage of the blebbistatin

inhibition reversibility [247], to regenerate tension upon drug washout. We observed that drug washout caused a reorganization of the actin cytoskeleton characterized by filopodia-like protrusions, concomitantly with a local stiffness increase.

4.4 The special case of focal adhesions

Our results showed that the nanomechanical response of the whole cell is sensitive to blebbistatin treatment, except for µm-sized, confined regions that were mainly localized at the cell edge (Figure 17). Talin fluorescent labeling identified those regions as focal adhesions.

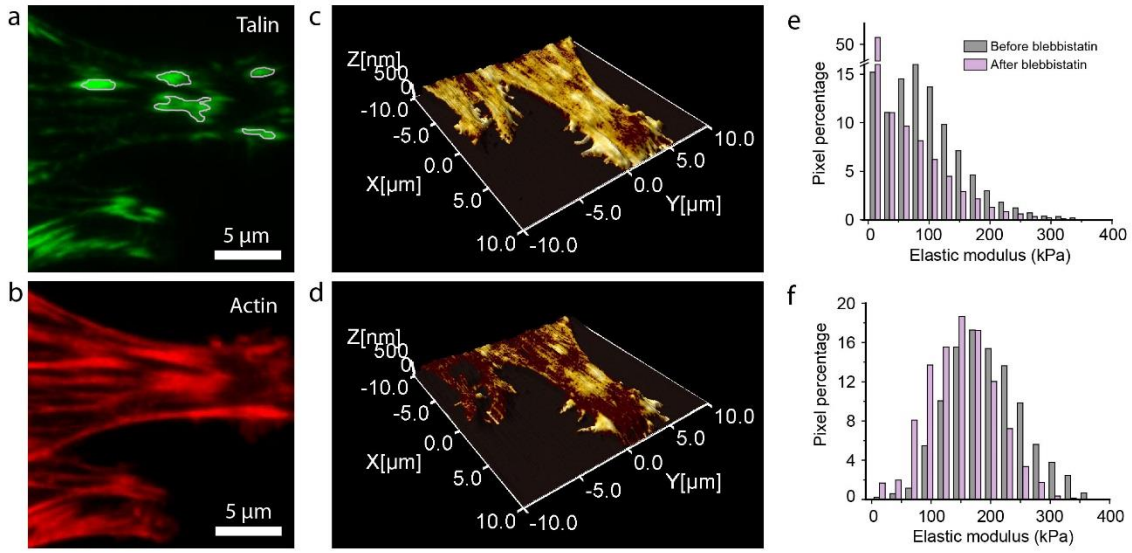

Figure 17: The mechanical response of focal adhesion is tension-independent

Talin (**a**) and actin (**b**) distribution within a fibroblast process. Elastic modulus map corresponding to the same region before (**c**) and after (**d**) myosin inhibition via blebbistatin. Elastic modulus distribution on focal adhesion (**e**) and throughout the rest of the cell (**f**), before (grey bars) and after (pink bars) myosin inhibition. We defined the substrate region based on topography data, and removed its stiffness from the overlays for clarity purpose.

Focal adhesions remain stiff upon blebbistatin treatment, despite the underlying stress fibers become more compliant, suggesting that tension does not dominate their nanomechanical response. This observation would be hard to reconcile with focal adhesions' physiological role, because they are primary sites of force transmission to the substrate [68]. This apparent paradox can be

explained by structural features of focal adhesions, namely their high protein density and their close contact with the substrate - both of which have been discussed in section 1.2.5. For this reason, we believe tension still contributes to counteracting heir indentation, but its component might be overwhelmed by the stronger contribution offered by the springy component of highly-packed proteins complexes, and their firm contact with the substrate.

In summary, this experiment suggests that, at length scales approaching molecular level, both force load and intrinsic stiffness of materials can contribute to the determination of mechanical properties and become dominant under certain circumstances. This highlights the capability of our platform to discriminate the relative contribution of different components to the origin of the nanomechanical response. In the next chapter we will quantitatively break down this problem through the introduction of the σ_c and K_{2D} terms, which, respectively, represent cortex tension and underlying cell elasticity.

4.5 Linearity in force vs. distance curves confirm the role of tension

As discussed in section 1.3.4.2, AFM indentation forces grow proportionally to the contact area between the tip and the sample. In turn, the growth of contact area as a function of indentation depends on the geometry of the tip. Except for the special case of cylindrical tips, which offer constant contact area [248], this dependency is non-linear and equal to the power of 2 for conical indenters [19] or equal to the power of 1.5 for parabolic and spherical indenters [249].

On the other hand, indentation forces of a tensioned material grown linearly with indentation for small indentations - Eq. (16). This relationship was experimentally measured in specialized cellular system where tension is believed to play a prominent role in cell's physiology [5, 250, 251].

We can compare the two aforementioned scenarios by a theoretical experiment performed with physiologically-relevant parameters (Figure 18). In one case a 1 μm-radius spherical tip indents a 4μm-tall cell, characterized by 1 kPa elastic modulus - a typical situation in force volume. In the other case, a 25μm-long actin bundle subjected to 5nN tensional force is indented and displaced by 30 nm (in line with the force curves shown in Figure 8). The comparison between the two curves shows that tension-induced reaction forces can be higher in magnitude than compression forces (and hence dominate the mechanical response) at small indentations. As indentation increases, the two components will become equivalent and the two curves will crossover, while at higher indentations - typical of force-volume measurements - the non-linear growth of compression-induced forces will dominate and become significantly larger than linear tension-induced forces.

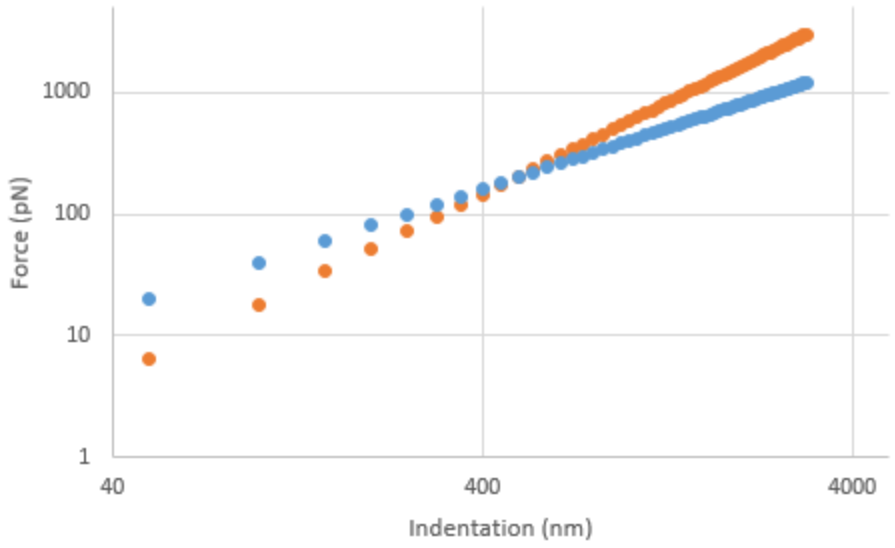

Figure 18: Simulation of dominant factors in the cell mechanical response

The red curves represents the compressive response of a 1kPa elastic hemi-space probed by a hemispherical indenter. The blue curve represents the mechanical response of a stretched filament subjected to 5nN prestress. Both curves are based on indentations typical for our platforms (blue curve) or force-volume (red curve) experiments The comparison between the two curves shows that for small indentations, the tension response might be dominant upon indentation, while it might become overwhelmed by the compression response as indentation becomes bigger.

If this is the case, we would expect forces to grow linearly for small indentations, and grow non-linearly at larger indentations. To verify this prediction, we acquired force curves with THCs in tapping mode – characterized by small indentation - and in force volume mode – characterized by large indentations - and looked for these mechanical signatures (Figure 19).

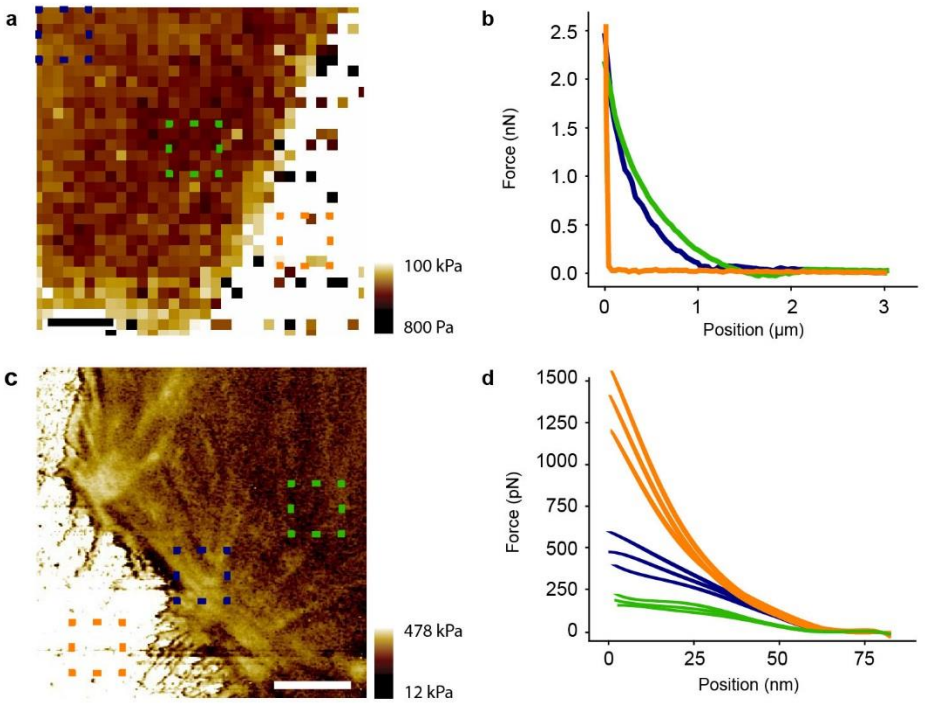

Figure 19: Nanomechanical cellular forces increase linearly with indentation

a, Mechanical map of a fibroblast edge acquired using THCs in force-volume mode. **b**, Force vs. indentation curves corresponding to single pixels in (**a**). Orange curves corresponds to measurements over the substrate, while blue and green corresponds to measurements over the cell. **c,** Mechanical map of a fibroblast edge acquired harnessing the torsional vibrations of THCs in tapping mode. **d**, Force vs. indentation curves corresponding to single pixels in (**c**). Green curves correspond to compliant cellular regions, blue curves correspond to stiffer cellular regions, while orange curves correspond to the substrate The approach and retract curves were averaged in all graphs for clarity purpose. Scale bars, 5 µm.

We found that THCs operated in force volume mode displayed the predicted non-linear dependency of forces from indentation, similarly to symmetrical cantilevers [130]. This was true over cells, but not over the substrate, because the latter is orders of magnitude stiffer than the cantilever and its mechanical response reflects the sum of the cantilever's flexural and torsional

spring constants. On the other hand, in tapping mode, THCs displayed forces increasing linearly as a function of indentations over cells, confirming the predominance of tension-reaction forces at smaller scales. We finally observe non-linear dependency on the substrate.

We conclude that depth of indentation plays a major role in the mechanical response of the cell and that, because indentations are small, our platform allows the detection of tension forces over the compression of bulk material. As a consequence, while elastic modulus might be a parameter truly representative of cell mechanics for big indentations, the relative contribution of forces deriving from material compression can be minimal at small indentations. In this case spring constant measurements - Eq. (1) - become more relevant, because they linearly relate a measured forces to displacement and are thus in line with the linear behavior of nanomechanical force vs. indentation curves.

A direct consequence is that, at the nanoscale, tip-sample contact area might not grow dramatically with indentation, but could be confined to a relatively-small region. As a consequence, tip shape and radius knowledge might not be as important for the characterization of cell mechanics, as they are for force volume-based methods.

To extend the validity of these findings, we mapped the error of linear fitting for force vs. indentation curves across the cell surface (Figure 20).

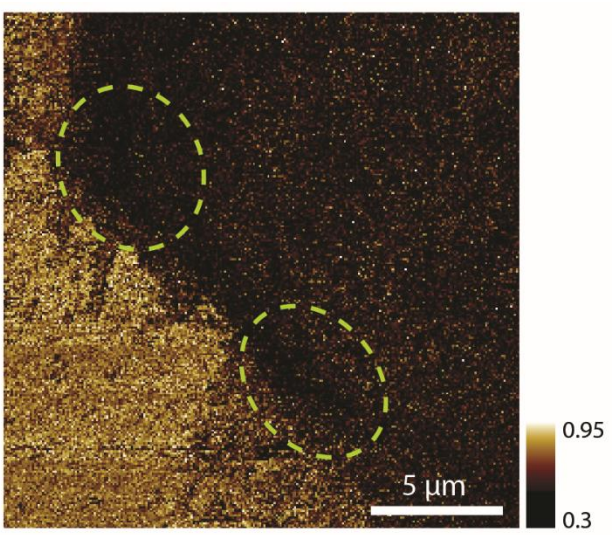

Figure 20: Linearity of force vs. indentation curves

Map showing the normalized error in linear fitting of force vs. indentation curves (error in linear fitting divided by error in linear fitting plus error in quadratic fitting). This map is acquired from the same cell displayed in Figure 19c. Regions surrounded by the dashed ellipses correspond to focal adhesions.

In this map, the brightest pixels correspond to the regions where force vs. indentation curves are farthest from being linear. The analysis reveals that the cell displays a rather uniform linearity, including regions corresponding to focal adhesions. Because focal adhesions' behavior is not dominated by tension, this indicates that cellular material displays surprisingly elastic behavior.

4.6 Small hysteresis in force vs. distance curves

As described in section 1.3.4.2, the area between the approach and retract curves of force vs. distance curves represents the dissipative behavior of the cell upon force stimulation (hysteresis of the system). The quantification of hysteresis would allow to calculate the parameter G'' – as

described in section 2.3.2 - thus quantifying the viscous behavior of cells in response to our oscillatory physical stimulation. Yet, the analysis of nanomechanical force curves revealed that the approach and retract portions of force vs. distance curves were surprisingly overlapping, indicating a relative lack in hysteresis (Figure 21). This finding is contrast with previous rheological studies monitoring microbeads displacement [110, 206] and AFM indentation [208, 209] at high frequencies. This apparent paradox will be discussed in greater detail in section 6.7.

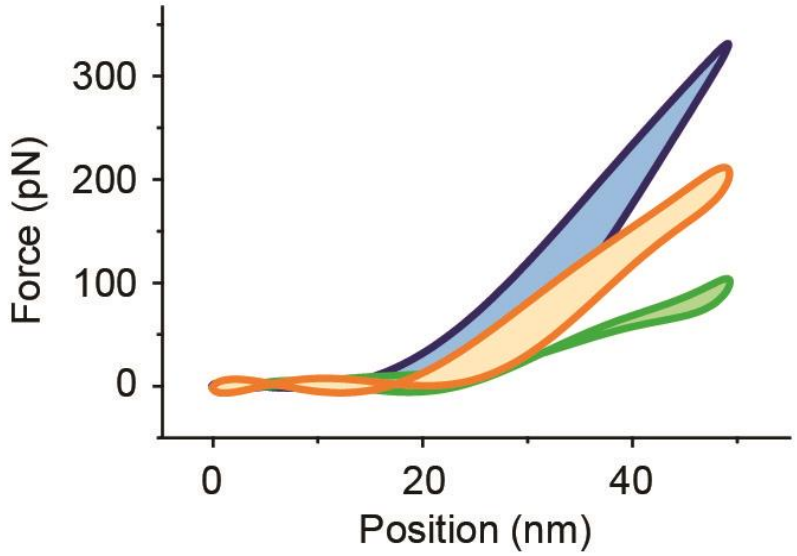

Figure 21: Force vs. distance curves display relatively-small hysteresis

Force vs. distance curves acquired over living fibroblasts. The lines indicate the approach and retract portion of the indentation, while the colored area within the lines indicates the hysteresis of the measurement.

The lack of hysteresis also supports the role of tension, as a response dominated by a constant tension would predict no viscoelastic dissipation.

Chapter 5: Relating nanoscale stiffness measurements to intracellular forces

The observations presented in Chapter 1: and Chapter 2: and the experiments presented in Chapter 4: support the hypothesis that intracellular forces determine the mechanical behavior of cells at the nanoscale. If this is the case, the knowledge of the nanoscale stiffness would, conversely, allow accessing the intracellular forces that determine them. This procedure would require a theoretical framework linking the two quantities, which would need to account for the heterogeneity in the locations of subcellular probing and in the distribution of force load across the cell.

5.1 One-dimensional model

5.1.1 Derivation of one-dimensional model

We started our formulation by investigating what determines the value of the AFM-measured spring constant, k_B, over actin bundles. If, on one hand, we expected our measurements to be influenced by an isometric tension, *T*, along the bundle, we also expected a contribution from the intrinsic stiffness of the underlying cellular material. This observation was corroborated by measurements over focal adhesions, where this additional component is indeed dominant. Furthermore, the lack of hysteresis typical of force vs. distance curves informed us that the stiffness

component must have been completely elastic. We thus modeled the stiffness component as a one-dimensional spring constant of cell material per unit length, K_{1D}.

Therefore, we modeled the response of an actin bundle to AFM indentation as the response of a stretched beam resting over an infinite number of independent springs – also known as the Filonenko-Borodich foundation [252]. We also assumed that the beam is infinitely long and that the tip makes contact with the bundle over a single point (this assumption is corroborated by our findings in section 4.5). As the AFM tip initially comes into contact with the bundle, a point with distance r = 0 and indentation z(x) = 0 is defined (Figure 22).

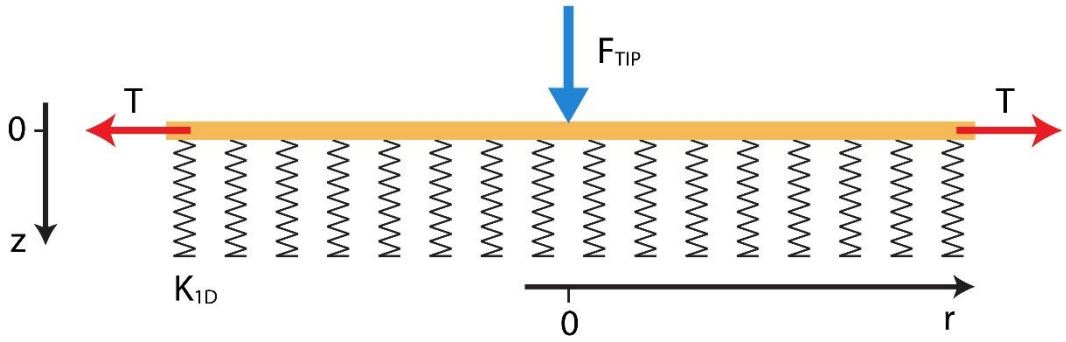

Figure 22: Modeling of actin bundle response to indentation

The AFM-measured spring constant, k_B, measured over an actin bundle (in yellow) is determined by the tension, T, across the bundle and by the spring constant per unit length of the underlying cellular material, K_{1D}. As the tip (represented by the blue arrow) contacts the bundle, we can define a point with distance, r, and indentation, z(r) equal to zero.

At r = 0, the tip pushes down the bundle with force F_{TIP} equal to

$$F_{TIP} = -h_{IND}\, k_B \qquad \text{Eq. (17)}$$

Where h_{IND} is the indentation and k_B is the spring constant felt by the tip over the bundle. Over this point, the only significant reaction force to indentation is offered by the tension's vertical component – the cellular spring constant contribution is negligible, because it is integrated over an infinitesimal distance – and is equal to:

$$F_{TIP} = 2T\frac{dz}{dr} \qquad \text{Eq. (18)}$$

Combining the two equation, we can obtain the relationship:

$$\frac{dz}{dr} = \frac{-h_{IND}\,k_B}{2T} \qquad \text{Eq. (19)}$$

On the other hand, at $r \neq 0$, for any bundle region of length *dr*, the tension will have two opposite components: one pointing downward - transmitting the force exerted by the tip - and the other pointing upward. We can write the sum of the two tension components, T_{VERT}, as:

$$T_{VERT}(x) = -\ T\ \frac{dz}{dr}\Big|_x\ +\ T\ \frac{dz}{dr}\Big|_{x+\,dr} \qquad \text{Eq. (20)}$$

, which can be rewritten as:

$$T_{VERT}(x) = T\ \frac{d^2z}{dr^2}\ dr \qquad \text{Eq. (21)}$$

This equation quantifies the downward tension component at each point at $r \neq 0$ along the bundle. This downwards tension is counteracted by the resistance of cellular material to compression, equal to $z\,K_{1D}\,dr$. Hence, for an infinitesimal portion of bundle length *at* $r \neq 0$, the force equilibrium can be written as:

$$\frac{d^2z}{dr^2} = \frac{z\,K_{1D}}{T} \qquad \text{Eq. (22)}$$

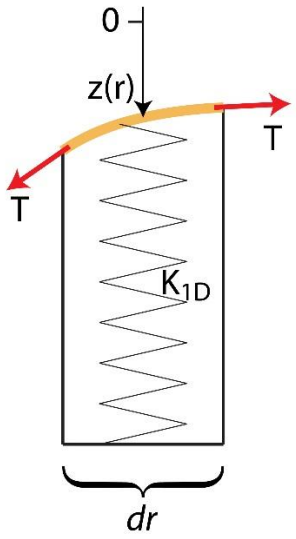

Figure 23: Force equilibrium over an actin bundle at r ≠ 0

At r≠0, three force components act over an infinitesimal portion of the bundle, *dr*: a downward tension component, $-\ T\ \frac{dz}{dr}\Big|_x$ caused by tip indentation at r = 0, an upward tension component, $T\ \frac{dz}{dr}\Big|_{x+\ dr}$ and the resistance to compression provided by the underlying elastic cellular material, $z\ K_{1D} dr$. These three components reach an equilibrium at a certain indentation, z.

This second order differential equation can be solved through the equation:

$$z(r) = C_1 e^{\sqrt{\frac{K_{1D}}{T}}r} + C_2 e^{-\sqrt{\frac{K_{1D}}{T}}r} \qquad \text{Eq. (23)}$$

, which can be simplified through two boundary conditions. First, because z(r) is expected to tend to zero as r increases, the term C_1 must be equal to zero. Second, at r = 0, the indentation is equal to h_{IND}, as expressed by Eq. (17). Hence the previous equation can be rewritten as:

$$z(r) = h_{IND}\ e^{-\sqrt{\frac{K_{1D}}{T}}r} \qquad \text{Eq. (24)}$$

, whose derivative at r = 0 is:

$$\left.\frac{dz}{dr}\right|_{r=0} = -\,h_{IND}\sqrt{\frac{K_{1D}}{T}} \qquad \text{Eq. (25)}$$

Finally, combining the previous relationship with Eq. (19), we come up with the following equivalence:

$$\frac{-h_{IND}\,k_B}{2T} = -\,h_{IND}\sqrt{\frac{K_{1D}}{T}} \qquad \text{Eq. (26)}$$

, which can be rewritten as:

$$k_B = 2\sqrt{T\,K_{1D}} \qquad \text{Eq. (27)}$$

This relationship, hence, relates the spring constant measured by AFM over an actin bundle, k_B, to the tension within the bundle, T, and the spring constant per unit length of the material supporting the bundle, K_{1D}.

5.1.2 Relating k_B with cell shape

In section 1.2.7, the quantitative relationship between tension of peripheral actin bundles and their radius of curvature has been discussed. It is therefore possible to combine Eq. (5) with Eq. (27) to generate a relationship between the nanomechanical response of peripheral actin bundles and their radius of curvature:

$$k_B = 2\sqrt{\sigma_m\,R\,K_{1D}} \qquad \text{Eq. (28)}$$

Based on this equation, we would expect that the spring constant measured over peripheral actin bundles would scale with the square root of their radii.

To test this hypothesis, we performed AFM mechanical imaging over the concave, uniformly-circular edges of living fibroblasts harboring peripheral actin bundles and interpolated their radii by fitting arcs. We found that data acquired from 11 bundles belonging to 4 different cells confirmed the predicted trend (Figure 24). These bundles spanned a wide range of radii - ranging between 3 and 30 µm - and end-to-end distances, substantiating the breadth of our findings. We did not detect a clear relationship between interpolated radii and distance between adhesion points, as reported by other studies [94].

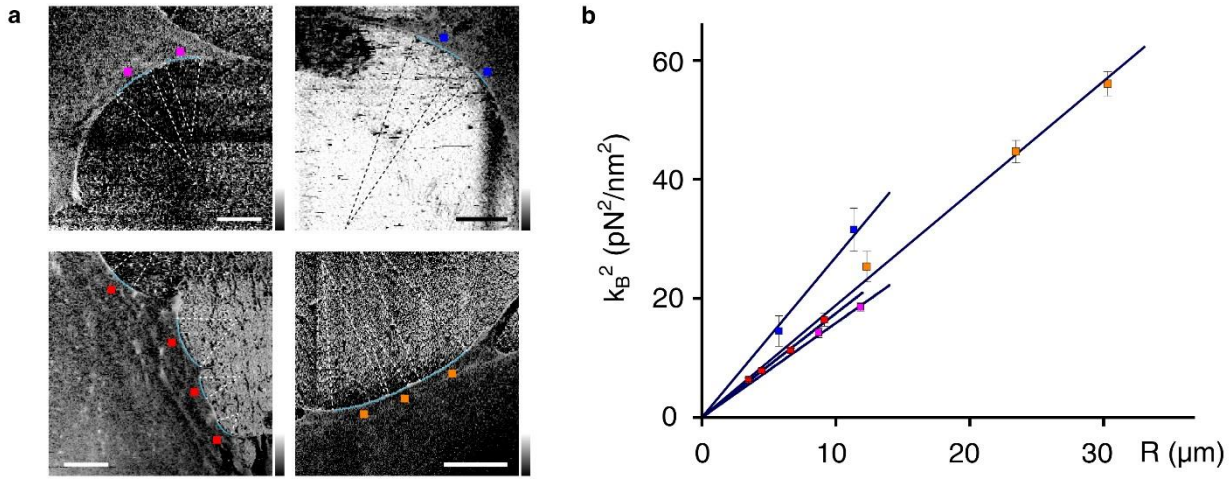

Figure 24: Relationship between nanomechanical response and cell shape

(**a**) Spring constant maps acquired from living fibroblast cells. Each colored square marks a single peripheral actin bundle. Circular arcs (in light blue) correspond to the circles that best fit the actin peripheral bundle trajectory. Dashed lines point towards the center of each circle. Going clockwise from the upper left panel, scale bars are 5, 15, 10 and 5 µm. The squares of spring constant values averaged over each bundle are plotted in (**b**) as a function of the fitted circle radius.

We also observed that each curve fits very well the data ($R > 0.97$), indicating that the parameter K_{1D} is uniform across the cell edge – assuming membrane tension is constant within each cell.

Furthermore, different cells displayed similar slopes, supporting the idea that membrane tension is tightly regulated in living fibroblasts, as previously postulated by other studies [244].

5.1.3 Mechanical coupling distance of the bundle

A very interesting aspect of the current model is its prediction that indentation forces are transmitted laterally up to a certain, finite distance, called coupling distance. To illustrate and demonstrate this concept, we will discuss two extremes cases whereas either the term *T* or the term K_{1D} is not taken into consideration within the model.

If an indentation model solely relies on the response of an elastic foundation composed of an infinite number of independent springs – i.e. the term K_{1D} is considered and the term T is ignored - the deflection of material outside of the loaded region is expected to be zero (practically, the deformation of the cellular material also depends on the finite tip size, which convolves into the measurement, but we assume indentation over a single point).

Conversely, if the indentation model only considers the stretched beam - i.e. the term T is considered and the term K_{1D} is ignored – the deflection of the beam extends to its entire length, L. In other words, the indentation force F_{TIP} is transmitted all the way to the beam's anchor points. In this model, the AMF-detected spring constant would vary along the length of the fiber with the following dependence on distance:

$$k_B(r) = \frac{T\, l_B}{x\,(l_B - x)} \qquad \text{Eq. (29)}$$

, where x corresponds to the position along the fiber and l_B represents the extent of force transmission, which in this model corresponds to the total length of the fiber, L [253].

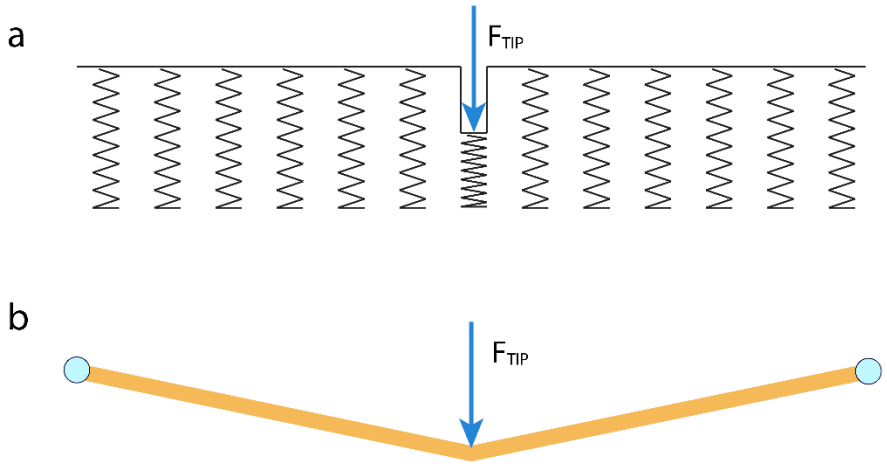

Figure 25: Extreme alternative models of cell response to AFM indentation

(**a**) If the response to cell indentation is only determined by the term K_{1D}, we would expect deformation to be confined to the indented region. (**b**) If the response to cell indentation is only determined by the term T, indentation force is propagated for the whole length of the fiber, L.

To calculate the extent of force transmission in our model, we can relate Eq. (27) to Eq. (29) and solve for l_B:

$$l_B = \sqrt{\frac{T}{K_{1D}}} \qquad \text{Eq. (30)}$$

Hence our model predicts that mechanical coupling distance of the bundle, l_B – i.e. how far the effects of a force applied perpendicularly to a bundle will be transmitted along that bundle - is

larger than a single point, but has finite length. Its extent is modulated by tension – tending to expand the region of force transmission – and cell material spring constant – tending to decrease the region of force transmission.

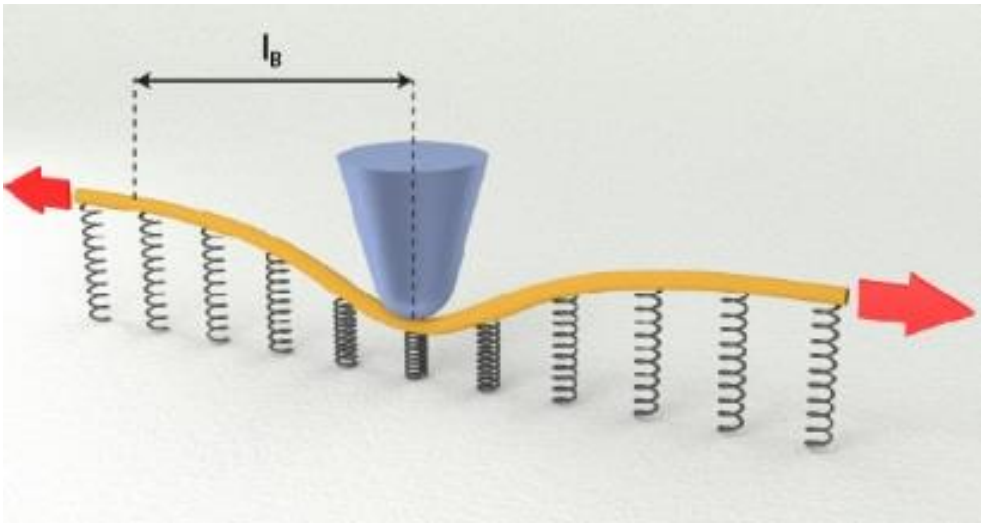

Figure 26: Mechanical coupling distance of actin bundles

Mechanical coupling distance over the bundle, l_B, specifies how far the force applied by the AFM tip (in blue) are transmitted along the bundle (in yellow).

As a consequence, the spring constant felt by the tip will not solely depend upon the elasticity of the cellular material directly under it, but on the collective elasticity of a cellular region spanning 2 l_B lengths. Hence, any rigid object within an l_B distance would be, in principle, felt at a distance from the AFM tip. Previous experiments (Figure 14) showed that focal adhesions are the most rigid objects within a fibroblast cell. Because focal adhesions are found at the end most of the actin bundles, we reasoned that the measurement of l_B could be determined experimentally by analyzing the spring constant profile between FAs and actin bundles. We expect the stiffness to vary along the bundle length according to the following relationship:

$$k_B(x) = \frac{2\sqrt{k_{1D}\,T}}{1 - \frac{m-1}{m}e^{-2x/l_B}} \qquad \text{Eq. (31)}$$

, where x represents the distance from the focal adhesion and m is the ratio between the stiffness measured at the focal adhesion and the stiffness measured at x >> l_B.

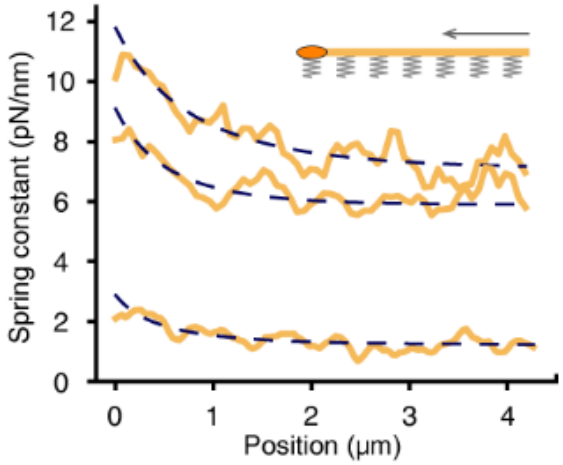

Figure 27: Interpolation of l_B

Stiffness profiles along three actin bundles terminating in focal adhesions. The dotted lines represent the best fit of l_B according to Eq. (31). The inset diagram represents the orientation of bundles and focal adhesion with respect to the orientation of the graph. A smoothing filter (Savitzky-Golay, order: 1, side-points: 2) was applied before displaying stiffness profiles.

We indeed observed gradual increase in stiffness towards the focal adhesions that fit our equation very well (Figure 27). The best fitting values according to Eq. (31) gave l_B values of 1.4, 1.9, and 2.3 µm. We can also predict the extent of l_B to be proportional to the actomyosin activity within the bundle. This relationship could be experimentally verified by measuring a gradual decrease in l_B upon increasing concentrations of actomyosin inhibitor drugs, such as blebbistatin.

Besides confirming the validity of our model and its predictions, the quantification of l_B allows the quantification of a physiologically-relevant cellular parameter – this will be discussed in more detail in the next chapter. Additionally, it allows the calculation of tension within peripheral bundles through the combination of Eq. (27) with Eq. (30). The tension values calculated based on the fittings shown in Figure 27 were 1.2, 2.8, and 8.2 nN, in line with estimates based on micropillars in living cells [67] and on bundles extracted from cells [88].

5.2 Two-dimensional model

5.2.1 Derivation of two-dimensional model

The validity of the model on actin bundles spurred us to extend its physical principles to the rest of the cell, with the intent of harnessing its predictive power for the determination other cell physiological quantities. We reasoned that tension is indeed present throughout the rest of cell surface, because both cell membrane and the underlying cortex are under prestress. Hence, we summed their contribution into the term σ_C, which mainly reflects cortex contribution, due to its higher value of tension compared with membrane. Similarly to the 1-D case, we also modeled the elastic component of the underlying cell material through a spring term. In the 2-D case, K_{2D} represents the spring constant of underlying cellular material per unit area. Therefore, we modeled the response of the cortex to AFM indentation as the response of a stretched sheet resting on an elastic foundation, where the spring constant measured over the cell cortex, k_C, should depend on both the σ_C and K_{2D} terms (Figure 28).

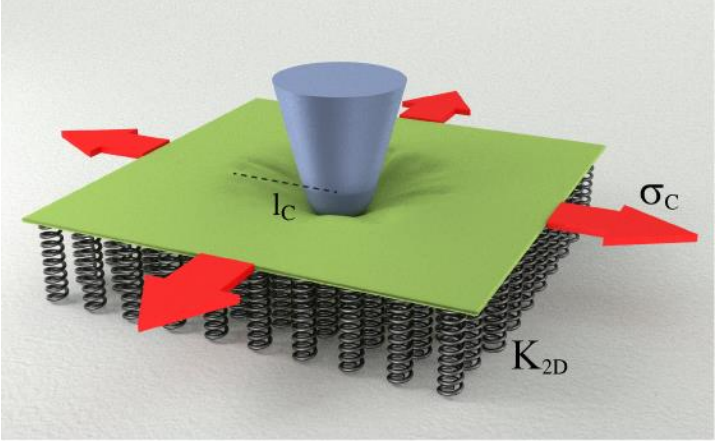

Figure 28: Modeling of cell cortex response to indentation

The AFM-measured spring constant, k_C, measured over the cortex (in green) is determined by the tension, σ_C, across the cortex (represented by the red arrows) and by the spring constant per unit area of the underlying cellular material, K_{2D} (represented by the grey springs).

Analogously to the 1-D case - Eq. (20) - we can assume the tension vertical contribution for a ring of cell material at a distance $r \neq 0$ from the indentation to be equal to:

$$\sigma_{C\,VERT}(r) = -\sigma_C 2\pi r \left.\frac{dz}{dr}\right|_{r_0} + \sigma_C 2\pi (r + dr) \left.\frac{dz}{dr}\right|_{r_0+dr} \qquad \text{Eq. (32)}$$

in cylindrical coordinates This component is in equilibrium with the force exerted by the compression of cellular material within the same ring, equal to $z\ k_{2D}\ 2\pi r\ dr$. This leads to the following force equilibrium:

$$r\,\frac{d^2z}{dr^2} + \frac{dz}{dr} - \frac{K_{2D}}{\sigma_C} = 0 \qquad \text{Eq. (33)}$$

This second-order differential equation can be solved through a modified Bessel function of the second kind, leading to solution:

$$z(r) = \beta \mathrm{K}_0\left(r\sqrt{\frac{K_{2D}}{\sigma_C}}\right) \qquad \text{Eq. (34)}$$

, where K_0 is the modified Bessel function of the second kind. Differently from the 1-D model, the assumption that indentation occurs over a single point cannot be made, due to the singularity of K_0 at the origin (r = 0). Hence, tip radius and shape have to be taken into account to calculate the force balance in the contact area under the indenting tip. Furthermore, the integration of forces under the tip cannot be directly solved, and requires approximations. However, it can be shown that k_C depends only weakly on the tip radius (~25% change upon two-fold change in radius) and on the tip shape. In case of a flat punch with radius *a*, k_C can be written as:

$$k_C = \frac{2\,\pi\,\sigma_C}{\mathrm{K}_0\left(\frac{a}{l_C}\right)} \qquad \text{Eq. (35)}$$

where l_C is the mechanical coupling distance of the cortex. For values between 10 and 100 nm (typical of this work) and l_C estimated from data (shown later in Figure 29), the previous equation can be approximated as:

$$k_C \cong 2\,\sigma_C \qquad \text{Eq. (36)}$$

Although this relationship indicates that the spring constant measurements over the cortex mainly depends on the cortex tension, the intrinsic rigidity of cellular material can still influence mechanical response over the cortex via the coefficient preceding σ_C, which could be different from 2 over distinct cellular regions. Additionally, we would expect this equation to reflect the contribution of membrane tension, rather than cortex tension within regions of cortical network

unsupported by actin filaments and their associated proteins – i.e. over the gaps of the cortical mesh.

5.2.2 Mechanical coupling distance of the cortex

Stemming from Eq. (35), we can calculate the mechanical coupling length of the cortex. Analogously to the one-dimensional case, the mechanical coupling distance of the cortex, l_C, can be expressed as:

$$l_C = \sqrt{\frac{\sigma_C}{K_{2D}}} \qquad \text{Eq. (37)}$$

As a consequence, k_c will depend collectively on the behavior of a cellular region spanning a circle with radius approximately equal to l_c. As shown in Figure 24, actin bundles are consistently more rigid than the neighboring actin cortex regions, hence they can be used to experimentally determine values of l_C – similarly to how FAs were used to experimentally determine l_B. In the 2-D model, we expect the stiffness to vary along the actin cortex according to an equation well approximated by the following function:

$$k_c(x) \cong \beta \mathrm{K}_0(4x/l_C) + k_c(\infty) \qquad \text{Eq. (38)}$$

Spring constant fitting over cortex regions flanked or intersected by an actin bundle gives l_C values between 250 nm to 1000 nm (Figure 29).

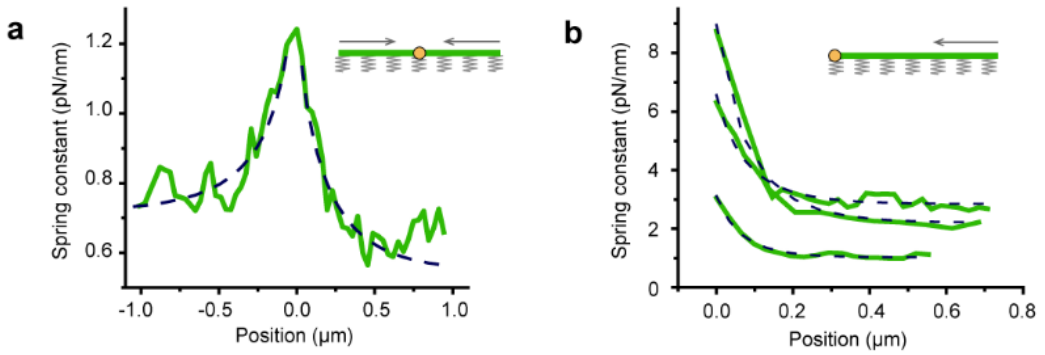

Figure 29: Interpolation of l_C

(**a**) Stiffness profile acquired along a cortex region intersected by a linear stress fiber. (**b**) Stiffness profiles acquired along three cortical regions, each ending in a single peripheral actin bundle. For both panels the dotted lines represent the best fit of l_C according to Eq. (38) and the insets are diagrams representing the orientation of cortex and bundles with respect to the orientation of the graphs.

Just as in the 1-D formulation, the presence of mechanical coupling distances on the cortex confirms the validity of the model and allows the quantification of a physiologically-relevant cellular parameter. Additionally, we found that the cortex tension values measured through Eq. (36) appeared to positively correlate with the corresponding l_C values acquired via fitting of Eq. (38) over cortical regions, as expected from Eq. (37) (Figure 30).

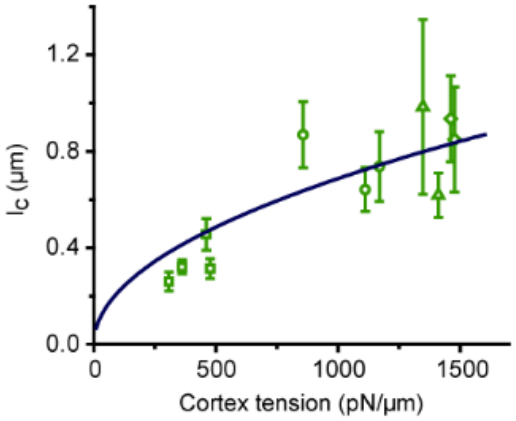

Figure 30: Relationship between σ_C and l_C

σ_C values were plotted against the corresponding l_C values. The blue line represent the best fit for the data points, following the relationship described by Eq. (37).

Finally, it should be noticed that l_B values appear generally larger than l_C values. This relationship is in line with the notion that tension along actin bundles is generally higher than the tension within the actin cortex.

5.2.3 Relating k_C with cell physiological parameters

Similarly to the 1-D model, the 2-D model has testable predictions that confirm its validity and allow relating mechanical measurements to cellular parameters. First, Eq. (36) provides a straightforward way to estimate a cell's cortex tension and it variation across the cell body. k_C values acquired from the cell surface typically range between 0.15 and 0.75 pN/nm, predicting cortex tension to range between 300 and 1500 pN/µm. These values are in line with measurements performed on living cell with different techniques from independent groups (See Table 1 for details).

Additionally, K_{2D} can be related to the tension-free elastic modulus of cellular material. This can be achieved simply combining the definition of elastic modulus - shown in Eq. (2) - and the definition of K_{2D}:

$$E_{TF} \cong K_{2D}\, h \qquad \text{Eq. (39)}$$

, where E_{TF} is the tension-free elastic modulus of the cell and h is the height of the cell. Due to Eq. (37) and given approximate values of 500 nm for l_C and 900 pN/µm for cortex tension, we can estimate K_{2D} to be ~ 3600 pN/µm^3 and E_{TF} to be ~1.8 kPa, in line with elastic modulus values of fibroblast found in literature [97, 254].

5.3 Combination of 1-D and 2-D models

To create a comprehensive framework understanding the collective behavior of a cell across its whole surface, we sought to connect the 1-D model with its 2-D counterpart.

We reasoned that actin bundles should be physically connected to the cell membrane. Hence, actin bundle indentation would not only result in the deformation of the bundle itself, but also in the deformation of the neighboring cortex, whose shape would be recapitulated by the previously discussed parameter l_C , as illustrated in Figure 31.

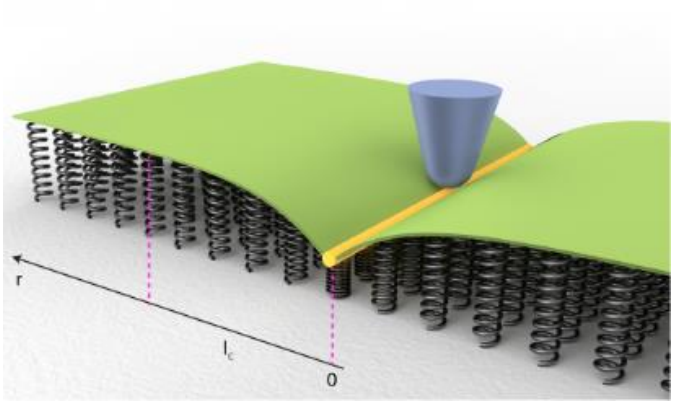

Figure 31: Combination of 1-D and 2-D models

To combine the two models, we assume to push down a unit length of the bundle (in yellow) uniformly. Because of physical connections between bundles and membrane, the cortex will deform as well, following a profile described by l_C.

In the 1-D model, we can demonstrate that the spring constant measured over a bundle under tension T, with coupling distance l_B and supported by an elastic foundation characterized by the parameter K_{1D} is mathematically equivalent to the spring constant measured over an untensioned bundle which is indented over a length equal to 2 l_B (Figure 32a and b).

This relationship can be simply obtained by combining Eq. (27) and Eq. (30).

$$k_b = 2\, l_B\, K_{1D} \qquad \text{Eq. (40)}$$

Similarly, when indenting a bundle connected to the cortex (Figure 32c and d), the spring constant measured over the bundle, k_b, can be expressed as:

$$k_b = 2\ K_{2D}\, l_c\, l_B \qquad \text{Eq. (41)}$$

, where the l_b factor has to be introduced to take into account the different dimensionality of K_{2D} compared with K_{1D}.

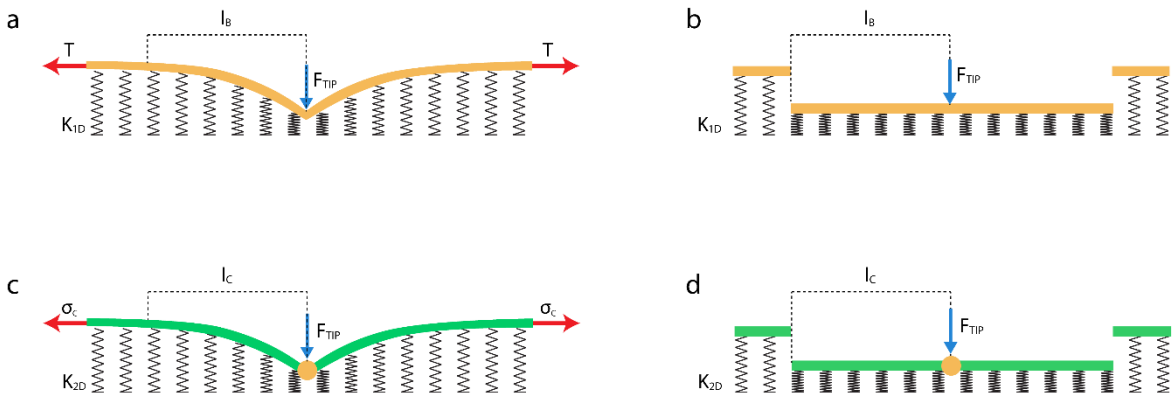

Figure 32: Derivation of K1D ≅ K2D l_C

The indentation of a tensioned bundle supported by an elastic foundation (**a**) is mathematically equivalent to the indentation of an untensioned bundle for a length = l_B (**b**). The indentation of a bundle supported by an elastic foundation and connected to a tensioned cortex (**c**) is mathematically equivalent to the indentation of an untensioned cortex for an area = l_B * l_C (**d**).

Combining the two previous equations leads to the equivalence:

$$K_{1D} \cong K_{2D} l_c \qquad \text{Eq. (42)}$$

, which allows relating the 1-D model to its 2-D counterpart.

To verify this mechanical linking, we created a new relationship combining Eq. (27), Eq. (30), and Eq. (36):

$$\frac{k_B}{l_B} = \frac{k_C}{l_C} \qquad \text{Eq. (43)}$$

To test the equivalence of the two ratios we measured these four parameters from four different bundles and their neighboring cortical regions. Despite the large variability of each individual parameter – which varied more than twofold across bundles – and the variability of each ratio

across bundles, the equivalence between the two ratios k_B/l_B and k_C/l_C was strikingly, with an approximate error of 20% (Figure 33).

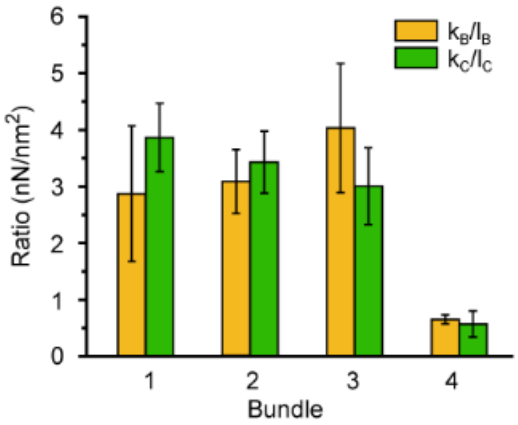

Figure 33: Prediction $k_B/l_B = k_C/l_C$

We measured the ratios k_B/l_B and k_C/l_C for each bundle within a single cell. Despite the large variability of each parameter and ratio within the cell, the two ratios k_B/l_B and k_C/l_C were surprisingly similar across different bundles.

5.4 Determination of intracellular forces

The presented framework not only provides a way to interpret nanomechanical data, but also allowed us to test its assumption through the multiple predictions that have been verified in the previous paragraphs. Once tested its validity, we sought to harness our model to systematically quantify intracellular forces from stiffness values and their gradients across the cell surface.

The first quantity that can be extracted from the interpretation of nanomechanical data is the isometric tension across actin bundles, T. The estimation of this value is possible by combining Eq. (27) and Eq. (30), which results in the following equation:

$$T = 0.5\, k_B\, {l_B}^2 \qquad \text{Eq. (44)}$$

While k_B can be simply acquired through the knowledge of the AFM-measured spring constant over actin bundles, l_B can be interpolated from the stiffness variation over actin bundles through Eq. (31) or, alternatively, by using Eq. (43). Our data shown in Figure 34a reflects the latter approach, due its broader applicability – it does not require fitting over the steep stiffness gradients caused by the presence of focal adhesions. Both approaches predict T values in living cells in the order of few to several nN.

We were also able to measure the tension across cortical regions, σ_C, through Eq. (36). Figure 34b shows σ_C values extracted from regions adjacent to those used to provide T values for panel a. Typical cortex tension values estimated through this formula range between a few hundred pN/µm to approximately 1500 pN/µm.

Finally, combining Eq. (5) with Eq. (44) and Eq. (43), we measured membrane tension, σ_m, through the following relationship:

$$\sigma_m = \frac{{k_B}^2\, l_C}{4\, R\, k_C} \qquad \text{Eq. (45)}$$

Membrane tension values acquired range between 121 and 191 pN/µm (Figure 34c). Furthermore, using this formula, we could obtain multiple, independent estimates of σ_m for a single cell from

multiple peripheral bundles. We found that the σ_m range of values for each cells is surprisingly small - error bars in Figure 34c. – thus confirming the precision of our method.

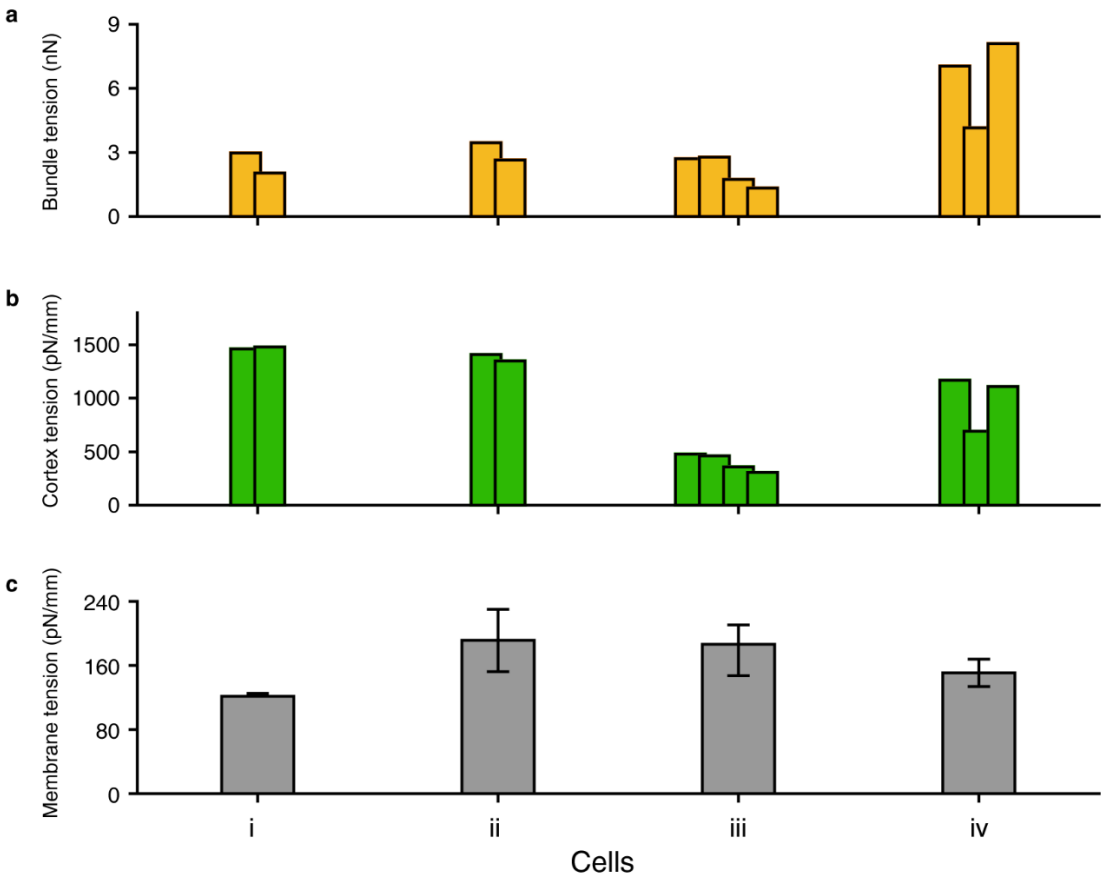

Figure 34: Determination of intracellular forces from stiffness images

Determination of bundle tension (**a**), cortex tension (**b**) and membrane tension (**c**) values from four living fibroblast cells. For each cell, different bundles can be analyzed, each represented by a single bar. Data presented for cells (i-iv) are calculated from the stiffness maps in panels (a-d) of Figure 24, respectively. Bars are placed in the same order as their respective bundles appear in each panel, i.e. from left to right.

5.5 Conclusions

In this chapter, a model relating nanoscale mechanical measurement to intracellular forces has been presented, whereas nanoscale stiffness depends on tension components, in addition to an underlying elastic foundation. While we initially modelled the response of actin bundles, the model has been subsequently extended to the rest of the cell cortex. Furthermore, connections have been found between the 1-D and the 2-D formulation - through the indentation of actin bundles connected to the cortex, and between the model and cell shape – through the Laplace rule.

Using the model, stiffness values across the cell and their micrometer-scale patterns of variation become easily-acquirable observables that can be used to determine physiologically-relevant parameters of cells, namely isometric forces and mechanical coupling distances across the cell surface. The physiological importance of knowing intracellular forces has been extensively discussed in Chapter 2:, while the importance of the mechanical coupling distance will be discussed in the next chapter.

A few aspects allow this model to differentiate itself from other theoretical views of cell mechanics. First, our model not only explains and fits the acquired data, but is as well able to make several predictions. These could, in turn, be experimentally verified, allowing us to confirm the assumptions and the validity of our model.

Second, while most of the mechanobiology studies are either interested in the dissection of mechanical properties or the dissection of intracellular forces, and address them by separate experimental set-ups and theoretical frameworks, our model allow unprecedented and quantitative

connections between these two fields. The breath of our findings is further increased by the connection with cell shape, provided by the modified Laplace law.

Additionally, our framework allows the estimation of bundle tension, cortex tension, membrane tension, tension-free elastic modulus, and mechanical coupling distances of actin bundles and cortex, all from a single AFM nanoscale stiffness image. While other techniques and model might allow the determination of one or two of the aforementioned parameters, [221] no other model or technique can map all of them simultaneously. In addition, our extrapolated parameters are generally based on local mechanical properties of the cell, whereas other model tend to provide forces and mechanical parameters representative of the collective response of the cell.

Finally, in some cases, more than one set of variables can be used to determine a single mechanical parameter. Values acquired through different formulas are consistent with each other, further confirming the validity of our model.

Chapter 6: Discussion

6.1 Technical advantages of the imaging platform

A net advantage of using THCs comes from their intrinsic capability of decoupling viscous drag from the measurements, resulting in considerable improvement in force sensitivity. The convolution of cellular forces with viscous drag is indeed a serious issue for measurements performed in force volume and in tapping mode, resulting in difficulties to reconstruct accurate force vs. indentation curves. This issue has recently gained the attention of the community, spurring Wang and Butte to manufacture tall (18 μm) cantilevers tip [255]. These tips, besides improving the imaging of lower parts of the cell next to steep regions, allow a reduction of squeeze-damping film, resulting in improved signal-to-noise ratios. Another promising approach to tip lengthening is represented by the deposition of amorphous carbon over pre-existing tips, although the latter approach might result in challenging imaging conditions [256]. An alternative successful approach to viscous drag reduction has been followed by other groups through the reduction of cantilever size [146].

Further improvements of our platform would be possible by further optimization of THC design and their miniaturization, allowing to combine them with high-speed AFM technology [120], potentially leading to one to two orders of magnitude increase in the speed of mechanical measurements.

6.2 Combination with super-resolution optical techniques

The present work was performed using the AFM platform in conjunction with a conventional epifluorescence microscope, which has resolution limits imposed by the diffraction properties of light (~250nm). To further correlate mechanical phenotypes with the dynamic of fine intracellular components, our platform could be potentially mounted on top of super-resolution optical platforms. The combination between AFM mechanical measurements and super-resolution techniques is technically feasible and will likely become popular in the following years, but it is currently challenging and resources-demanding, mainly due to the novelty of the super-resolution techniques and their limits, which will be described in the following paragraphs.

PALM (PhotoActivated Localization Microscopy) and STORM (STochastic Optical Reconstruction Microscopy) offer the highest resolution within the realm of the state of the art super-resolution techniques (up to 20 nm in XY). STORM has been recently performed on fixed cells in conjunction with force volume mechanical measurements [257], while PALM has been performed on living cells after AFM topographical imaging [258]. Yet, the combination of PALM/STORM with AFM is currently hampered by the time required to acquire thousands of frames necessary to reconstruct a single image (currently within the minute timescale) and the need of special buffers to allow PALM and STORM imaging.

Combination of our platform with SIM (Structured Illumination Microscopy) and STED (STimulated Emission Depletion) might be easier to implement and amenable to live cell imaging. STED greatly improves spatial resolution (up to ~ 50 nm in XY), is compatible with living cell imaging, and has already been performed on fixed cells in combination with force volume imaging

[257]. Yet, while this work was conducted on the stage of a wide-field fluorescence microscope, STED setup would requires the implementation of a scanning laser confocal microscope in addition to the purchase and set up of two different wavelength lasers (including a femtolaser).

The use of SIM would also lead to a net increase in resolution (up to 100 nm in XY) and would be easier to implement compared with PALM/STORM and STED, because it would still rely on a setup very similar to those commonly used in wide-field fluorescence microscopy (including light source, cameras, and fluorophores). Yet, its operation would still be dependent on the implementation of a structured illumination setup and on the reconstruction of optical images from illuminated grid patterns.

6.3 Combination with micropillars

To provide an additional and independent readout of cellular forces, our platform can be combined with micropatterned substrates such as micropillars, as schematically shown in Figure 35.

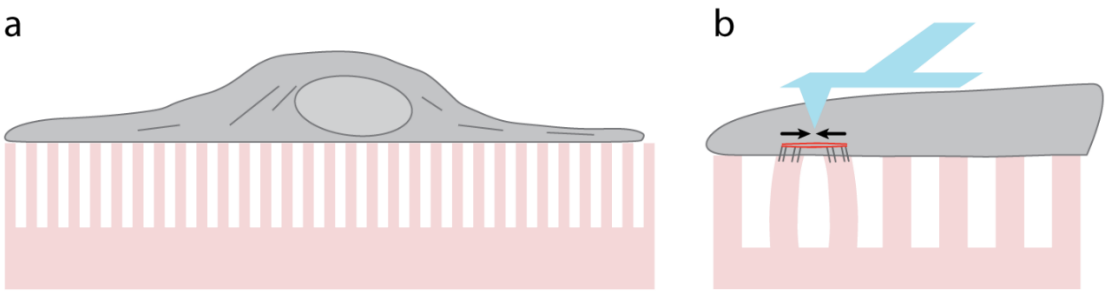

Figure 35: Combination of AFM with micropillars

(**a**) A cell is spread over micrometric pillars (in pink). (**b**) Drawing depicting the combination between our platform and micropatterned pillars. Intracellular isometric forces (black arrows) along actin cables (in red) can be measured simultaneously via our AFM platform (in light blue) and by measuring micrometric pillars deflection via optical microscopy.

This combination allows the simultaneous measurement of intracellular forces via AFM and optical monitoring of the pillar top deflection. Because the contribution of isometric tension was found to be dominant in the nanomechanical response of actin bundles, we expect to see a correlation between deflection of pillars tops and the stiffness of the cellular region pulling over those pillar tops.

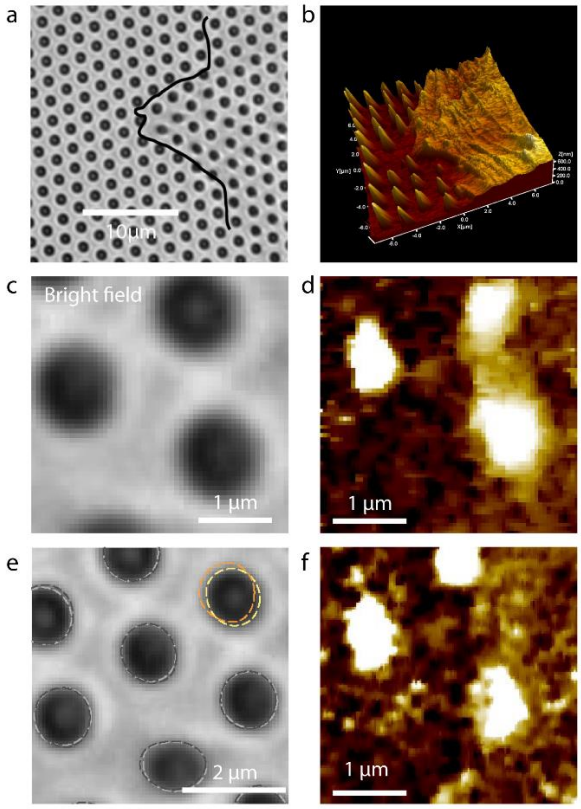

Figure 36: Simultaneous detection of isometric forces via AFM and micropillars

(**a**) Bright field image of a living fibroblast cell plated on 1µm-diameter pillars. The cell edge has been drawn for clarity purpose. (**b**) AFM topographical map acquired from the cell shown in (a). Notice that most of the cell keeps a relatively-flat shape, indicating that imaging with our platform does not cause the cell to sink dramatically between the pillars. (**c**) Zoom in on three pillar tops supporting the same fibroblast cell. (**d**) AFM elastic modulus map corresponding to the cell region on top of (c). The cell region between the two pillars shown on the right is particularly stiff. (**e**) The pillar top position is monitored over time and represented by dotted contour lines. One of the pillar tops is significantly displaced over time (it changes its position from the yellow to the orange contour). (**f**) AFM elastic modulus map corresponding to the regions in (c) and (d), later in time. The pillar top corresponding to the top part of the image is now more distant from the pillar top at the bottom of the image and the cell elastic modulus measured between these two pillars is greatly reduced.

Figure 36 shows preliminary results of an experiment whereas a fibroblast cell is plated on micrometric pillars and simultaneously probed with our nanomechanical platform. The time-dependent analysis of pillar top displacement (Figure 36c) and cell mechanical maps (Figure 36d and f) shows high stiffness over cell regions pulling pillar tops close to each other relative to their equilibrium position. Conversely, as pillar tops are released and returns to their equilibrium position, the stiffness of the cell portion lying between those pillar tops drops dramatically, in line with our predictions.

6.4 Effects of AFM measurements

It could be argued that repeated mechanical measurements of cells might alter cell physiology. Throughout two decades, the general consensus has been that AFM measurements cause a very limited amount of cellular damage. If this is true for force volume measurements, which indent hundreds of nm of cellular materials and apply few nN of forces, it should thus also be the case for our platform, which applies forces and indentation one to two orders of magnitude smaller than force volume. A fiducial readout of AFM invasiveness could be represented by the imaging of unsupported or lightly-supported cellular structures, such as membrane ruffles and moving filopodia. The comparison between trace (tip scans in one direction) and retrace (tip scans in the opposite direction) images displayed little variation in height and mechanical information, supporting the idea that AFM measurements don’t significantly interfere with cell’s fine functionalities.

On the other hand, the application of pN-level forces via our instrumentation can potentially activate cellular mechanotransduction machineries, which might cause a variety of effects on cell physiology – as described in section 2.1. While this makes our platform a potential tool to locally stimulate mechanotransduction and force-induced processes, it raises the question of whether our measurements could be influenced by AFM indentation. Although this is indeed a possibility for the flat regions of cells, mechanotransduction is believed to be activated by the simultaneous binding of receptors to specific ECM ligands, such as collagen and fibronectin. Additionally, our measurements are mainly targeted to the concave regions at the cell edge, which are known to be particularly stable during a cultured cell's lifetime. Finally, application of forces might in principle induce various topographical mechanical and rearrangements, but the physical principles behind our framework would, nevertheless, still be valid.

6.5 Effect of substrate mechanics

Most animal cells are embedded within an animal body's soft tissues. As a consequence, to more closely resemble the morphological features and functions typical of cells residing within a living organism, cultured cells must be plated on relatively-soft substrates (Pa to kPa range, depending on the tissue of origin) [97]. However, the current work was performed on cells plated on fibronectin-coated plastic and glass (~ GPa range stiffness). Because these materials are orders of magnitude more rigid than animal tissues and the cellular machineries believed to sense rigidity, we made the assumption that cells felt those substrate as infinitely rigid. This condition, which is

typical of most of biological studies performed on cultured cells, represents an intrinsic bias of our study.

Indeed, cells not only respond to rigidity by modulating aspects of their physiology such as differentiation, shape, and migration (as described in section 1.4.1.1), but tend to match their stiffness to that of the underlying substrate – i.e. stiffer substrates induce an increase in cell rigidity [259]. This dependence seems to rely on cell prestress and actomyosin activity, because blebbistatin inhibition concomitantly decreases cortex stiffness and traction forces regardless of the stiffness of the substrate [260]. This is confirmed by studies showing that cells exert higher traction forces on stiffer micrometric pillars [67].

Another interesting consideration about potential effects of substrate mechanics on our measurement is provided by substrate force load. Although cells generally prefer keeping isometric forces across structures at a given setpoint, we might expect that substrate stretching would induce a temporary increase of measured spring constant, as a result of an increase of the parameters T σ_C and σ_m within the cell.

6.6 Elastic modulus values

The *E* values interpolated from our living cells measurements are generally in the order of tens of kPa, and often exceed 100 kPa. The magnitude of these values is surprisingly high, since AFM measurements of cell mechanics performed in force-volume mode typically provide elastic modulus values ranging between 100 Pa and 10 kPa [97]. According to recent AFM microrheology

experiments, elastic modulus values are expected to further increase at high frequency of stimulation [129], although not as much as shown by our measurements (performed at ~12 kHz).

To address this apparent paradox we previously argued that elastic modulus might not be the right parameter to fit force vs. distance curves and describe cell stiffness at the nanoscale. Indeed, nanomechanical force vs. distance curves display striking linearity (Figure 19), whereas elastic modulus fitting is based on contact mechanics models predicting tip-sample contact area and tip-sample forces growing non-linearly with indentation (See section 1.3.4.2). Additionally, our results are in line with AFM studies that recently quantified the magnitude of *E* at high frequency. All these studies (performed using force stimulations ranging from 5 to 220 kHz) report values of elastic modulus one to two order of magnitude higher than in FV [152, 153, 155] , confirming the trend we observed in our experiments. Finally, *E* values depend on a large number of factors, including convolved contribution of tension, subcellular location of probing, indentation depths, and physiological state of the cell under analysis. Discrepancies might also be readily attributed to these factors.

It is also interesting noticing that our tension-free values of elastic modulus E_{TF} are approximately in the kPa range, much lower than those estimated considering the collective response of the cell (generally exceeding hundreds of kPa), which is dominated by tension.

6.7 Small hysteresis

According to microrheology studies, the viscous behavior of cells (quantified by the loss modulus) is expected to increase faster than the elastic behavior (quantified by the elastic modulus) upon

high-frequency mechanical probing (see section 2.3.2). This would result into force vs. distance curves characterized by large hysteresis. Yet, our nanoscale measurements are in contrast with this notion and display relatively little hysteresis. Although we do not have a definite answer to this paradox, we formulated some hypotheses.

First, a cell's measured viscosity is partly due to dissociation of structural and crosslinking components from the cell surface, leading to stress dissipation. Because half-life of these components is generally in the order of seconds [50], mechanical measurements performed within those timescales might reveal prominent viscosity. On the other hand, measurements at shorter timescales, such as those typical of our experiments (~13 kHz) exert indentations significantly faster than the half-life of those components.

Second, it is possible that, as measurements are performed faster, the biphasic nature of the cytoplasm hypothesized by the poroelastic model might play an important role, delaying the movement of water across the pores, and resulting in higher cytoplasm elasticity. We can verify whether this is the case by adapting Eq. (15) to our experimental conditions using rough parameter estimations. Assuming $\delta \sim 30$ nm, $R \sim 100$ nm (which roughly takes into account l_C), and $D_P \sim 40$ $\mu m^2/s$ [215], poroelastic behavior would emerge for timescales shorter than ~ 0.009 s. Because our measurement rate is ~ 13 kHz, we believe this is our case.

6.8 Membrane tension vs. cortex tension

The original formulation of the Laplace law for cell shape equilibrium (See section 1.2.7) predicts that membrane tension is the only component resisting line tension within the cell edge. However,

some groups have argued that cortex tension should have also been taken into account within the model. In this work, we assumed surface tension to correspond to σ_m. Although cortex tension is generally one order of magnitude higher than membrane tension and should, in theory, be a strong contributor of surface tension, we ruled out this possibility, based on two main considerations.

First, multiple experiments showed that peripheral arcs decrease their radius of curvature upon actin inhibition. These results were obtained upon incubation with a wide variety of drugs, such actin monomer-depleting Latrunculin A, actomyosin inhibitors BDM [91] and blebbistatin [94], and ROCK inhibitor Y27632 [93, 94]. These experiments suggest that a passive component – i.e. membrane tension – still acts on the periphery, regardless of actomyosin contractility or presence of polymerized actin. It should be pointed out, though, that blebbistatin has also been found to increase the radius of curvature of arcs [261].

Second, whereas the cell membrane engulfs the peripheral actin bundles, we are not aware of any direct evidence of physical connection between cortical filaments and peripheral actin bundles.

Nevertheless, we recognize that it is possible that cortex tension might partly support membrane tension in the creation of a force balance at the cell edge. In that case, although our measurements of membrane tension would no longer be valid, all other formulas would still be completely relevant by simply exchanging the σ_m with σ_C term. Numerical values of other mechanical parameters would also still be very close to those currently indicated.

6.9 Cortex tension values

Our study estimates cortex tension of fibroblasts to range between ~ 300 and 1500 pN/µm. These values are in line with values found in literature. Table 1 lists a collection of cortex tension values acquired by independent groups, using different techniques and underlying assumptions.

	VALUE	SYSTEM	TECHNIQUE	AUTHORS
σ_C	20 pN/µm	Neutrophils	Bead indentation	Lomakina et al. 2004[250]
σ_C	1500 pN/µm	Dictyostelium	Micropipette aspiration	Dai et al. 1999[262]
σ_C	35 pN/µm	Neutrophils	Bead indentation	Simon et al. 2007[263]
σ_C	33 pN/µm	Neutrophils	Micropipette aspiration	Herant et al. 2005[264]
σ_C	4100 pN/µm	Dictyostelium	Indentation	Pasternak et al. 1989[265]
σ_C	1500 pN/µm	Lymphocyte	Indentation	Pasternak et al. 1985[251]
σ_C	35 pN/µm	Granulocytes	Micropipette aspiration	Evans and Yeung 1989[113]
σ_C	4330 pN/µm	Dictyostelium	Micropipette aspiration	Schwarz et al. 2000[266]
σ_C	300 pN/µm	Chick fibroblasts	Micropipette aspiration	Thoumine et al. 1999[52]
σ_C	413 pN/µm	Mouse fibroblasts	Micropipette aspiration	Tinevez et al. 2009[190]
σ_C	55 pN/nm	Zebrafish ectoderm	AFM indentation	Krieg et al. 2008[267]
σ_C	200 pN/µm	HeLa in metaphase	Cell compression	Fischer-Friedrich et al. 2014[221]
σ_C	1600 pN/µm	HeLa in mitosis	Compression	Fischer-Friedrich et al. 2014[221]

Table 1: Cortex tension literature values

Sample of cortex tension measurements from the current literature. In most of the cases, values technically refer to the collective surface tension and might, hence, be slightly overestimated due to the unsubtracted contribution of membrane tension.

6.10 Membrane tension values

Our study estimates membrane tension values between 121 and 191 pN/μm. These values are in broad agreement with those obtained with other techniques, namely tether pulling assays and measurement based on thermal vibrations (Table 2). The numerical disagreement between our values and some of those acquired harnessing tether pulling assays might be due to the underlying assumptions and limitations of both techniques. For example, as described in section 2.2.6, σ_m values determined via tether pulling assays directly depend on the bending modulus of the plasma membrane and the thickness of the tether. While bending modulus might vary across cell types - but is assumed to be constant - the tether diameter might not be constant across the tether length and its diameter might not be accurately determined from diffraction limited-optical images.

Tether pulling assays mostly rely on Eq. (11) and thus measure apparent membrane tension, rather than the in-plane membrane tension. Even when tether pulling assays are performed on blebs, in-plane tension values are based on the assumption that the pulled tethers are not influenced by neighboring membrane proteins. On the other hand, our measurements might offer membrane tension values unaffected by the term γ.

	VALUE	SYSTEM	TECHNIQUE	AUTHORS
σ_m	11 pN/µm	Melanoma cells	OT tether pulling	Dai and Sheetz 1999[200]
σ_m	3 pN/µm	Renal epithelial cells	OT tether pulling	Dai and Sheetz 1999[200]
σ_m	90 pN/µm	Nerve growth cone	Leading edge model	Craig et al. 2012[268]
σ_m	250 pN/µm	"Cyber" cells	Area-based estimation	Herant and Dembo 2010[269]
σ_m	1000 pN/µm	Red blood cells	AFM indentation	Sen et al. 2005 [19]
σ_m	39 pN/µm	Mouse fibroblasts	Micropipette asp.	Tinevez et al. 2009[190]
σ_{mAPP}	36 pN/µm	Melanoma cells	OT tether pulling	Dai and Sheetz 1999[200]
σ_{mAPP}	15 pN/µm	Renal epithelial cells	OT tether pulling	Dai and Sheetz 1999[200]
σ_{mAPP}	2 pN/µm	Red blood cells	Optical interferometry	Popescu et al. 2006[20]
σ_{mAPP}	150 pN/µm	C. elegans sperm cell	OT tether pulling	Batchelder et al. 2011[270]
σ_{mAPP}	520 pN/µm	Kidney epith. cells	AFM tether pulling	Brückner et al 2015[271]
σ_{mAPP}	30 pN/µm	Mouse fibroblasts	OT tether pulling	Raucher and Sheetz 2000[11]
σ_{mAPP}	276 pN/µm	Fish keratocytes	OT tether pulling	Lieber et al. 2013[201]
σ_{mAPP}	250 pN/µm	Kidney epith. cells	AFM tether pulling	Pietuch et al. 2013[272]
σ_{mAPP}	365 pN/µm	Fish keratocyte edge	OT tether pulling	Lieber et al. 2015[273]
σ_{mAPP}	280 pN/µm	Fish keratocyte rear	OT tether pulling	Lieber et al. 2015[273]

Table 2: Membrane tension literature values

Sample of membrane tension measurements from the current literature. σ_m stands for membrane tension. σ_{mAPP} stands for apparent membrane tension, OT stands for optical trap.

Although some studies show that σ_m is a constant parameters within a given cell type, it is currently unclear whether cells keep σ_m at a preferred value [244]. Our study show that membrane tension is relatively uniform across the different cells tested, hence supporting the idea that cells prefer keeping membrane tension at a defined set-point, and confirming the notion that membrane tension is a tightly-regulated parameter.

6.11 Peripheral bundle tension values

Based on our model, we estimate tension within peripheral bundles to range between ~ 1 and 8 nN. Although a high number of studies characterized traction forces *in vivo*, force measurements across single actin bundles or stress fibers have so far been limited. Cells plated on micropillars and on elastic gels generally exhibit average ~10 nN centripetal forces, and peak forces around 30 nN for focal adhesions at the edge of the cell [68], setting an approximate upper limit to the traction forces possibly exerted by stress fibers. Indeed, we would expect peripheral bundle forces to be lower, due to the possibility of membrane tension, cortex tension and actomyosin contraction pulling along the same direction.

A few approaches have been employed to measure forces in single bundles. Deguchi et al. measured peripheral actin bundle length, extracted them from cells allowing strain relaxation, and applied the tensile stress necessary for bundles to return to their original lengths – similarly to experiments previously described in section 1.2.6. They reported stresses around 4 nN in peripheral actin bundles of endothelial cells [88]. Others cultured cells on special substrates designed to access peripheral bundles from the side through soft cantilevers. Their estimate was 95 nN, but their modeling neglected other force components acting at the cell edge besides bundle tension [124]. A similar approach by the same group reported tension within the 1 to 18 nN range when the fiber was indeed isolated from the neighboring cell material [274]. Finally, it is possible to estimate peripheral bundle tension considering the force equilibrium resulting from a modified Laplace law - as discussed in section 1.2.7. This procedure involves measuring the radius of curvature of the bundle and estimating either the membrane [93] or cortex tension [275], depending

on the specific assumption of the underlying model. Bundle tension estimated with this method range between several to a few tens of nN.

Regardless of the actual force value, it should be mentioned that cell traction forces certainly depend on the rigidity of the substrate. Generally, traction forces increase linearly with rigidity, then they reach a saturation once at a certain rigidity threshold [67]. In the present study, and in most of the studies presented in this paragraph, estimated forces should relate to the saturation regime.

6.12 A unified view of nanoscale mechanics of cells

Taken together, our results point to a novel view of cell mechanics, whereas nanodeformability of cells and force transmission are intimately connected and easily convertible into each other.

A powerful link between these two is provided by coupling distances. These quantities represent the lateral extent of force transmission upon vertical force application, i.e. they quantify the "mechanical horizon" of a given force application. While in this work pN-scale forces were generated by an AFM tip, the same principles can be applied to the pN-range forces generated between neighboring cells, across a cell's volume, and between a cell and its substrate. As a consequence, the knowledge of coupling distances can inform us on how these forces can be transmitted across cellular lengthscales and between different structures. Importantly, cells could in principle regulate their physiology by modifying their tension or their local stiffness, resulting in opposite effects in the extent of force propagation. This regulation could be useful, for example,

to spatially confine opening of membrane channels, activation of molecules, and formation of bonds.

We will now discuss the latter case in more detail. It is known that cell prestress helps integrin clustering and FA maturation. This is generally believed to be mediated by mechanotransduction events caused by protein conformational changes, and by allosteric changes in integrins that extend to their intracellular domains. Our results support the view that tension and intrinsic stiffness can offer an additional layer of regulation through an additional mechanism. Indeed, it is possible that the nanorigidity of intracellular elements such as cortex and focal adhesion materials, would regulate the isometric forces between ligand and receptor, thus changing a bond's lifetime [276]. Additionally, the regulation of cellular coupling distances could change the likelihood of distant bond formation by modulating the distance between ligands and receptors. This was suggested to be the case for glycocalyx, whose rigidity has been regarded an important factor in integrin clustering [277]. A similar mechanism based on actomyosin tension along bundles could also explain the unidirectional growth of focal adhesion and their elongated shape in their mature form.

Bibliography

1. Iskratsch, T., H. Wolfenson, and M.P. Sheetz, *Appreciating force and shape-the rise of mechanotransduction in cell biology.* Nat Rev Mol Cell Biol, 2014. **15**(12): p. 825-33.

2. Wang, N., J.D. Tytell, and D.E. Ingber, *Mechanotransduction at a distance: mechanically coupling the extracellular matrix with the nucleus.* Nature Reviews Molecular Cell Biology, 2009. **10**(1): p. 75-82.

3. Dumont, S. and M. Prakash, *Emergent mechanics of biological structures.* Molecular Biology of the Cell, 2014. **25**(22): p. 3461-3465.

4. Rief, M., et al., *Reversible unfolding of individual titin immunoglobulin domains by AFM.* Science, 1997. **276**(5315): p. 1109-1112.

5. Kole, T.P., et al., *Intracellular mechanics of migrating fibroblasts.* Molecular Biology of the Cell, 2005. **16**(1): p. 328-338.

6. Shao, J.Y., H.P. Ting-Beall, and R.M. Hochmuth, *Static and dynamic lengths of neutrophil microvilli.* Proceedings of the National Academy of Sciences of the United States of America, 1998. **95**(12): p. 6797-6802.

7. Singer, S.J. and G.L. Nicolson, *The fluid mosaic model of the structure of cell membranes.* Science, 1972. **175**(4023): p. 720-31.

8. Nicolson, G.L., *The Fluid-Mosaic Model of Membrane Structure: still relevant to understanding the structure, function and dynamics of biological membranes after more than 40 years.* Biochim Biophys Acta, 2014. **1838**(6): p. 1451-66.

9. Apodaca, G., *Modulation of membrane traffic by mechanical stimuli.* Am J Physiol Renal Physiol, 2002. **282**(2): p. F179-90.

10. Sheetz, M.P., *Cell control by membrane-cytoskeleton adhesion.* Nat Rev Mol Cell Biol, 2001. **2**(5): p. 392-6.

11. Raucher, D. and M.P. Sheetz, *Cell spreading and lamellipodial extension rate is regulated by membrane tension.* Journal of Cell Biology, 2000. **148**(1): p. 127-136.

12. Keren, K., et al., *Mechanism of shape determination in motile cells.* Nature, 2008. **453**(7194): p. 475-U1.

13. Gauthier, N.C., et al., *Temporary increase in plasma membrane tension coordinates the activation of exocytosis and contraction during cell spreading.* Proc Natl Acad Sci U S A, 2011. **108**(35): p. 14467-72.

14. Houk, A.R., et al., *Membrane tension maintains cell polarity by confining signals to the leading edge during neutrophil migration.* Cell, 2012. **148**(1-2): p. 175-88.

15. Togo, T., T.B. Krasieva, and R.A. Steinhardt, *A decrease in membrane tension precedes successful cell-membrane repair.* Mol Biol Cell, 2000. **11**(12): p. 4339-46.

16. Clark, A.G., et al., *Stresses at the Cell Surface during Animal Cell Morphogenesis.* Current Biology, 2014. **24**(10): p. R484-R494.

17. Parton, R.G. and M.A. del Pozo, *Caveolae as plasma membrane sensors, protectors and organizers.* Nature Reviews Molecular Cell Biology, 2013. **14**(2): p. 98-112.

18. Sinha, B., et al., *Cells respond to mechanical stress by rapid disassembly of caveolae.* Cell, 2011. **144**(3): p. 402-13.

19. Sen, S., S. Subramanian, and D.E. Discher, *Indentation and adhesive probing of a cell membrane with AFM: theoretical model and experiments.* Biophys J, 2005. **89**(5): p. 3203-13.

20. Popescu, G., et al., *Optical measurement of cell membrane tension.* Physical Review Letters, 2006. **97**(21).

21. GM, C. *The Cell: A Molecular Approach. . 2nd edition.*; Available from: http://www.ncbi.nlm.nih.gov/books/NBK9834/.

22. Reitsma, S., et al., *The endothelial glycocalyx: composition, functions, and visualization.* Pflugers Archiv-European Journal of Physiology, 2007. **454**(3): p. 345-359.

23. Fels, J., et al., *Nanomechanics of vascular endothelium.* Cell Tissue Res, 2014. **355**(3): p. 727-37.

24. Marsh, G. and R.E. Waugh, *Quantifying the mechanical properties of the endothelial glycocalyx with atomic force microscopy.* J Vis Exp, 2013(72): p. e50163.

25. Dahl, K.N., A.J.S. Ribeiro, and J. Lammerding, *Nuclear shape, mechanics, and mechanotransduction.* Circulation Research, 2008. **102**(11): p. 1307-1318.

26. Guilak, F., J.R. Tedrow, and R. Burgkart, *Viscoelastic properties of the cell nucleus.* Biochemical and Biophysical Research Communications, 2000. **269**(3): p. 781-786.

27. Haga, H., et al., *Elasticity mapping of living fibroblasts by AFM and immunofluorescence observation of the cytoskeleton.* Ultramicroscopy, 2000. **82**(1-4): p. 253-8.

28. Fletcher, D.A. and D. Mullins, *Cell mechanics and the cytoskeleton.* Nature, 2010. **463**(7280): p. 485-492.

29. Gittes, F., et al., *Flexural Rigidity of Microtubules and Actin-Filaments Measured from Thermal Fluctuations in Shape.* Journal of Cell Biology, 1993. **120**(4): p. 923-934.

30. Brangwynne, C.P., et al., *Microtubules can bear enhanced compressive loads in living cells because of lateral reinforcement.* Journal of Cell Biology, 2006. **173**(5): p. 733-741.

31. Stamenovic, D., et al., *Cell prestress. II. Contribution of microtubules.* American Journal of Physiology-Cell Physiology, 2002. **282**(3): p. C617-C624.

32. Dumont, S., *Chromosome Segregation: Spindle Mechanics Come To Life.* Current Biology, 2011. **21**(18): p. R688-R690.

33. Dumont, S., E.D. Salmon, and T.J. Mitchison, *Deformations Within Moving Kinetochores Reveal Different Sites of Active and Passive Force Generation.* Science, 2012. **337**(6092): p. 355-358.

34. Elting, M.W., et al., *Force on spindle microtubule minus ends moves chromosomes.* Journal of Cell Biology, 2014. **206**(2): p. 245-256.

35. Gruenbaum, Y. and U. Aebi, *Intermediate filaments: a dynamic network that controls cell mechanics.* F1000Prime Rep, 2014. **6**: p. 54.

36. Harada, T., et al., *Nuclear lamin stiffness is a barrier to 3D migration, but softness can limit survival.* Journal of Cell Biology, 2014. **204**(5): p. 669-682.

37. Jerome Irianto, C.R.P., Avathamsa Athirasala, Irena L. Ivanovska, Roger E. Greenberg, Dennis E. Discher, *Cell Invasion through Stiff Constrictions causes Mutations While Damaging the Nucleus*, in *Biolphysical Society Meeting 2016*. 2016.

38. Swift, J., et al., *Nuclear lamin-A scales with tissue stiffness and enhances matrix-directed differentiation.* Science, 2013. **341**(6149): p. 1240104.

39. Guo, M., et al., *The Role of Vimentin Intermediate Filaments in Cortical and Cytoplasmic Mechanics.* Biophysical Journal, 2013. **105**(7): p. 1562-1568.

40. Guo, M., et al., *Probing the Stochastic, Motor-Driven Properties of the Cytoplasm Using Force Spectrum Microscopy.* Cell, 2014. **158**(4): p. 822-832.

41. Herrmann, H., et al., *Intermediate filaments: from cell architecture to nanomechanics.* Nature Reviews Molecular Cell Biology, 2007. **8**(7): p. 562-573.

42. Goley, E.D., et al., *An actin-filament-binding interface on the Arp2/3 complex is critical for nucleation and branch stability.* Proceedings of the National Academy of Sciences of the United States of America, 2010. **107**(18): p. 8159-8164.

43. Prass, M., et al., *Direct measurement of the lamellipodial protrusive force in a migrating cell.* Journal of Cell Biology, 2006. **174**(6): p. 767-772.

44. Mattila, P.K. and P. Lappalainen, *Filopodia: molecular architecture and cellular functions.* Nature Reviews Molecular Cell Biology, 2008. **9**(6): p. 446-454.

45. Chaudhuri, O., S.H. Parekh, and D.A. Fletcher, *Reversible stress softening of actin networks.* Nature, 2007. **445**(7125): p. 295-298.

46. Gardel, M.L., et al., *Elastic Behavior of cross-linked and bundled actin networks.* Science, 2004. **304**(5675): p. 1301-1305.

47. Storm, C., et al., *Nonlinear elasticity in biological gels.* Nature, 2005. **435**(7039): p. 191-194.

48. Parekh, S.H., et al., *Loading history determines the velocity of actin-network growth.* Nature Cell Biology, 2005. **7**(12): p. 1219-1223.

49. Gardel, M.L., et al., *Prestressed F-actin networks cross-linked by hinged filamins replicate mechanical properties of cells.* Proceedings of the National Academy of Sciences of the United States of America, 2006. **103**(6): p. 1762-1767.

50. Salbreux, G., G. Charras, and E. Paluch, *Actin cortex mechanics and cellular morphogenesis.* Trends Cell Biol, 2012. **22**(10): p. 536-45.

51. Xu, K., H.P. Babcock, and X. Zhuang, *Dual-objective STORM reveals three-dimensional filament organization in the actin cytoskeleton.* Nat Methods, 2012. **9**(2): p. 185-8.

52. Thoumine, O., O. Cardoso, and J.J. Meister, *Changes in the mechanical properties of fibroblasts during spreading: a micromanipulation study.* Eur Biophys J, 1999. **28**(3): p. 222-34.

53. Ingber, D.E., *Tensegrity: The architectural basis of cellular mechanotransduction.* Annual Review of Physiology, 1997. **59**: p. 575-599.

54. Alert, R., et al., *Model for probing membrane-cortex adhesion by micropipette aspiration and fluctuation spectroscopy.* Biophys J, 2015. **108**(8): p. 1878-86.

55. Charras, G. and E. Paluch, *Blebs lead the way: how to migrate without lamellipodia.* Nat Rev Mol Cell Biol, 2008. **9**(9): p. 730-6.

56. Stewart, M.P., et al., *Hydrostatic pressure and the actomyosin cortex drive mitotic cell rounding.* Nature, 2011. **469**(7329): p. 226-30.

57. Chaigne, A., et al., *A narrow window of cortical tension guides asymmetric spindle positioning in the mouse oocyte.* Nature Communications, 2015. **6**.

58. Bergert, M., et al., *Cell mechanics control rapid transitions between blebs and lamellipodia during migration.* Proceedings of the National Academy of Sciences of the United States of America, 2012. **109**(36): p. 14434-14439.

59. Izzard, C.S. and L.R. Lochner, *Cell-to-substrate contacts in living fibroblasts: an interference reflexion study with an evaluation of the technique.* J Cell Sci, 1976. **21**(1): p. 129-59.

60. Giebel, K., et al., *Imaging of cell/substrate contacts of living cells with surface plasmon resonance microscopy.* Biophys J, 1999. **76**(1 Pt 1): p. 509-16.

61. Kim, S.H., et al., *Study of Cell-Matrix Adhesion Dynamics Using Surface Plasmon Resonance Imaging Ellipsometry.* Biophysical Journal, 2011. **100**(7): p. 1819-1828.

62. Zaidel-Bar, R., et al., *Functional atlas of the integrin adhesome.* Nature Cell Biology, 2007. **9**(8): p. 858-868.

63. Kanchanawong, P., et al., *Nanoscale architecture of integrin-based cell adhesions.* Nature, 2010. **468**(7323): p. 580-U262.

64. Roca-Cusachs, P., et al., *Clustering of alpha(5)beta(1) integrins determines adhesion strength whereas alpha(v)beta(3) and talin enable mechanotransduction.* Proceedings of the National Academy of Sciences of the United States of America, 2009. **106**(38): p. 16245-16250.

65. Patla, I., et al., *Dissecting the molecular architecture of integrin adhesion sites by cryo-electron tomography.* Nature Cell Biology, 2010. **12**(9): p. 909-915.

66. Franz, C.M. and D.J. Muller, *Analyzing focal adhesion structure by atomic force microscopy.* Journal of Cell Science, 2005. **118**(22): p. 5315-5323.

67. Ghibaudo, M., et al., *Traction forces and rigidity sensing regulate cell functions.* Soft Matter, 2008. **4**(9): p. 1836-1843.

68. Balaban, N.Q., et al., *Force and focal adhesion assembly: a close relationship studied using elastic micropatterned substrates.* Nat Cell Biol, 2001. **3**(5): p. 466-72.

69. Stricker, J., et al., *Myosin II-mediated focal adhesion maturation is tension insensitive.* PLoS One, 2013. **8**(7): p. e70652.

70. Oakes, P.W. and M.L. Gardel, *Stressing the limits of focal adhesion mechanosensitivity.* Curr Opin Cell Biol, 2014. **30**: p. 68-73.

71. Kong, F., et al., *Demonstration of catch bonds between an integrin and its ligand.* Journal of Cell Biology, 2009. **185**(7): p. 1275-1284.

72. Buckley, C.D., et al., *Cell adhesion. The minimal cadherin-catenin complex binds to actin filaments under force.* Science, 2014. **346**(6209): p. 1254211.

73. del Rio, A., et al., *Stretching single talin rod molecules activates vinculin binding.* Science, 2009. **323**(5914): p. 638-41.

74. Margadant, F., et al., *Mechanotransduction in vivo by repeated talin stretch-relaxation events depends upon vinculin.* PLoS Biol, 2011. **9**(12): p. e1001223.

75. Sawada, Y., et al., *Force sensing by mechanical extension of the Src family kinase substrate p130Cas.* Cell, 2006. **127**(5): p. 1015-26.

76. Choquet, D., D.P. Felsenfeld, and M.P. Sheetz, *Extracellular matrix rigidity causes strengthening of integrin-cytoskeleton linkages.* Cell, 1997. **88**(1): p. 39-48.

77. Hu, K., et al., *Differential transmission of actin motion within focal adhesions.* Science, 2007. **315**(5808): p. 111-5.

78. Case, L.B. and C.M. Waterman, *Integration of actin dynamics and cell adhesion by a three-dimensional, mechanosensitive molecular clutch.* Nat Cell Biol, 2015. **17**(8): p. 955-63.

79. Grashoff, C., et al., *Measuring mechanical tension across vinculin reveals regulation of focal adhesion dynamics.* Nature, 2010. **466**(7303): p. 263-6.

80. Pellegrin, S. and H. Mellor, *Actin stress fibres.* Journal of Cell Science, 2007. **120**(20): p. 3491-3499.

81. Kim, D.H., A.B. Chambliss, and D. Wirtz, *The multi-faceted role of the actin cap in cellular mechanosensation and mechanotransduction.* Soft Matter, 2013. **9**(23): p. 5516-5523.

82. Katoh, K., et al., *Isolation and contraction of the stress fiber.* Molecular Biology of the Cell, 1998. **9**(7): p. 1919-1938.

83. Deguchi, S., T. Ohashi, and M. Sato, *Tensile properties of single stress fibers isolated from cultured vascular smooth muscle cells.* Journal of Biomechanics, 2006. **39**(14): p. 2603-2610.

84. Thoresen, T., M. Lenz, and M.L. Gardel, *Reconstitution of Contractile Actomyosin Bundles.* Biophysical Journal, 2011. **100**(11): p. 2698-2705.

85. Kassianidou, E. and S. Kumar, *A biomechanical perspective on stress fiber structure and function.* Biochimica Et Biophysica Acta-Molecular Cell Research, 2015. **1853**(11): p. 3065-3074.

86. Burridge, K. and E.S. Wittchen, *The tension mounts: Stress fibers as force-generating mechanotransducers.* Journal of Cell Biology, 2013. **200**(1): p. 9-19.

87. Ikai, A., et al., *Mechanics of Intracellular Stress Fibers: A Short Review.* Japanese Journal of Applied Physics, 2011. **50**(8).

88. Deguchi, S., T. Ohashi, and M. Sato, *Evaluation of tension in actin bundle of endothelial cells based on preexisting strain and tensile properties measurements.* Mol Cell Biomech, 2005. **2**(3): p. 125-33.

89. Katoh, K., et al., *Stress fiber organization regulated by MLCK and Rho-kinase in cultured human fibroblasts.* Am J Physiol Cell Physiol, 2001. **280**(6): p. C1669-79.

90. Tanner, K., et al., *Dissecting regional variations in stress fiber mechanics in living cells with laser nanosurgery.* Biophys J, 2010. **99**(9): p. 2775-83.

91. Bar-Ziv, R., et al., *Pearling in cells: a clue to understanding cell shape.* Proc Natl Acad Sci U S A, 1999. **96**(18): p. 10140-5.

92. Zand, M.S. and G. Albrechtbuehler, *What Structures, Besides Adhesions, Prevent Spread Cells from Rounding Up.* Cell Motility and the Cytoskeleton, 1989. **13**(3): p. 195-211.

93. Thery, M., et al., *Cell distribution of stress fibres in response to the geometry of the adhesive environment.* Cell Motil Cytoskeleton, 2006. **63**(6): p. 341-55.

94. Bischofs, I.B., et al., *Filamentous network mechanics and active contractility determine cell and tissue shape.* Biophys J, 2008. **95**(7): p. 3488-96.

95. Oakes, P.W., et al., *Geometry regulates traction stresses in adherent cells.* Biophys J, 2014. **107**(4): p. 825-33.

96. Ingber, D.E., *Tensegrity I. Cell structure and hierarchical systems biology.* J Cell Sci, 2003. **116**(Pt 7): p. 1157-73.

97. Levental, I., P.C. Georges, and P.A. Janmey, *Soft biological materials and their impact on cell function.* Soft Matter, 2007. **3**(3): p. 299-306.

98. Gossett, D.R., et al., *Hydrodynamic stretching of single cells for large population mechanical phenotyping.* Proceedings of the National Academy of Sciences of the United States of America, 2012. **109**(20): p. 7630-7635.

99. Guido, I., M.S. Jaeger, and C. Duschl, *Dielectrophoretic stretching of cells allows for characterization of their mechanical properties.* European Biophysics Journal with Biophysics Letters, 2011. **40**(3): p. 281-288.

100. Sraj, I., et al., *Cell deformation cytometry using diode-bar optical stretchers.* Journal of Biomedical Optics, 2010. **15**(4).

101. Dao, M., C.T. Lim, and S. Suresh, *Mechanics of the human red blood cell deformed by optical tweezers.* Journal of the Mechanics and Physics of Solids, 2003. **51**(11-12): p. 2259-2280.

102. Fredberg, J.J., et al., *Airway smooth muscle, tidal stretches, and dynamically determined contractile states.* American Journal of Respiratory and Critical Care Medicine, 1997. **156**(6): p. 1752-1759.

103. Thoumine, O. and A. Ott, *Time scale dependent viscoelastic and contractile regimes in fibroblasts probed by microplate manipulation.* Journal of Cell Science, 1997. **110**: p. 2109-2116.

104. Bader, D.L., et al., *Deformation properties of articular chondrocytes: A critique of three separate techniques.* Biorheology, 2002. **39**(1-2): p. 69-78.

105. Tseng, Y., T.P. Kole, and D. Wirtz, *Micromechanical mapping of live cells by multiple-particle-tracking microrheology.* Biophys J, 2002. **83**(6): p. 3162-76.

106. Jonas, M., et al., *Fast fluorescence laser tracking microrheometry, II: quantitative studies of cytoskeletal mechanotransduction.* Biophys J, 2008. **95**(2): p. 895-909.

107. Yamada, S., D. Wirtz, and S.C. Kuo, *Mechanics of living cells measured by laser tracking microrheology.* Biophys J, 2000. **78**(4): p. 1736-47.

108. Wirtz, D., *Particle-tracking microrheology of living cells: principles and applications.* Annu Rev Biophys, 2009. **38**: p. 301-26.

109. Bausch, A.R., et al., *Local measurements of viscoelastic parameters of adherent cell surfaces by magnetic bead microrheometry.* Biophys J, 1998. **75**(4): p. 2038-49.

110. Fabry, B., et al., *Scaling the microrheology of living cells.* Phys Rev Lett, 2001. **87**(14): p. 148102.

111. Heidemann, S.R. and D. Wirtz, *Towards a regional approach to cell mechanics.* Trends Cell Biol, 2004. **14**(4): p. 160-6.

112. Hochmuth, R.M., *Micropipette aspiration of living cells.* J Biomech, 2000. **33**(1): p. 15-22.

113. Evans, E. and A. Yeung, *Apparent viscosity and cortical tension of blood granulocytes determined by micropipet aspiration.* Biophys J, 1989. **56**(1): p. 151-60.

114. Lim, C.T., E.H. Zhou, and S.T. Quek, *Mechanical models for living cells--a review.* J Biomech, 2006. **39**(2): p. 195-216.

115. Needham, D. and R.M. Hochmuth, *Rapid flow of passive neutrophils into a 4 microns pipet and measurement of cytoplasmic viscosity.* J Biomech Eng, 1990. **112**(3): p. 269-76.

116. Theret, D.P., et al., *The application of a homogeneous half-space model in the analysis of endothelial cell micropipette measurements.* J Biomech Eng, 1988. **110**(3): p. 190-9.

117. Rodriguez, M.L., P.J. McGarry, and N.J. Sniadecki, *Review on Cell Mechanics: Experimental and Modeling Approaches.* Applied Mechanics Reviews, 2013. **65**(6).

118. Pelling, A.E. and M.A. Horton, *An historical perspective on cell mechanics.* Pflugers Archiv-European Journal of Physiology, 2008. **456**(1): p. 3-12.

119. Radmacher, M., et al., *From Molecules to Cells - Imaging Soft Samples with the Atomic Force Microscope.* Science, 1992. **257**(5078): p. 1900-1905.

120. Ando, T., T. Uchihashi, and N. Kodera, *High-speed AFM and applications to biomolecular systems.* Annu Rev Biophys, 2013. **42**: p. 393-414.

121. Zhang, J., et al., *Real-space identification of intermolecular bonding with atomic force microscopy.* Science, 2013. **342**(6158): p. 611-4.

122. Schneider, S.W., et al., *Surface dynamics in living acinar cells imaged by atomic force microscopy: identification of plasma membrane structures involved in exocytosis.* Proc Natl Acad Sci U S A, 1997. **94**(1): p. 316-21.

123. Schafer, C., et al., *Aldosterone signaling pathway across the nuclear envelope.* Proc Natl Acad Sci U S A, 2002. **99**(10): p. 7154-9.

124. Piacentini, N., et al., *Ultra-soft cantilevers and 3-D micro-patterned substrates for contractile bundle tension measurement in living cells.* Lab Chip, 2014. **14**(14): p. 2539-47.

125. Bhushan, B. and O. Marti, *Scanning Probe Microscopy – Principle of Operation, Instrumentation, and Probes*, in *Springer Handbook of Nanotechnology*, B. Bhushan, Editor. 2004, Springer Berlin Heidelberg: Berlin, Heidelberg. p. 325-369.

126. Radmacher, M., *Studying the mechanics of cellular processes by atomic force microscopy.* Methods Cell Biol, 2007. **83**: p. 347-72.

127. Derjaguin, B.V., V.M. Muller, and Y.P. Toporov, *Effect of Contact Deformations on the Adhesion of Particles.* Progress in Surface Science, 1994. **45**(1-4): p. 131-143.

128. Smith, B.A., et al., *Probing the viscoelastic behavior of cultured airway smooth muscle cells with atomic force microscopy: Stiffening induced by contractile agonist.* Biophysical Journal, 2005. **88**(4): p. 2994-3007.

129. Rigato, A., *Characterization of cell mechanics with atomic force microscopy: mechanical mapping and high speed microrheology*. 2015, Aix-Marseille Université.

130. Plodinec, M., M. Loparic, and U. Aebi, *Imaging Fibroblast Cells Using Atomic Force Microscopy (AFM).* Cold Spring Harbor Protocols, 2010. **2010**(10): p. pdb.prot5500.

131. Kuznetsova, T.G., et al., *Atomic force microscopy probing of cell elasticity*. Micron, 2007. **38**(8): p. 824-833.

132. Rotsch, C., K. Jacobson, and M. Radmacher, *Dimensional and mechanical dynamics of active and stable edges in motile fibroblasts investigated by using atomic force microscopy.* Proc Natl Acad Sci U S A, 1999. **96**(3): p. 921-6.

133. Rotsch, C. and M. Radmacher, *Drug-induced changes of cytoskeletal structure and mechanics in fibroblasts: an atomic force microscopy study.* Biophys J, 2000. **78**(1): p. 520-35.

134. Martens, J.C. and M. Radmacher, *Softening of the actin cytoskeleton by inhibition of myosin II.* Pflugers Arch, 2008. **456**(1): p. 95-100.

135. Schafer, A. and M. Radmacher, *Influence of myosin II activity on stiffness of fibroblast cells.* Acta Biomater, 2005. **1**(3): p. 273-80.

136. Matzke, R., K. Jacobson, and M. Radmacher, *Direct, high-resolution measurement of furrow stiffening during division of adherent cells.* Nat Cell Biol, 2001. **3**(6): p. 607-10.

137. Oberleithner, H., et al., *Potassium softens vascular endothelium and increases nitric oxide release.* Proc Natl Acad Sci U S A, 2009. **106**(8): p. 2829-34.

138. Stolz, M., et al., *Early detection of aging cartilage and osteoarthritis in mice and patient samples using atomic force microscopy.* Nat Nanotechnol, 2009. **4**(3): p. 186-92.

139. Jin, H., et al., *Detection of erythrocytes influenced by aging and type 2 diabetes using atomic force microscope.* Biochemical and Biophysical Research Communications, 2010. **391**(4): p. 1698-1702.

140. Cross, S.E., et al., *Nanomechanical analysis of cells from cancer patients.* Nat Nanotechnol, 2007. **2**(12): p. 780-3.

141. Plodinec, M., et al., *The nanomechanical signature of breast cancer.* Nat Nanotechnol, 2012. **7**(11): p. 757-65.

142. Iyer, S., et al., *Atomic force microscopy detects differences in the surface brush of normal and cancerous cells.* Nat Nanotechnol, 2009. **4**(6): p. 389-93.

143. Dufrene, Y.F., et al., *Multiparametric imaging of biological systems by force-distance curve-based AFM.* Nature Methods, 2013. **10**(9): p. 847-854.

144. Gavara, N. and R.S. Chadwick, *Determination of the elastic moduli of thin samples and adherent cells using conical atomic force microscope tips.* Nat Nanotechnol, 2012. **7**(11): p. 733-6.

145. Rigato, A., et al., *Atomic Force Microscopy Mechanical Mapping of Micropatterned Cells Shows Adhesion Geometry-Dependent Mechanical Response on Local and Global Scales.* Acs Nano, 2015. **9**(6): p. 5846-5856.

146. Braunsmann, C., et al., *High-speed force mapping on living cells with a small cantilever atomic force microscope.* Review of Scientific Instruments, 2014. **85**(7).

147. Eghiaian, F., A. Rigato, and S. Scheuring, *Structural, Mechanical, and Dynamical Variability of the Actin Cortex in Living Cells.* Biophysical Journal, 2015. **108**(6): p. 1330-1340.

148. Sahin, O., et al., *High-resolution imaging of elastic properties using harmonic cantilevers.* Sensors and Actuators a-Physical, 2004. **114**(2-3): p. 183-190.

149. Sahin, O. and A. Atalar, *Simulation of higher harmonics generation in tapping-mode atomic force microscopy.* Applied Physics Letters, 2001. **79**(26): p. 4455-4457.

150. Garcia, R. and E.T. Herruzo, *The emergence of multifrequency force microscopy.* Nature Nanotechnology, 2012. **7**(4): p. 217-226.

151. Dulebo, A., et al., *Second harmonic atomic force microscopy imaging of live and fixed mammalian cells.* Ultramicroscopy, 2009. **109**(8): p. 1056-1060.

152. Raman, A., et al., *Mapping nanomechanical properties of live cells using multi-harmonic atomic force microscopy.* Nat Nanotechnol, 2011. **6**(12): p. 809-14.

153. Cartagena-Rivera, A.X., et al., *Fast, multi-frequency, and quantitative nanomechanical mapping of live cells using the atomic force microscope.* Sci Rep, 2015. **5**: p. 11692.

154. Sarioglu, A.F. and O. Solgaard, *Cantilevers with integrated sensor for time-resolved force measurement in tapping-mode atomic force microscopy.* Applied Physics Letters, 2008. **93**(2).

155. Wang, A., et al., *Fast Stiffness Mapping of Cells Using High-Bandwidth Atomic Force Microscopy.* Acs Nano, 2016. **10**(1): p. 257-264.

156. Steward, R.L., et al., *Illuminating human health through cell mechanics.* Swiss Medical Weekly, 2013. **143**.

157. Suresh, S., et al., *Connections between single-cell biomechanics and human disease states: gastrointestinal cancer and malaria.* Acta Biomaterialia, 2005. **1**(1): p. 15-30.

158. Kumar, S. and V. Weaver, *Mechanics, malignancy, and metastasis: The force journey of a tumor cell.* Cancer and Metastasis Reviews, 2009. **28**(1-2): p. 113-127.

159. Tamplenizza, M., et al., *Nitric oxide synthase mediates PC12 differentiation induced by the surface topography of nanostructured TiO2.* Journal of Nanobiotechnology, 2013. **11**.

160. Prager-Khoutorsky, M., et al., *Fibroblast polarization is a matrix-rigidity-dependent process controlled by focal adhesion mechanosensing.* Nature Cell Biology, 2011. **13**(12): p. 1457-U178.

161. Engler, A.J., et al., *Matrix elasticity directs stem cell lineage specification.* Cell, 2006. **126**(4): p. 677-689.

162. Lo, C.M., et al., *Cell movement is guided by the rigidity of the substrate.* Biophysical Journal, 2000. **79**(1): p. 144-152.

163. Mammoto, T., A. Mammoto, and D.E. Ingber, *Mechanobiology and Developmental Control.* Annual Review of Cell and Developmental Biology, Vol 29, 2013. **29**: p. 27-61.

164. Wirtz, D., K. Konstantopoulos, and P.C. Searson, *The physics of cancer: the role of physical interactions and mechanical forces in metastasis.* Nat Rev Cancer, 2011. **11**(7): p. 512-22.

165. Guck, J., et al., *Optical deformability as an inherent cell marker for testing malignant transformation and metastatic competence.* Biophysical Journal, 2005. **88**(5): p. 3689-3698.

166. Jonietz, E., *MECHANICS The forces of cancer.* Nature, 2012. **491**(7425): p. S56-S57.

167. Lam, W.A., M.J. Rosenbluth, and D.A. Fletcher, *Increased leukaemia cell stiffness is associated with symptoms of leucostasis in paediatric acute lymphoblastic leukaemia.* British Journal of Haematology, 2008. **142**(3): p. 497-501.

168. Mitchison, T.J., G.T. Charras, and L. Mahadevan, *Implications of a poroelastic cytoplasm for the dynamics of animal cell shape.* Seminars in Cell & Developmental Biology, 2008. **19**(3): p. 215-223.

169. Hoffman, B.D., C. Grashoff, and M.A. Schwartz, *Dynamic molecular processes mediate cellular mechanotransduction.* Nature, 2011. **475**(7356): p. 316-323.

170. Ingber, D.E., *Mechanobiology and diseases of mechanotransduction.* Annals of Medicine, 2003. **35**(8): p. 564-577.

171. Piston, D.W. and G.J. Kremers, *Fluorescent protein FRET: the good, the bad and the ugly.* Trends Biochem Sci, 2007. **32**(9): p. 407-14.

172. Borghi, N., et al., *E-cadherin is under constitutive actomyosin-generated tension that is increased at cell-cell contacts upon externally applied stretch (vol 109, 12568, 2012).* Proceedings of the National Academy of Sciences of the United States of America, 2012. **109**(46): p. 19034-19034.

173. Chang, C.W. and S. Kumar, *Vinculin tension distributions of individual stress fibers within cell-matrix adhesions.* J Cell Sci, 2013. **126**(Pt 14): p. 3021-30.

174. Zhang, Y., et al., *DNA-based digital tension probes reveal integrin forces during early cell adhesion.* Nat Commun, 2014. **5**: p. 5167.

175. Blakely, B.L., et al., *A DNA-based molecular probe for optically reporting cellular traction forces.* Nat Methods, 2014. **11**(12): p. 1229-32.

176. Gayrard, C. and N. Borghi, *FRET-based Molecular Tension Microscopy.* Methods, 2016. **94**: p. 33-42.

177. Paluch, E.K., et al., *Mechanotransduction: use the force(s).* Bmc Biology, 2015. **13**.

178. Harris, A.K., P. Wild, and D. Stopak, *Silicone-Rubber Substrata - New Wrinkle in the Study of Cell Locomotion.* Science, 1980. **208**(4440): p. 177-179.

179. Beningo, K.A., et al., *Nascent focal adhesions are responsible for the generation of strong propulsive forces in migrating fibroblasts.* J Cell Biol, 2001. **153**(4): p. 881-8.

180. Wang, Y.L., *Traction forces and rigidity sensing of adherent cells.* Conf Proc IEEE Eng Med Biol Soc, 2009. **2009**: p. 3339-40.

181. Ladoux, B. and A. Nicolas, *Physically based principles of cell adhesion mechanosensitivity in tissues.* Reports on Progress in Physics, 2012. **75**(11).

182. Galbraith, C.G. and M.P. Sheetz, *A micromachined device provides a new bend on fibroblast traction forces.* Proceedings of the National Academy of Sciences of the United States of America, 1997. **94**(17): p. 9114-9118.

183. Tan, J.L., et al., *Cells lying on a bed of microneedles: an approach to isolate mechanical force.* Proc Natl Acad Sci U S A, 2003. **100**(4): p. 1484-9.

184. Rossier, O.M., et al., *Force generated by actomyosin contraction builds bridges between adhesive contacts.* EMBO J, 2010. **29**(6): p. 1055-68.

185. Lemmon, C.A., C.S. Chen, and L.H. Romer, *Cell traction forces direct fibronectin matrix assembly.* Biophys J, 2009. **96**(2): p. 729-38.

186. Ghassemi, S., et al., *Cells test substrate rigidity by local contractions on submicrometer pillars.* Proc Natl Acad Sci U S A, 2012. **109**(14): p. 5328-33.

187. Wolfenson, H., et al., *Tropomyosin controls sarcomere-like contractions for rigidity sensing and suppressing growth on soft matrices.* Nat Cell Biol, 2016. **18**(1): p. 33-42.

188. le Digabel, J., et al., *Microfabricated substrates as a tool to study cell mechanotransduction.* Medical & Biological Engineering & Computing, 2010. **48**(10): p. 965-976.

189. Bergert, M., et al., *Force transmission during adhesion-independent migration.* Nat Cell Biol, 2015. **17**(4): p. 524-9.

190. Tinevez, J.Y., et al., *Role of cortical tension in bleb growth.* Proceedings of the National Academy of Sciences of the United States of America, 2009. **106**(44): p. 18581-18586.

191. Heisterkamp, A., et al., *Pulse energy dependence of subcellular dissection by femtosecond laser pulses.* Opt Express, 2005. **13**(10): p. 3690-6.

192. Kumar, S., et al., *Viscoelastic retraction of single living stress fibers and its impact on cell shape, cytoskeletal organization, and extracellular matrix mechanics.* Biophys J, 2006. **90**(10): p. 3762-73.

193. Colombelli, J., et al., *Mechanosensing in actin stress fibers revealed by a close correlation between force and protein localization.* J Cell Sci, 2009. **122**(Pt 10): p. 1665-79.

194. Lele, T.P., et al., *Mechanical forces alter zyxin unbinding kinetics within focal adhesions of living cells.* J Cell Physiol, 2006. **207**(1): p. 187-94.

195. Rauzi, M., et al., *Nature and anisotropy of cortical forces orienting Drosophila tissue morphogenesis.* Nat Cell Biol, 2008. **10**(12): p. 1401-10.

196. Jiang, G.Y., et al., *Two-piconewton slip bond between fibronectin and the cytoskeleton depends on talin.* Nature, 2003. **424**(6946): p. 334-337.

197. Sens, P. and J. Plastino, *Membrane tension and cytoskeleton organization in cell motility.* J Phys Condens Matter, 2015. **27**(27): p. 273103.

198. Dai, J. and M.P. Sheetz, *Mechanical properties of neuronal growth cone membranes studied by tether formation with laser optical tweezers.* Biophys J, 1995. **68**(3): p. 988-96.

199. Hochmuth, R.M., et al., *Deformation and flow of membrane into tethers extracted from neuronal growth cones.* Biophysical Journal, 1996. **70**(1): p. 358-369.

200. Dai, J.W. and M.P. Sheetz, *Membrane tether formation from blebbing cells.* Biophysical Journal, 1999. **77**(6): p. 3363-3370.

201. Lieber, A.D., et al., *Membrane Tension in Rapidly Moving Cells Is Determined by Cytoskeletal Forces.* Current Biology, 2013. **23**(15): p. 1409-1417.

202. Bo, L. and R.E. Waugh, *Determination of Bilayer-Membrane Bending Stiffness by Tether Formation from Giant, Thin-Walled Vesicles.* Biophysical Journal, 1989. **55**(3): p. 509-517.

203. Schmid-Schonbein, G.W., et al., *Passive mechanical properties of human leukocytes.* Biophys J, 1981. **36**(1): p. 243-56.

204. Kan, H.C., et al., *Hydrodynamics of a compound drop with application to leukocyte modeling.* Physics of Fluids, 1998. **10**(4): p. 760-774.

205. Mandadapu, K.K., S. Govindjee, and M.R. Mofrad, *On the cytoskeleton and soft glassy rheology.* J Biomech, 2008. **41**(7): p. 1467-78.

206. Deng, L., et al., *Fast and slow dynamics of the cytoskeleton.* Nat Mater, 2006. **5**(8): p. 636-40.

207. Stamenovic, D., et al., *Rheology of airway smooth muscle cells is associated with cytoskeletal contractile stress.* Journal of Applied Physiology, 2004. **96**(5): p. 1600-1605.

208. Alcaraz, J., et al., *Microrheology of human lung epithelial cells measured by atomic force microscopy.* Biophysical Journal, 2003. **84**(3): p. 2071-2079.

209. Rother, J., et al., *Atomic force microscopy-based microrheology reveals significant differences in the viscoelastic response between malign and benign cell lines.* Open Biology, 2014. **4**(5).

210. Hoffman, B.D. and J.C. Crocker, *Cell mechanics: dissecting the physical responses of cells to force.* Annu Rev Biomed Eng, 2009. **11**: p. 259-88.

211. Janmey, P.A., et al., *Resemblance of actin-binding protein/actin gels to covalently crosslinked networks.* Nature, 1990. **345**(6270): p. 89-92.

212. Stossel, T.P., *On the crawling of animal cells.* Science, 1993. **260**(5111): p. 1086-94.

213. Charras, G.T., et al., *Non-equilibration of hydrostatic pressure in blebbing cells.* Nature, 2005. **435**(7040): p. 365-369.

214. Charras, G.T., T.J. Mitchison, and L. Mahadevan, *Animal cell hydraulics.* Journal of Cell Science, 2009. **122**(18): p. 3233-3241.

215. Moeendarbary, E., et al., *The cytoplasm of living cells behaves as a poroelastic material.* Nature Materials, 2013. **12**(3): p. 253-261.

216. Ingber, D.E., *Cellular Tensegrity - Defining New Rules of Biological Design That Govern the Cytoskeleton.* Journal of Cell Science, 1993. **104**: p. 613-627.

217. Stamenovic, D., *Effects of cytoskeletal prestress on cell rheological behavior.* Acta Biomaterialia, 2005. **1**(3): p. 255-262.

218. Wang, N., J.P. Butler, and D.E. Ingber, *Mechanotransduction across the cell surface and through the cytoskeleton.* Science, 1993. **260**(5111): p. 1124-7.

219. Wang, N., et al., *Mechanical behavior in living cells consistent with the tensegrity model.* Proc Natl Acad Sci U S A, 2001. **98**(14): p. 7765-70.

220. Heidemann, S.R., P. Lamoureaux, and R.E. Buxbaum, *Opposing views on tensegrity as a structural framework for understanding cell mechanics.* Journal of Applied Physiology, 2000. **89**(4): p. 1670-1674.

221. Fischer-Friedrich, E., et al., *Quantification of surface tension and internal pressure generated by single mitotic cells.* Scientific Reports, 2014. **4**.

222. Canovic, E.P., et al., *Biomechanical imaging of cell stiffness and prestress with subcellular resolution.* Biomechanics and Modeling in Mechanobiology, 2014. **13**(3): p. 665-678.

223. Lu, L., et al., *Mechanical Properties of Actin Stress Fibers in Living Cells.* Biophysical Journal, 2008. **95**(12): p. 6060-6071.

224. Wakatsuki, T., et al., *Effects of cytochalasin D and latrunculin B on mechanical properties of cells.* Journal of Cell Science, 2001. **114**(5): p. 1025-1036.

225. Gardel, M.L., et al., *Stress-dependent elasticity of composite actin networks as a model for cell behavior.* Physical Review Letters, 2006. **96**(8).

226. Bhushan, B., *Springer Handbook of Nanotechnology*. 2010: Springer Berlin Heidelberg.

227. Sahin, O., et al., *An atomic force microscope tip designed to measure time-varying nanomechanical forces.* Nature Nanotechnology, 2007. **2**(8): p. 507-514.

228. Sahin, O., *Accessing Time-Varying Forces on the Vibrating Tip of the Dynamic Atomic Force Microscope to Map Material Composition.* Israel Journal of Chemistry, 2008. **48**(2): p. 55-63.

229. Sahin, O. and N. Erina, *High-resolution and large dynamic range nanomechanical mapping in tapping-mode atomic force microscopy.* Nanotechnology, 2008. **19**(44).

230. Husale, S., H.H.J. Persson, and O. Sahin, *DNA nanomechanics allows direct digital detection of complementary DNA and microRNA targets.* Nature, 2009. **462**(7276): p. 1075-U138.

231. Dong, M.D., S. Husale, and O. Sahin, *Determination of protein structural flexibility by microsecond force spectroscopy.* Nature Nanotechnology, 2009. **4**(8): p. 514-517.

232. Kim, D. and O. Sahin, *Imaging and three-dimensional reconstruction of chemical groups inside a protein complex using atomic force microscopy.* Nature Nanotechnology, 2015. **10**(3): p. 264-269.

233. Sahin, O., et al., *Resonant harmonic response in tapping-mode atomic force microscopy.* Physical Review B, 2004. **69**(16).

234. Harrison, C., et al., *On the response of a resonating plate in a liquid near a solid wall.* Sensors and Actuators a-Physical, 2007. **134**(2): p. 414-426.

235. Sun, M., et al., *Multiple membrane tethers probed by atomic force microscopy.* Biophys J, 2005. **89**(6): p. 4320-9.

236. Sader, J.E., J.W.M. Chon, and P. Mulvaney, *Calibration of rectangular atomic force microscope cantilevers.* Review of Scientific Instruments, 1999. **70**(10): p. 3967-3969.

237. Green, C.P., et al., *Normal and torsional spring constants of atomic force microscope cantilevers.* Review of Scientific Instruments, 2004. **75**(6): p. 1988-1996.

238. Cunningham, C.C., et al., *Actin-Binding Protein Requirement for Cortical Stability and Efficient Locomotion.* Science, 1992. **255**(5042): p. 325-327.

239. Su, J., M. Muranjan, and J. Sap, *Receptor protein tyrosine phosphatase alpha activates Src-family kinases and controls integrin-mediated responses in fibroblasts.* Current Biology, 1999. **9**(10): p. 505-511.

240. Smith, M.B., et al., *Segmentation and Tracking of Cytoskeletal Filaments Using Open Active Contours.* Cytoskeleton, 2010. **67**(11): p. 693-705.

241. Wu, C.T., et al., *Disease and region-related cardiac fibroblast potassium current variations and potential functional significance.* Cardiovasc Res, 2014. **102**(3): p. 487-96.

242. Sharma, V., et al., *Study and Manipulation of Charges Present in Silicon Nitride Films.* 2013 Ieee 39th Photovoltaic Specialists Conference (Pvsc), 2013: p. 1288-1293.

243. Fuchs, E. and D.W. Cleveland, *A structural scaffolding of intermediate filaments in health and disease.* Science, 1998. **279**(5350): p. 514-519.

244. Diz-Munoz, A., D.A. Fletcher, and O.D. Weiner, *Use the force: membrane tension as an organizer of cell shape and motility.* Trends in Cell Biology, 2013. **23**(2): p. 47-53.

245. Aratyn-Schaus, Y., P.W. Oakes, and M.L. Gardel, *Dynamic and structural signatures of lamellar actomyosin force generation.* Mol Biol Cell, 2011. **22**(8): p. 1330-9.

246. Straight, A.F., et al., *Dissecting temporal and spatial control of cytokinesis with a myosin II Inhibitor.* Science, 2003. **299**(5613): p. 1743-7.

247. Shutova, M., et al., *Functions of nonmuscle myosin II in assembly of the cellular contractile system.* PLoS One, 2012. **7**(7): p. e40814.

248. Rico, F., et al., *Cell dynamic adhesion and elastic properties probed with cylindrical atomic force microscopy cantilever tips.* J Mol Recognit, 2007. **20**(6): p. 459-66.

249. Lin, D.C., et al., *Spherical indentation of soft matter beyond the Hertzian regime: numerical and experimental validation of hyperelastic models.* Biomech Model Mechanobiol, 2009. **8**(5): p. 345-58.

250. Lomakina, E.B., et al., *Rheological analysis and measurement of neutrophil indentation.* Biophysical Journal, 2004. **87**(6): p. 4246-4258.

251. Pasternak, C. and E.L. Elson, *Lymphocyte Mechanical Response Triggered by Cross-Linking Surface-Receptors.* Journal of Cell Biology, 1985. **100**(3): p. 860-872.

252. Kerr, A.D., *Elastic and Viscoelastic Foundation Models.* Journal of Applied Mechanics, 1964. **31**(3): p. 491-498.

253. Cronin-Golomb, M. and O. Sahin, *High-resolution nanomechanical analysis of suspended electrospun silk fibers with the torsional harmonic atomic force microscope.* Beilstein J Nanotechnol, 2013. **4**: p. 243-8.

254. Janmey, P.A. and C.A. McCulloch, *Cell mechanics: integrating cell responses to mechanical stimuli.* Annu Rev Biomed Eng, 2007. **9**: p. 1-34.

255. Wang, A. and M.J. Butte, *Customized atomic force microscopy probe by focused-ion-beam-assisted tip transfer.* Applied Physics Letters, 2014. **105**(5).

256. Shibata, M., et al., *Long-tip high-speed atomic force microscopy for nanometer-scale imaging in live cells.* Sci Rep, 2015. **5**: p. 8724.

257. Chacko, J.V., F.C. Zanacchi, and A. Diaspro, *Probing Cytoskeletal Structures by Coupling Optical Superresolution and AFM Techniques for a Correlative Approach.* Cytoskeleton, 2013. **70**(11): p. 729-740.

258. Odermatt, P.D., et al., *High-Resolution Correlative Microscopy: Bridging the Gap between Single Molecule Localization Microscopy and Atomic Force Microscopy.* Nano Letters, 2015. **15**(8): p. 4896-4904.

259. Solon, J., et al., *Fibroblast adaptation and stiffness matching to soft elastic substrates.* Biophysical Journal, 2007. **93**(12): p. 4453-4461.

260. Tee, S.Y., et al., *Cell Shape and Substrate Rigidity Both Regulate Cell Stiffness.* Biophysical Journal, 2011. **100**(5): p. L25-L27.

261. Labouesse, C., et al., *Cell shape dynamics reveal balance of elasticity and contractility in peripheral arcs.* Biophys J, 2015. **108**(10): p. 2437-47.

262. Dai, J.W., et al., *Myosin I contributes to the generation of resting cortical tension.* Biophysical Journal, 1999. **77**(2): p. 1168-1176.

263. Simon, S.I., et al., *Dynamics of neutrophil membrane compliance and microstructure probed with a micropipet-based piconewton force transducer.* Annals of Biomedical Engineering, 2007. **35**(4): p. 595-604.

264. Herant, M., V. Heinrich, and M. Dembo, *Mechanics of neutrophil phagocytosis: behavior of the cortical tension.* Journal of Cell Science, 2005. **118**(9): p. 1789-1797.

265. Pasternak, C., J.A. Spudich, and E.L. Elson, *Capping of Surface-Receptors and Concomitant Cortical Tension Are Generated by Conventional Myosin.* Nature, 1989. **341**(6242): p. 549-551.

266. Schwarz, E.C., et al., *Dictyostelium myosin IK is involved in the maintenance of cortical tension and affects motility and phagocytosis.* Journal of Cell Science, 2000. **113**(4): p. 621-633.

267. Krieg, M., et al., *Tensile forces govern germ-layer organization in zebrafish.* Nature Cell Biology, 2008. **10**(4): p. 429-U122.

268. Craig, E.M., et al., *Membrane Tension, Myosin Force, and Actin Turnover Maintain Actin Treadmill in the Nerve Growth Cone.* Biophysical Journal, 2012. **102**(7): p. 1503-1513.

269. Herant, M. and M. Dembo, *Form and Function in Cell Motility: From Fibroblasts to Keratocytes.* Biophysical Journal, 2010. **98**(8): p. 1408-1417.

270. Batchelder, E.L., et al., *Membrane tension regulates motility by controlling lamellipodium organization.* Proceedings of the National Academy of Sciences of the United States of America, 2011. **108**(28): p. 11429-11434.

271. Bruckner, B.R., et al., *Ezrin is a Major Regulator of Membrane Tension in Epithelial Cells.* Scientific Reports, 2015. **5**.

272. Pietuch, A., B.R. Bruckner, and A. Janshoff, *Membrane tension homeostasis of epithelial cells through surface area regulation in response to osmotic stress.* Biochimica Et Biophysica Acta-Molecular Cell Research, 2013. **1833**(3): p. 712-722.

273. Lieber, A.D., et al., *Front-to-Rear Membrane Tension Gradient in Rapidly Moving Cells.* Biophysical Journal, 2015. **108**(7): p. 1599-1603.

274. Labouesse, C., et al., *Microsurgery-aided in-situ force probing reveals extensibility and viscoelastic properties of individual stress fibers.* Sci Rep, 2016. **6**: p. 23722.

275. Bischofs, I.B., S.S. Schmidt, and U.S. Schwarz, *Effect of adhesion geometry and rigidity on cellular force distributions.* Phys Rev Lett, 2009. **103**(4): p. 048101.

276. Gao, H., J. Qian, and B. Chen, *Probing mechanical principles of focal contacts in cell-matrix adhesion with a coupled stochastic-elastic modelling framework.* J R Soc Interface, 2011. **8**(62): p. 1217-32.

277. Paszek, M.J., et al., *Integrin Clustering Is Driven by Mechanical Resistance from the Glycocalyx and the Substrate.* Plos Computational Biology, 2009. **5**(12).